UNIVERSITY OF VERONA

DEPARTMENT OF NEUROSCIENCES, BIOMEDICINE AND MOVEMENT SCIENCES

PHD IN APPLIED LIFE AND HEALTH SCIENCES

CYCLE XXXIII/2018

DEVELOPMENT OF ANTIBACTERIAL MEDICAL DEVICES BY COUPLING 3D PRINTING AND DRUG REPURPOSING

IN CO-TUTELLE DE THÉSE WITH APTUIT, AN EVOTEC COMPANY

S.S.D.: BIO/19

Coordinator: Prof. Giovani Malerba
Signature _____

Tutor: Prof.ssa Annarita Mazzariol (University of Verona)
Signature _____

Tutor: PhD Antonio Felici (Aptuit, an Evotec company
Signature _____

Tutor: MSc. Livia Ferrari (Aptuit, an Evotec company
Signature _____

PhD candidate: Jesus Augusto Vazquez Rodriguez

Signature:_____

Cover page

UNIVERSITÀ di VERONA

The experimental work described in this thesis research project was performed in the Department of Microbiology at Aptuit, an Evotec Company, Verona, Italy. This research was funded by the research project PRINTAID, the EU Framework Programme for Research and Innovation within Horizon 2020—Marie Skłodowska-Curie Innovative Training Networks under grant agreement No. 722467.

ACKNOWLEDGEMENTS

Antes que nada, me gustaría agradecer muy sinceramente a Antonio y Livia, por toda su confianza y basta paciencia para la realización de este proyecto de tesis. A mi familia, en especial a mis padres, Jesus y Lucy, a mis hermanos Diego y Kathia, que siempre creyeron en mi durante mi PhD y me dieron su apoyo incondicional.
Agradecer también mis compañeros de Aptuit, con los cuales compartí muchas vivencias durante los 3 años que estuve en la empresa. A todo el grupo de In vitro, con los cuales aprendí todas las bases de microbiología de laboratorio para poder desarrollar nuevos antimicrobianos. A Isabelle y Marinella, de las cuales aprendí como poder organizarse para llevar a cabo los experimentos en el laboratorio. A Michelle que siempre estuvo disponible para todas las dudas que tenía, a Anna, Diana, Luisa y Alessia con las cuales tuve muchas charlas matutinas y vespertinas en el laboratorio. A Vanessa que me ayudo a adaptarme a un nuevo país, con un nuevo idioma y una cultura muy diferente a la mía, ¡muchas gracias!

A mis compañeros del grupo In vivo, los cuales tuvieron mucha paciencia para enseñarme todo lo que sé de la experimentación animal, como olvidar las mañanas y las tardes donde ayude a colectar muestras. En general a todo el grupo In vivo (Elisa, Paola, Vivian, Livia, Jhon, Tommaso, Valeria, Giulio, Gabriella y Silvia) los cuales me compartieron sus opiniones y consejos para desarrollar mi trabajo con los ratones. A Vivian que muchas veces tuvimos discusiones científicas en el laboratorio y siempre me daba ideas para poder plantear y planificar mis experimentos. A Giulio y Jhon, que durante la etapa crítica de mi doctorado me apoyaron en realizar correctamente los modelos de infección. Como olvidar las largas horas trabajando y colectando muestras, tomando el desayuno y comiendo juntos.
A todos mis colaboradores e investigadores de PRINT-AID, en especial a Clara, Bahaa' y David con los cuales pudimos desarrollar de excelente manera diversos proyectos de investigación. Agradecer a la comunidad europea la cual por medio del proyecto PRINTAID H2020-MSCA-ITN-2017 financiaron la odisea para inicia mi vida científica en este PhD

CONTENTS

EXECUTIVE SUMMARY

Antibiotic resistance has been deemed as one of the biggest menaces for human health at a global scale. According to recent reports from the World Health Organization, in 2050 there will be an estimated of 10 million deaths per year due to antimicrobial resistance. In order to properly reduce the latent risk of antimicrobial resistance, multiple strategies have been explored to develop effective antibiotics in the short term. Drug repurposing has been deemed as one of the most promising strategies to generate novel antimicrobial drugs to treat infectious diseases. Drug repurposing is based on unravelling novel therapeutic indications for already approved drugs, which reduces drug development related costs as well as undesired toxicity related effects of the novel drug. Regarding the application of drug repurposing for developing novel antibiotics, the potential emergence of bacterial is greatly reduced, as bacterial cells are challenged with molecules acting with different antibacterial mechanisms of action of those known from current antibiotics.

Niclosamide has been identified as a potential antibacterial drug due to its high inhibitory activity against Gram-positive bacteria, in particular *Staphylococcus* aureus (*S. aureus*) which is considered one of the main causative agents of device-related infections. The present PhD research project is focused on evaluating the antibacterial activity of niclosamide in order to develop anti-infective medical devices by using 3D printing technologies.

In Chapter 2, the antibacterial activity of niclosamide was characterized against different relevant strains of *S. aureus* and *Staphylococcus epidermidis* (*S. epidermidis*). The inhibitory effect of niclosamide against both planktonic and biofilm growth of *S. aureus* was further studied. Moreover, the effect of niclosamide on the main metabolic pathways was studied in order to understand the possible antibacterial mechanism of action.

In chapter 3, thermoplastic polyurethane (TPU) catheters loaded with niclosamide were developed as a novel way to circumvent device-associated infections caused by *Staphylococcus aureus*. In order to produce such devices, niclosamide was loaded into the polymeric matrix of the TPU via solvent casting, and then hot melt extruded using a 3D printing to produce catheters loaded with niclosamide. The mechanical properties of the fabricated catheters were accordingly studied as well as the drug release of niclosamide from the catheters. Moreover, our results also demonstrated that niclosamide-loaded catheters were capable of release therapeutic concentrations of niclosamide under in vivo conditions. The *in vivo* therapeutic antibacterial effect was then confirmed using a foreign body infection model.

Finally, in chapter 4, antibacterial coatings were formulated in order to coat medical devices. The antibacterial coatings were developed by incorporating niclosamide into a polymer ink comprised of Poly(DL-lactide)/polyethylene glycol (PDLA-PEG). The coating was then deposited on the surface of catheters segments using ink jet printing technology, assuring the deposition of precise amounts of niclosamide per catheter. Furthermore, we demonstrated the *in vivo* efficacy and the protective activity of the developed coatings using a foreign body infection model.

LIST OF ABBREVIATIONS

AM	Additive manufacturing
AMR	Antimicrobial resistance
API	Active pharmaceutical ingredient
ATR	Attenuated total reflectance
BAI	Biomaterial associated infection
CDC	Center for disease control
CFU	Colony forming units
CLSI	Clinical and laboratory standards institute
CO2	Carbon dioxide
CRBIs	Catheter related bloodstream infections
CV	Cristal violet
DMEM	Dulbecco's modified Eagle's medium
DMSO	Dimethyl sulfoxide
DNA	deoxyribonucleic acid
EDTA	ethylenediaminetetraacetic acid
EM	Elastic modulus
FBS	Fetal bovine serum
FTIR	Fourier-transform infrared spectroscopy
HAIs	Health care-associated infections
HME	Hot melt extrusion
IJP	Ink jet printing
LDPE	Low density polyethylene
MBC	Minimal bactericidal concentration
MBIC	Minimum biofilm inhibitory concentration
MHB	Muller Hilton broth
MIC	Minimal inhibitory concentration
MMS	Macromolecule synthesis
MRSA	Methicilin resistant *Staphylococcus aureus*
MRSE	Methicilin resistant *Staphylococcus epidermidis*
MSSA	Methicilin susceptible *Staphylococcus aureus*
MSSE	Methicilin susceptible *Staphylococcus epidermidis*
MTP	Microtiterplate
MTT	(3-[4,5-dimethylthiazol-2-yl]-2,5 diphenyl tetrazolium bromide)
NIC	Niclosamide
OD	Optical density
PBS	Phosphate buffered saline
PCL	Polycaprolactone
PDLA	Poly (DL-lactide)
PEG	Polyethylene glycol
Pen	Penicillin

PLGA	Poly(lactic-co-glycolic acid)
PMF	Proton motive force
RNA	Ribonucleic acid
rpm	revolutions per minute
RT	room temperature
SD	Standard deviation
SEM	Scanning electron microscopy
Strep	Streptomycin
TCA	Trichloroacetic acid
TPU	Thermoplastic polyurethane
TSA	Tryptone soy agar
TSB	Tryptone soy broth
v/v	volume/volume
WHO	Wold health organization
WT	Wild type
XRPD	X-ray power diffraction
ZOI	Zone of inhibition

CHAPTER 1

GENERAL INTRODUCTION

GENERAL INTRODUCTION

HEALTHCARE ASSOCIATED INFECTIONS AND PATHOGENENESIS OF MEDICAL DEVICE-ASSOCIATED INFECTIONS

Healthcare associated infections (HCAI) are infections originated in a healthcare setting. These infections are often caused by microbes already present in the patient's organism or in the environment of the healthcare facility[1]. Worldwide, millions of patients are affected by HCAIs each year, resulting in massive health-related costs and unnecessary deaths[2]. HCAIs annually account for about 100, 000 deaths in USA and approximately 37, 000 fatalities in Europe[3]. Overall, financial costs are estimated to reach at least $ 10 billion each year worldwide[4]. According to US National Institute of Health, 60 % of HCAIs are caused by the biofilm (either in biotic or abiotic surfaces), whereas a huge fraction (~ 25 %) are directly related with the use of medical devices [5-7]. The most common medical devices associated infections are Ventilator-Associated Pneumonia (VAP), Central-Line-Associated Blood Stream Infections (CLABSI), and Catheter-Related Urinary Tract Infection (CAUTI)[8, 9]. In the table 1 is reported the most common device associated infections and their etiological pathogens[10].

Medical device	Major causative microorganism
Central Venous catheter	*S.aureus*, coagulase negative *Staphylococcus* spp, *Enterococcus* spp. , *Candida* spp., *Klebsiella pneumoniae,*
Urinary catheter	*Escherichia coli, Candida spp., CoNS, Enterococcus faecalis, Proteus mirabilis*
Peritoneal catheter	*S. aureus*, *Pseudomonas aeruginosa*, *Candida* spp.
Mechanical heart valve	CoNS, *S. aureus*, *Streptococcus* spp., *Enterococcus* spp
Coronary stents	*S. aureus*, CoNS, *P. aeruginosa*, *Candida* spp
Cardiac pacemakers	*S. aureus*, CoNS, *Streptococcus* spp., *Candida* spp.
Vascular graft	*S.aureus, Staphylococcus epidermidis*, *Pseudomonas* spp., *Enterococcus* spp., *Enterobacter* spp

Fracture fixation device	CoNS; *S. aureus*, *Propionibacterium* spp., *Streptococcus* spp., *Corynebacterium* spp.
Hip/knee implants	*S. aureus*, CoNS, *Streptococcus* spp., *Enterobacteriaceae*
Pelvic mesh	CoNS; *Streptococcus* spp., *P. mirabilis*, *Enterococcus* spp., *Actinomyces* spp.
Cochlear implants	*S. aureus*, *P. aeruginosa*, *Haemophilus influenzae*, *Streptococcus* spp.
Breast implants	*S. aureus*, CoNS, *Streptococcus*, *Propionibacterium* spp.

Table 1. Most common causative pathogens of medical-device associated infections. Coagulase-negative staphylococci (CoNS). Figure adapted from [10].

BACTERIAL COLONIZATION AND BIOFILM FORMATION ON MEDICAL DEVICES

Bacterial colonization on device surfaces is the most crucial step in the multifaceted process that led to medical device- associated infections. Bacterial cells attaching to medical devices eventually form bacterial microaggregates which are encased into an abundant extracellular polymeric matrix[11]. Bacterial cells residing within biofilm structures display different phenotypic and genotypic characteristics than their planktonic counterpart[12]. These differential features result in having several biofilm bacterial communities exhibiting physiological and metabolic properties which in fact affects the bacterial susceptibility to antibiotic treatments [6]. As a matter of fact, it has been reported that biofilms are 10-1000 times more resistant to antibiotic treatment than their respective planktonic cells[6, 13]. In addition, the polymeric matrix represents a physical barrier to antibiotics and other antimicrobial molecules. These protective biofilm phenotype enables bacterial cells to resist not only to antibiotics but also to the immune host response for prolonged period of times[14].

Frequently, these factors may result in recalcitrant infections that may lead to device removal, bacterial dissemination to other body sites or treatment failure. In most of the cases, biofilm on medical devices includes multiple type of microorganisms which represent a fitness survival benefit to the microbial

community[15]. The transition of planktonic cells to biofilm phenotype involves several biological, chemical, and physical mechanisms and components which differ between bacterial species and strains[12]. However, biofilm formation and development on medical devices most commonly follows a 3-stage lifecycle involving: initial bacterial adhesion, accumulation/maturation and finally dispersal. The biofilm lifecycle is schematically depicted in figure 1[16].

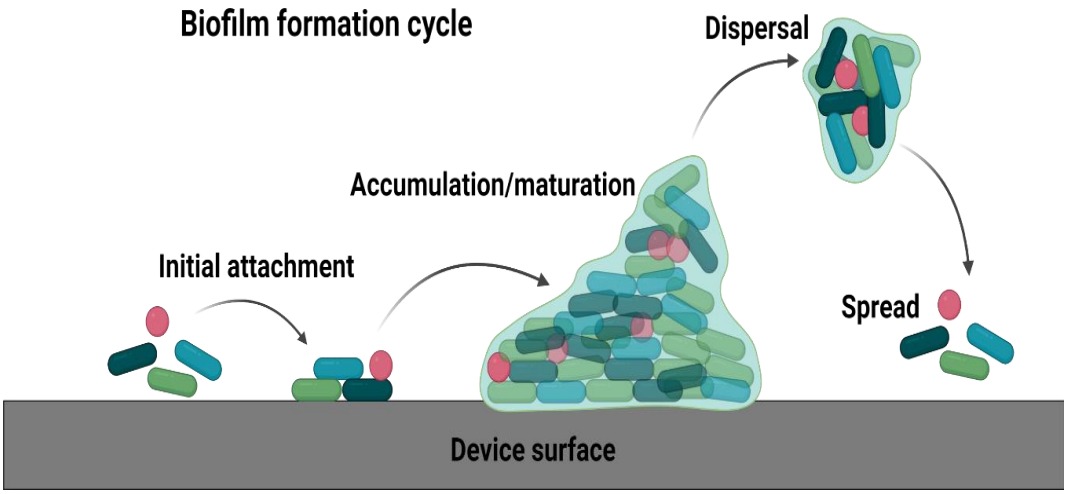

Figure 1. Biofilm development include 3 stages: Initial attachment, accumulation maturation and dispersal.

The biofilm formation process begins with the attachment of bacterial cells to the device surface which is mainly mediated by bacterial factors such as pili, flagella, receptors, or other adhesive appendages. This initial bacterial contamination on the medical device might originate from the patient or health professional microbiota leading to the subsequent bacterial colonization throughout the device surface[17]. Once bacteria have adhered to the device surface, cells initiate to proliferate resulting in the formation of multi-layered microaggregates. Subsequently, bacterial cells secrete polymeric substances to the immediate environment including proteins, exopolysaccharides, and extracellular DNA[18]. These extracellular polymeric substances (EPS) form a polymeric matrix embedding bacterial cells and providing physical structure and mechanical integrity to the biofilm) [19]. EPS serves as well as a 3D-scaffold for further bacterial proliferation while promoting cell-cell adhesion, cell-cell communication, and aggregation. The

composition of EPS significantly varies between different bacterial species, for instance *P. aeruginosa* biofilms are mainly composed of Pel, Psl and alginate whereas poly-β(1-6)-N-acetylglucosamine (PNAG) and polysaccharide intercellular adhesin (PIA) constitute most of the polymeric matrix of staphylococcal biofilms[6, 12, 17].

Mature biofilms are comprised of microcolonies surrounded by EPS which boost a complex dynamic of chemical and biological interactions resulting in the characteristic genetic and phenotypic heterogeneity of biofilms. In this stage, bacterial virulence factors are produced, contributing to the recalcitrance of biofilm infections. Once the maturation process is completed, tower-like structures are prevalent in the biofilm 3D structure which in fact characterizes fully stablished biofilms[20].

The last stage of biofilm development is characterized by detachment of bacterial cells from cell clusters. Dispersal is induced by passive and active mechanisms. The passive detachment of cells is governed by external influences, such as mechanical and shear stress[19]. Additionally, biofilm components could be removed by grazing, erosion, abrasion, and sloughing. On the other hand, active dispersal mechanisms are triggered by a series of changes in the cellular signals such as changes in oxygen levels, metal concentrations, nutrient availability, waste products and inducing molecules [21, 22]. Dispersal response mainly involves the production of bacterial factors with the ability to modulate the biofilm integrity, EPS-degrading enzymes, surfactant-like molecules and inhibitors of matrix production are the main effectors in active dispersal. It is worth highlighting that dispersed cells regain a planktonic-like phenotype with higher motility which in fact increases the colonization of new surfaces and the dissemination of the infection to distant sites within the body [19].

Gram-positive staphylococci are responsible for most part of the device associated infections. Specifically, *S. aureus* stands as the most recurrent pathogen in these infections[23]. *S. aureus* produces a wide variety of toxins and virulence factors

which highly attenuate the host defences, rendering the host susceptible to further biofilm infection[24]. Initially, bacterial cells attach to device surfaces either by nonspecific forces (electrostatic, mechanical, surface tension, hydrophobicity) or bacterial factors such as adhesive appendages, pili or flagella. Biofilm formation of *S. aureus* on medical devices highly relies on the interaction of bacterial cells to host matrix proteins, particularly fibrinogen, collagen, and fibronectin[25]. These proteinous host factors, rapidly adhere to medical devices after implantation. *S. aureus* cells attach to such host ligands via a group of surface proteins termed Microbial Surface Components Recognizing Adhesive Matrix Molecules (MSCRAMM). The most studied MSCRAMM include Fibronectin binding protein A (FnbpA) and Fibronectin binding protein B (FnbpB) which attach to fibronectin, elastin and fibrinogen, Clumping factor A (ClfA) that binds to fibrinogen, and collagen-binding adhesin which binds to collagen[24, 26].

As mentioned before, host proteins promote bacterial attachment mainly through MSCRAMM-host ligand interactions. Consequently, attachment and accumulation of host proteins on medical devices highly influence the biofilm formation process and further infection development within the host. For instance, several studies have demonstrated that *S. aureus* cells binds more often to protein-covered devices than uncoated devices[20, 23].

On the other hand, host factors, especially those involved in the immune system promote the persistence of bacterial infection. *S. aureus* infections have been reported to modulate the host immune response as bacterial toxins and virulence factors decrease both the complement-mediated opsonic effect and the bactericidal activity of leucocytes in device-surrounding tissue[27]. Additionally, the biofilm structure per se constitutes an immune evasion mechanism since the polymeric matrix prevents from neutrophils attack , moreover biofilm cells produce signalling factors that control inflammatory response[12].

The presence of the medical device within the host produces a foreign body response in the surrounding tissue. In this reaction, there is an inflammatory

response which involves the complement system, platelets, and immune cells, particularly neutrophils. Neutrophils under these specific conditions are overstimulated for which its bactericidal activity is greatly reduced promoting device bacterial colonization[28]. Additionally, the medical device offers a substratum surface for bacterial adhesion and subsequent biofilm development[29]. The device material properties such as chemical nature (e.g., charge and hydrophobicity), topography, roughness, and stiffness conditionate the cellular and immune responses, tissue integration and bacterial adhesion[11, 29, 30].

ANTIFOULING AND ANTIMICROBIAL STRATEGIES TO PREVENT DEVICE ASSOCIATED INFECTIONS

All medical devices are prone to microbial colonization, hence halting microbial adhesion on device surfaces is a key step to control the spreading of device-associated infections[20]. As bacterial attachment to medical devices depends partially on the properties of the device surface, the material modification, and the antimicrobial functionalization of medical devices would be the most suitable approach for preventing bacterial infections. Overall, anti-infective device approaches can be divided in two categories: antimicrobial and antifouling. In brief, antimicrobial approaches are those in which approaching microorganisms are inhibited or killed by antimicrobial agents, while in antifouling approaches, the physicochemical properties of the biomaterial are modified in order to prevent bacterial attachment onto the device surface[31-33].

In antimicrobial approaches, the antimicrobial effect is achieved through: (1) antibacterial agent release and (2) contact-killing surface. Whereas antifouling strategies employ the following mechanisms: (1) steric repulsion/hydration, (2) electrostatic repulsion, or (3) low surface energy[30].

Antimicrobial release approaches have demonstrated to be efficacious as a plethora of antimicrobials can be employed in different substratum surfaces, however the main drawback relies on the fact that once the antimicrobial agent is released both

its activity and concentration can decrease and not be longer effective against the microbes[32]. Moreover, the drug reservoir can be depleted, hence exhausting the antibacterial protection. Some antibacterial agents, used for this application, are metallic nanoparticles, salt metals, antibodies, antibacterial peptides, antibiotics, signalling molecules, disinfectants, and repurposed drugs[12, 20, 32, 34].

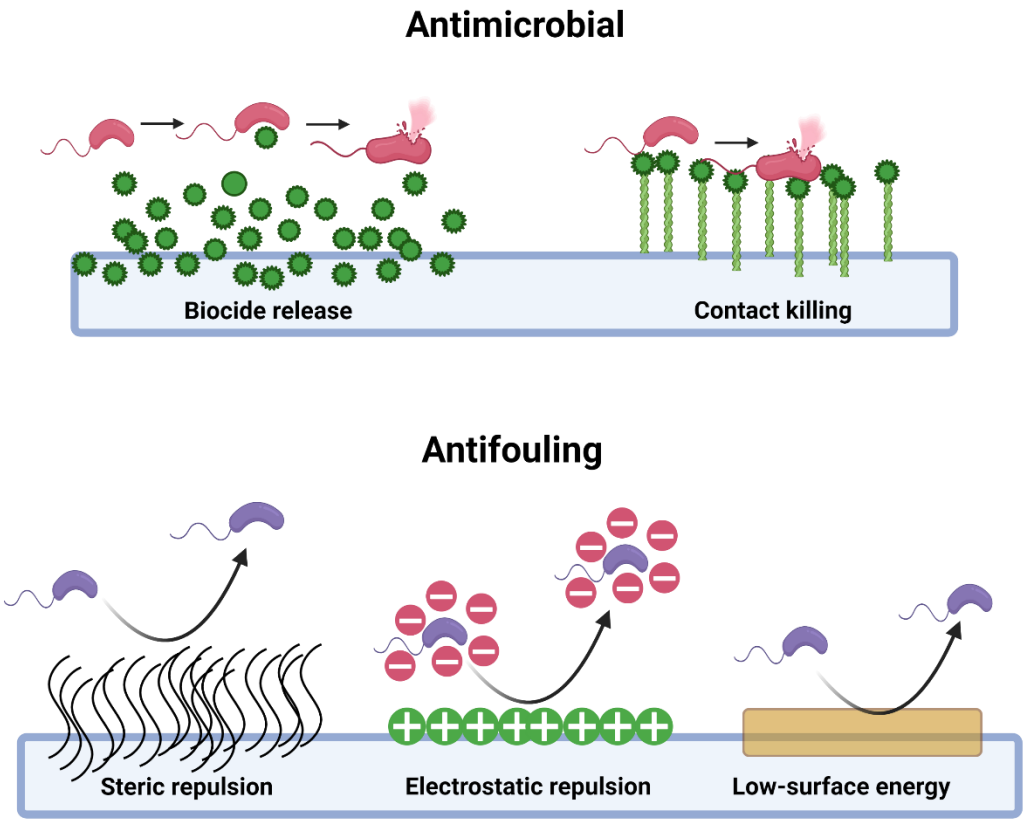

Figure 2. Classification of strategies to achieve antimicrobial and antifouling surfaces to prevent medical device associated infection.

In contact killing strategies, device surfaces can be functionalized mainly with monomers, side chains or grafted moieties. The main mechanism of action of this approach is the disruption /damage of the microbial surface. This damage is achieved by opposite charge attraction and penetration of the active group into the bacterial surface leading to cell disruption, or by affecting the charge of the membrane potential[31]. Many contact active materials are based on cationic monomers, side chains and covalent surface grafts. Most of these materials are functionalized with quaternary ammonium compounds, antibacterial peptides, or cationic biocides[35]. The main drawback of this strategy is the potential

accumulation of cellular components from dead bacteria which eventually may mask the contact-active surface properties. Additionally, device material can be affected due to the functionalization and may lead to changes in the material integrity[35, 36].

Antifouling strategies can be categorized in coatings, blends and micropatterned surfaces[31]. The most investigated mechanism employs hydration forces/steric repulsion to generate antifouling surfaces. For instance, one of the first polymers used as antifouling coating was polyethylene glycol (PEG) which through its hydrophilicity is capable to produce a hydration layer, creating an energetic barrier[30]. This energetic barrier interferes with proteins, rendering bacterial interactions unfavourable to attain bacterial attachment on the material. Other polymers such as polyglycerols, polyoxazolines, zwitterionic polymers and hydrophobic polymers have been explored extensively to protect device from bacterial adhesion[36-38].

On the other hand, antifouling polymers can be incorporated into the backbone or the device material by copolymerization. The amount and the properties of the material can be tailored according to the final application of the device[38]. Bulk modification, in contrast to surface modifications, may be advantageous for long-term protection since improved physical and chemical properties can be obtained in the bulk material[31]. However, the potential drawback of this approach is that the production of specific polymeric blends may include complex processes and may lead to the deterioration of the components of the device. Some polyurethanes such as Poly Tetra Methylene Oxide (PTMO), a polyether obtained from the polymerization of tetrahydrofuran (THF) are commonly used to fabricate medical catheters[37].

In addition, another antifouling approach that has been recently explored is micropatterning. By modifying the topography/roughness of device surfaces, some properties as hydrophobicity and surface energy can be impacted and thus bacterial adhesion limited[29]. Most of the micropatterns that have been exploited to be

applied in medical devices arises from antifouling textures found in nature like the skin of dolphins, sharks, and the cuticle of insects [33]. The commercially available sharklet technology, mimics the surface micropatterns of shark skin, exerting anti-infective properties to polymers[30]. Nevertheless, one of the main drawbacks of this approach is the lack of *in vivo* studies demonstrating the efficacy of this material to prevent device infections in physiologically relevant conditions[31].

ADDITIVE MANUFACTURING FOR DEVELOPING ANTIBACTERIAL MEDICAL DEVICES

Additive manufacturing (AM) is defined as the process of assembling materials to make objects from 3D model data, usually layer by layer. This definition has been adopted by the International Organization for Standardization (ISO) and American Society for Testing and Materials (ASTM) standard (ISO/ASTM 52900:2016)[39]. Generally, the 3D printing of objects follows the next steps:

1) 3D-models of the product are designed and transferred to the 3D-printer machine.
2) The model is digitalized and deconstructed into layers.
3) Printing parameters are selected (temperature, material, laser intensity, Z resolution, etc), and the machine prints the 3D construct layer by layer and finally the support material is removed from the construct.
4) Once the final product is printed, post-printing modification may be performed for the intended application[40-43].

As AM models are designed and modelled using a 3D dedicated software, complex 3D structures can be fabricated accurately to resemble closely the original model. It is worth highlighting that by conventional fabrication techniques such a degree of structure precision in the final product would be scarcely achieved[44]. By exploiting this feature of 3D printing technologies, a myriad of personalized medical devices has been previously fabricated for improving current biomedical technologies and satisfy medical needs[45]. Among other, these devices include

wound dressings, catheters, endotracheal tubes, abdominal and vaginal meshes, hearth valves, prothesis, implants, stents, and drug delivery systems[41, 46].

One of the most promising applications of 3D printing is the fabrication of tailor-made medical devices to fulfil a specific function once inserted into the patient[45]. Despite these advantages, materials, especially polymers, for biomedical applications are at risk of microbial contamination, which in fact, can affect the integrity and functionality of 3D-printed medical devices[42] and lead to more serious health complications[20]. One approach to circumvent the potential risk of microbial contamination is loading drugs within the structure of the device construct[40]. Different types of drugs such as antimicrobials, can be directly incorporated into the polymer carrier of the medical devices to prevent device-associated infections[43]. An antibiotic-loaded medical device allows for controlled and localized drug delivery. Consequently, drug concentration at the site of implant is normally higher with respect to those achieved after systemic administration. Moreover, localized drug delivery overcomes the potential toxic adverse effects that may arise after systemic administration of high doses of drug[47].

FUSED DEPOSITION MODEL AND INK JET PRINTING

Among the different current AM techniques, extrusion-based 3D printing technologies, namely Fused Deposition Model (FDM) and Ink jet printing are the more common techniques for the preparation of drug loaded devices[40, 48]. In FDM, a polymeric filament or film is melt-extruded through a heated nozzle and then deposited layer by layer to finally generate 3D construct based in the digital model (Figure 3)[41]. FDM allows for customization of several properties such geometry, density and the size of the printed products[45]. Additionally, another remarkable advantage of this technology is that a variety of medical grade polymers such as PEG, hydroxypropylcellulose (HPC), Eudragit, polyvinylpyrrolidone (PVP), thermoplastic polyurethane (TPU), polycaprolactone (PCL), polylactic acid (PLA), etc can be utilized for printing devices[43]. The process for printing

antibiotic loaded devices by FDM requires the preparation of a thermoplastic polymer loaded with an antibiotic agent[40].

The production of polymer loaded materials is usually achieved by different processes such as melt-blending, physical mixing, and homogenization prior to be fed into the 3D printer; however, a large variation in the particle size between the polymer and the drug can produce a non-homogenous drug distribution in the material[48]. Mixing techniques, specifically, solvent casting assures a homogenous distribution of the drug within the polymeric matrix since both the drug and the polymer are dissolved in an organic solvent. In this case, the polymer-drug solution is casted and the solvent evaporated to produce drug-loaded films which will be then fed into the 3D printer machine to fabricate an antibiotic-release device[49]. A critical aspect of FDM is the potential material degradation during 3D printing. Usually, high melting temperatures (>100 °C) are used to 3D print the drug-loaded polymeric material, thus the importance of selecting heat-resistant antibiotics to avoid possible adverse effects such as decrease in the drug activity and the production of hazardous byproducts[50].

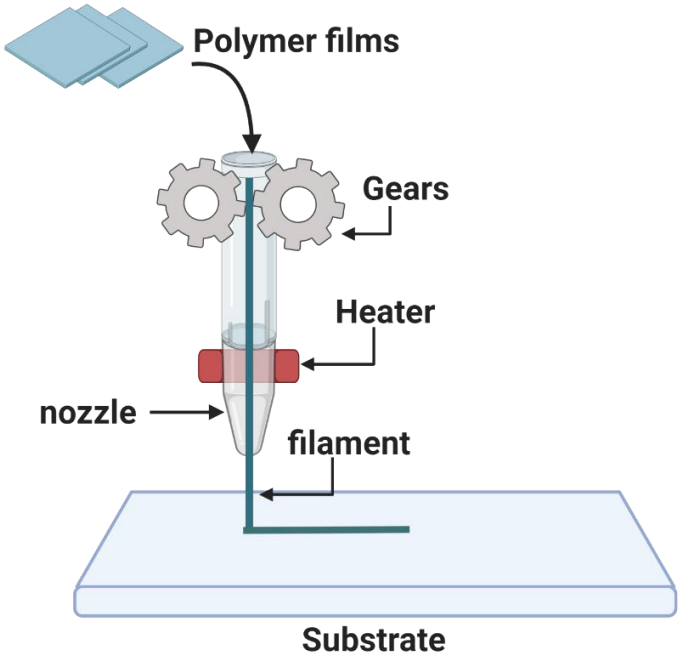

Figure 3. Fused Deposition Model (FDM) printing process

Previous studies report the use of FDM to produce antibiotic-loaded medical devices such as PLA nasal stents loaded with penicillin, anti-infective PLA vascular stents loaded with iodine, antibacterial PCL wound dressings loaded with metals, tetracycline-eluting PLA orthopaedic liners and dialysis catheters loaded with gentamycin[51-54]. However, most of the studies regarding the production of antibiotic-loaded devices by FDM have been tested for antibacterial-anti biofilm activity just by *in vitro* methods[47]. As far as we are concerned, only one study has reported the evaluation of the efficacy of 3D-printed scaffolds impregnated with tobramycin in a rat osteomyelitis model. Interestingly, in such study, animals implanted with tobramycin-loaded scaffolds showed a significant reduction of tissue and osseous infections with respect to control group[55].

Ink jet printing (IJP) is an AM technology which allows the deposition of 1-100 pL droplets of liquid material to produce 2D and 3D structures. This approach involves dissolving/dispersing a material in a liquid to form an ink[56]. Usually, polymeric solutions are used as inks in IJP which are dissolved in a solvent such as dichloromethane, dimethyl sulfoxide, tetrahydrofuran, chloroform, etc. The most common polymers used for ink preparation include PEG, gelatine, collagen, fibrin, alginate, gelatin methacryloyl (GelMA), poly (lactic-co-glycolic acid) (PLGA), poly (DL-lactide) (PDLA), etc. These polymeric inks evaporate after material deposition, resulting in a dry polymeric material[57].

In inkjet printing, ink drops are ejected from a micro nozzle and are usually created by heating the ink further than the boiling temperature or by application of a voltage to a piezoelectric transducer, which leads to a vibration of the material (Figure 4) [58]. The piezoelectric ink jetting is the predominant technology for research nowadays, given its flexibility in the use of different material to formulate inks[59]. Moreover, piezoelectric Drop on demand injection (DOD) has a fully automated injection which provides accurate control on the droplet size leading to minimum material losses, reduction of contamination of deposited material and precise design of deposition patterns on different surfaces[58]. The Ink jet technology has successfully been used in the health research field, and,

according to the final application, inks can be categorized in screening platforms for drug discovery, drug formulations, bio-inks (inks containing cells) and drug-containing inks[57]. IJP allows for the controllable and reproducible deposition pattern of droplets on almost all suitable surfaces. For this reason this technology has been explored to functionalize medical devices with drug-containing inks[60]. This approach offers a significant reduction of wasting materials during the manufacturing process since an exact amount of ink containing specific amount of drug can be deposited on the device, achieving high coating yields[56].

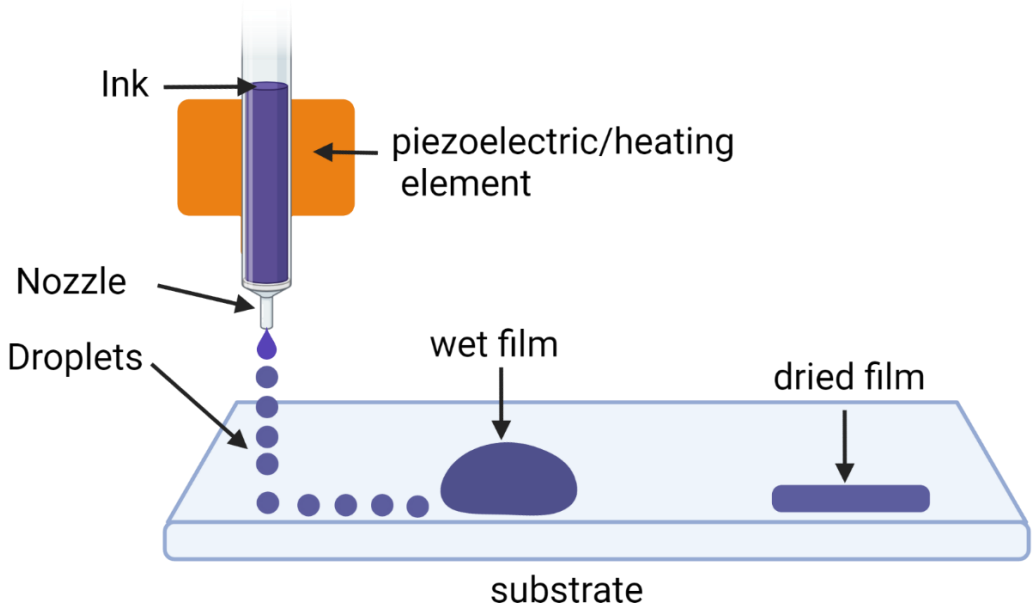

Figure 4. Schematic showing the printing process of the drop-on demand inkjet technology.

In contrast to IJP, other techniques used to coat medical devices, namely spray and dip coating, show different drawbacks. In one hand, in spray coatings, a drug-polymer solution is sprayed onto the device, dried and sprayed a second time. The main disadvantages of spray coating for medical devices are: the requirement of specialized equipment and that an inhomogeneous coating is quite often obtained [61]. On the other hand, dip coating involves the submersion of the device in a drug-polymer solution and then the device is spinned to remove the coating excess[62]. This process is usually repeated until an appropriate amount of drug-coating is achieved. Usually, dip coating yields high drug concentration, but it is a time-consuming process[61, 62].

Several proof-of-principle studies have proved that IPJ can be used to functionalized medical devices with different pharmacological agents. Tarche et al, applied IJP technology to coat stents by depositing droplets of phosorylcholine-linked methacrylate tetracopolymer loaded with fenofibrate and ABT-578 on their surface[63]. In a different study, coronary metal stents were coated with inks of PDLA loaded with simvastatin and paclitaxel[61]. Interestingly, the coated stents were able to exert an *in vivo* effect showing intrastent restenosis, the stents also presented neither inflammatory response nor *in vivo* cytotoxicity. Additionally, other devices have been coated such as wound dressings and microneedle systems[56]. Wu et al [64] coated a bone implant with a polymer loaded with isoniazid-rifampicin to treat bone tuberculosis. Similarly, Gu et al, deposited phosphate nanoparticles loaded with rifampicin on titanium substrates using IJP[65]. Finally, in a recent study amphotericin B solution was deposited on the surface of microneedles by IJP [66]. The amphotericin-loaded microneedles showed activity against *Candida parapsilosis* in a disk diffusion assay.

ANTIMICROBIAL DRUG REPURPOSING AND ANTIBACTERIAL ACTIVITY OF NICLOSAMIDE

Drug repurposing is reported as the process of generating novel therapeutic applications for known approved drugs[67]. Drug repurposing is based on two principles: (I) the drug has undescribed inherent biological activities and (II) diseases may often share common molecular and/or genetic factors, thus they can be treated using diverse drugs[68]. The application of drug repurposing to generate novel antibacterial treatments displays several advantages , including: reduction in research and development related costs, pharmacokinetic, pharmacodynamic and toxicological profiles are already known, risk failure reduction for the novel drug indication and minimizing the emergence of antimicrobial resistance[68-70].

In recent years, several studies have been focused on tackling antibacterial infections by exploring the use of repurposed drugs. Among the recent discoveries, niclosamide has been been proposed as a promising candidate to treat bacterial

infections, particularly those caused by Gram-positive bacterial pathogens[71-74]. Niclosamide, a halogenated salicylanilide, was first developed in 1953 by Bayer research laboratory to kill snails and then stop the spread of schistosomiasis[75]. Afterwards, it was discovered that niclosamide was highly active against cestodes and, thus, it was approved for the therapy of nematode infestation in humans[76]. Currently, niclosamide is considered as an essential medicine by the World Health Organization to treat nematode infections in humans. [77]. The proposed molluscicide mechanism of action is mainly related to its activity as ionophore which may uncouple the mitochondrial oxidative phosphorylation of tapeworms and hence interfere with the metabolism of these organisms[78]. Niclosamide may exhibit a similar mechanism of action towards bacterial cells by uncoupling the electron chain transport and then dissipating the proton motive force (PMF). The negative impact on the PMF would eventually increase the oxygen consumption while decreasing the ATP production. Due to reduced ATP production, macromolecular synthesis pathways are severely affected and finally cell death occurs [79].

Niclosamide has been proven highly effective against different bacteria such as *Mycobacterium tuberculosis*, *S. aureus*, *S. epidermidis*, *Enterococcus Faecium*, *Clostridium dificcile* and *Helycobacter pylori*[71, 72, 80-88]. Moreover, niclosamide is able to prevent the biofilm formation and partially disaggregate mature biofilms of *S. aureus* and *S. epidermidis* at concentrations comparable to those of the MIC[73, 88]. Considering niclosamide antibiofilm activity, Gwisai et al[72], deposited niclosamide on different material substrates, inhibiting the biofilm formation of *S. aureus*. This study provided a proof of concept of how this drug could be potentially applied to medical device surfaces and thus prevent biofilm infections.

Even though niclosamide has potent activity not only as antibacterial but also as anticancer drug, its use in the clinic is limited due to its poor solubility in water[89]. Given these characteristics, this drug may be ineffective to treat systemic infections.

Interestingly, different approaches have been employed such as HME and IJP to increase niclosamide solubility and thus its *in vivo* bioavailability.

In this research thesis, we aimed to confirm the therapeutic potential use of niclosamide to treat device-associated infections caused by *Staphylococcus* spp. Under this rationale, 2 different additive manufacturing technologies (HME and IJP) were used to develop niclosamide-releasing devices. Such devices were then analysed for their antibacterial activity using different *in vitro* models and ultimately, the devices were tested for their *in vivo* efficacy using a murine foreign body infection

REFERENCES

1. *Collins, A.S. and R. Hughes,* Patient safety and quality: an evidence-based handbook for nurses. *Preventing health care–associated infections, 2008.*
2. *Horan, T.C., M. Andrus, and M.A. Dudeck,* CDC/NHSN surveillance definition of health care–associated infection and criteria for specific types of infections in the acute care setting. *American journal of infection control, 2008. 36(5): p. 309-332.*
3. *Klevens, R.M., et al.,* Estimating health care-associated infections and deaths in U.S. hospitals, 2002. *Public Health Rep, 2007. 122(2): p. 160-6.*
4. *Organization, W.H.,* WHO guidelines on hand hygiene in health care: first global patient safety challenge clean care is safer care. *2009: World Health Organization.*
5. *Jamal, M., et al.,* Bacterial biofilm and associated infections. *Journal of the Chinese Medical Association, 2018. 81(1).*
6. *Davies, D.,* Understanding biofilm resistance to antibacterial agents. *Nature Reviews Drug Discovery, 2003. 2(2): p. 114-122.*
7. *Bjarnsholt, T.,* The role of bacterial biofilms in chronic infections. *Apmis, 2013. 121: p. 1-58.*
8. *Organization, W.H.,* Report on the burden of endemic health care-associated infection worldwide. *2011.*
9. *Zell, B.L. and D.A. Goldmann,* Healthcare-associated infection and antimicrobial resistance: moving beyond description to prevention. *Infection Control & Hospital Epidemiology, 2007. 28(3): p. 261-264.*
10. *Salwiczek, M., et al.,* Emerging rules for effective antimicrobial coatings. *Trends in Biotechnology, 2014. 32(2): p. 82-90.*
11. *Weinstein, R.A. and R.O. Darouiche,* Device-associated infections: a macroproblem that starts with microadherence. *Clinical infectious diseases, 2001. 33(9): p. 1567-1572.*
12. *Arciola, C.R., D. Campoccia, and L. Montanaro,* Implant infections: adhesion, biofilm formation and immune evasion. *Nature Reviews Microbiology, 2018. 16(7): p. 397-409.*
13. *Harriott, M.M.,* Biofilms and Antibiotics, *in* Reference Module in Biomedical Sciences. *2019, Elsevier.*
14. *Mah, T.-F.C. and G.A. O'Toole,* Mechanisms of biofilm resistance to antimicrobial agents. *Trends in microbiology, 2001. 9(1): p. 34-39.*

15. *Del Pozo, J. and R. Patel,* The challenge of treating biofilm-associated bacterial infections. *Clinical Pharmacology & Therapeutics, 2007. 82(2): p. 204-209.*
16. *Mack, D., et al.,* Biofilm formation in medical device-related infection. *The International journal of artificial organs, 2006. 29(4): p. 343-359.*
17. *Busscher, H.J., et al.,* Biomaterial-associated infection: locating the finish line in the race for the surface. *Science translational medicine, 2012. 4(153): p. 153rv10-153rv10.*
18. *Floyd, K.A., A.R. Eberly, and M. Hadjifrangiskou,* 3 - Adhesion of bacteria to surfaces and biofilm formation on medical devices, *in* Biofilms and Implantable Medical Devices, *Y. Deng and W. Lv, Editors. 2017, Woodhead Publishing. p. 47-95.*
19. *Rumbaugh, K.P. and K. Sauer,* Biofilm dispersion. *Nature Reviews Microbiology, 2020. 18(10): p. 571-586.*
20. *Khatoon, Z., et al.,* Bacterial biofilm formation on implantable devices and approaches to its treatment and prevention. *Heliyon, 2018. 4(12): p. e01067.*
21. *Wille, J. and T. Coenye,* Biofilm dispersion: The key to biofilm eradication or opening Pandora's box? *Biofilm, 2020. 2: p. 100027.*
22. *Solano, C., M. Echeverz, and I. Lasa,* Biofilm dispersion and quorum sensing. *Current opinion in microbiology, 2014. 18: p. 96-104.*
23. *Zheng, Y., et al.,* Colonization of medical devices by staphylococci. *Environmental microbiology, 2018. 20(9): p. 3141-3153.*
24. *Oliveira, D., A. Borges, and M. Simões,* Staphylococcus aureus toxins and their molecular activity in infectious diseases. *Toxins, 2018. 10(6): p. 252.*
25. *Zapotoczna, M., E. O'Neill, and J.P. O'Gara,* Untangling the Diverse and Redundant Mechanisms of Staphylococcus aureus Biofilm Formation. *PLoS Pathog, 2016. 12(7): p. e1005671.*
26. *Moormeier, D.E. and K.W. Bayles,* Staphylococcus aureus biofilm: a complex developmental organism. *Molecular microbiology, 2017. 104(3): p. 365-376.*
27. *DeLeo, F.R., B.A. Diep, and M. Otto,* Host defense and pathogenesis in Staphylococcus aureus infections. *Infectious disease clinics of North America, 2009. 23(1): p. 17-34.*
28. *Moriarty, T.F., S.A. Zaat, and H.J. Busscher,* Biomaterials associated infection: immunological aspects and antimicrobial strategies. *2012: Springer Science & Business Media.*

29. *Song, F., H. Koo, and D. Ren,* Effects of material properties on bacterial adhesion and biofilm formation. *Journal of dental research, 2015. 94(8): p. 1027-1034.*
30. *Zheng, S., et al.,* Implication of Surface Properties, Bacterial Motility, and Hydrodynamic Conditions on Bacterial Surface Sensing and Their Initial Adhesion. *Frontiers in Bioengineering and Biotechnology, 2021. 9(82).*
31. *Zander, Z.K. and M.L. Becker,* Antimicrobial and antifouling strategies for polymeric medical devices. *2018, ACS Publications.*
32. *Cloutier, M., D. Mantovani, and F. Rosei,* Antibacterial coatings: challenges, perspectives, and opportunities. *Trends in biotechnology, 2015. 33(11): p. 637-652.*
33. *Adlhart, C., et al.,* Surface modifications for antimicrobial effects in the healthcare setting: A critical overview. *Journal of Hospital Infection, 2018. 99(3): p. 239-249.*
34. *Amin Yavari, S., et al.,* Combating Implant Infections: Shifting Focus from Bacteria to Host. *Advanced Materials, 2020. 32(43): p. 2002962.*
35. *Siedenbiedel, F. and J.C. Tiller,* Antimicrobial Polymers in Solution and on Surfaces: Overview and Functional Principles. *Polymers, 2012. 4(1): p. 46-71.*
36. *Babutan, I., A.-D. Lucaci, and I. Botiz,* Antimicrobial Polymeric Structures Assembled on Surfaces. *Polymers, 2021. 13(10): p. 1552.*
37. *Singha, P., J. Locklin, and H. Handa,* A review of the recent advances in antimicrobial coatings for urinary catheters. *Acta Biomater, 2017. 50: p. 20-40.*
38. *Jain, A., et al.,* Antimicrobial polymers. *Advanced healthcare materials, 2014. 3(12): p. 1969-1985.*
39. *DIN, E.,* ISO/ASTM 52900: 2017-06 additive manufacturing—general principles—terminology (ISO/ASTM 52900: 2015). *German version EN ISO/ASTM, 2017. 52900.*
40. *Borandeh, S., et al.,* Polymeric drug delivery systems by additive manufacturing. *Advanced Drug Delivery Reviews, 2021.*
41. *Ahangar, P., et al.,* Current biomedical applications of 3D printing and additive manufacturing. *Applied sciences, 2019. 9(8): p. 1713.*
42. *González-Henríquez, C.M., M.A. Sarabia-Vallejos, and J. Rodríguez Hernandez,* Antimicrobial polymers for additive manufacturing. *International journal of molecular sciences, 2019. 20(5): p. 1210.*
43. *Mokhena, T.C., et al.,* Antibiotic 3D printed Materials for healthcare applications. *Antibiotic Materials in Healthcare, 2020: p. 141.*

44. *Ngo, T.D., et al.,* Additive manufacturing (3D printing): A review of materials, methods, applications and challenges. *Composites Part B: Engineering, 2018. 143: p. 172-196.*
45. *Francis, M.P., et al.,* Additive manufacturing for biofabricated medical device applications, *in* Additive Manufacturing. *2018, Elsevier. p. 311-344.*
46. *Culmone, C., G. Smit, and P. Breedveld,* Additive manufacturing of medical instruments: A state-of-the-art review. *Additive Manufacturing, 2019. 27: p. 461-473.*
47. *Ballard, D.H., et al.,* Antibiotics in 3D-printed implants, instruments and materials: benefits, challenges and future directions. *Journal of 3D printing in medicine, 2019. 3(2): p. 83-93.*
48. *Wang, J., et al.,* Emerging 3D printing technologies for drug delivery devices: Current status and future perspective. *Advanced Drug Delivery Reviews, 2021.*
49. *Shaqour, B., et al.,* 3D-Printed Drug Delivery Systems: The Effects of Drug Incorporation Methods on Their Release and Antibacterial Efficiency. *Materials, 2020. 13(15): p. 3364.*
50. *Shaqour, B., et al.,* Production of drug delivery systems using fused filament fabrication: a systematic review. *Pharmaceutics, 2020. 12(6): p. 517.*
51. *Weisman, J.A., et al.,* Antibiotic and chemotherapeutic enhanced three-dimensional printer filaments and constructs for biomedical applications. *International journal of nanomedicine, 2015. 10: p. 357.*
52. *Weisman, J.A., et al.,* 3D printed antibiotic and chemotherapeutic eluting catheters for potential use in interventional radiology: in vitro proof of concept study. *Academic radiology, 2019. 26(2): p. 270-274.*
53. *Ballard, D.H., et al.,* Three-dimensional printing of bioactive hernia meshes: In vitro proof of principle. *Surgery, 2017. 161(6): p. 1479-1481.*
54. *Muwaffak, Z., et al.,* Patient-specific 3D scanned and 3D printed antimicrobial polycaprolactone wound dressings. *International journal of pharmaceutics, 2017. 527(1-2): p. 161-170.*
55. *Shim, J.-H., et al.,* Three-dimensional printing of antibiotics-loaded poly-ε-caprolactone/poly (lactic-co-glycolic acid) scaffolds for treatment of chronic osteomyelitis. *Tissue Engineering and Regenerative Medicine, 2015. 12(5): p. 283-293.*

56. *Scoutaris, N., S. Ross, and D. Douroumis,* Current trends on medical and pharmaceutical applications of inkjet printing technology. *Pharmaceutical research, 2016. 33(8): p. 1799-1816.*

57. *Azizi Machekposhti, S., S. Mohaved, and R.J. Narayan,* Inkjet dispensing technologies: recent advances for novel drug discovery. *Expert opinion on drug discovery, 2019. 14(2): p. 101-113.*

58. *Li, K., et al.,* Controllable printing droplets on demand by piezoelectric inkjet: applications and methods. *Microsystem technologies, 2018. 24(2): p. 879-889.*

59. *Barui, S.,* 3D inkjet printing of biomaterials: Principles and applications. *Medical Devices & Sensors, 2021. 4(1): p. e10143.*

60. *Boehm, R.D., et al.,* Inkjet printing for pharmaceutical applications. *Materials Today, 2014. 17(5): p. 247-252.*

61. *Scoutaris, N., et al.,* Development and Biological Evaluation of Inkjet Printed Drug Coatings on Intravascular Stent. *Molecular Pharmaceutics, 2016. 13(1): p. 125-133.*

62. *Heldman, A.W., et al.,* Paclitaxel stent coating inhibits neointimal hyperplasia at 4 weeks in a porcine model of coronary restenosis. *Circulation, 2001. 103(18): p. 2289-2295.*

63. *Tarcha, P.J., et al.,* The application of ink-jet technology for the coating and loading of drug-eluting stents. *Annals of biomedical engineering, 2007. 35(10): p. 1791-1799.*

64. *Wu, W., et al.,* A programmed release multi-drug implant fabricated by three-dimensional printing technology for bone tuberculosis therapy. *Biomedical Materials, 2009. 4(6): p. 065005.*

65. *Gu, Y., et al.,* Inkjet printed antibiotic-and calcium-eluting bioresorbable nanocomposite micropatterns for orthopedic implants. *Acta biomaterialia, 2012. 8(1): p. 424-431.*

66. *Boehm, R.D., et al.,* Inkjet Printing of Amphotericin B onto Biodegradable Microneedles Using Piezoelectric Inkjet Printing. *JOM, 2013. 65(4): p. 525-533.*

67. *Langedijk, J., et al.,* Drug repositioning and repurposing: terminology and definitions in literature. *Drug discovery today, 2015. 20(8): p. 1027-1034.*

68. *Farha, M.A. and E.D. Brown,* Drug repurposing for antimicrobial discovery. *Nature microbiology, 2019. 4(4): p. 565-577.*

69. *Kaul, G., et al.,* Update on drug-repurposing: is it useful for tackling antimicrobial resistance? *2019, Future Medicine.*

70. *Domínguez, A.V., M.E.J. Mejías, and Y. Smani,* Drugs Repurposing for Multi-Drug Resistant Bacterial Infections, *in* Drug Repurposing-Hypothesis, Molecular Aspects and Therapeutic Applications. *2020, IntechOpen.*

71. *Rajamuthiah, R., et al.,* Repurposing salicylanilide anthelmintic drugs to combat drug resistant Staphylococcus aureus. *PloS one, 2015. 10(4): p. e0124595.*

72. *Gwisai, T., et al.,* Repurposing niclosamide as a versatile antimicrobial surface coating against device-associated, hospital-acquired bacterial infections. *Biomedical Materials, 2017. 12(4): p. 045010.*

73. *Torres, N.S., et al.,* Screening a commercial library of pharmacologically active small molecules against Staphylococcus aureus biofilms. *Antimicrobial agents and chemotherapy, 2016. 60(10): p. 5663-5672.*

74. *Gilbert-Girard, S., et al.,* Optimization of a High-Throughput 384-Well Plate-Based Screening Platform with Staphylococcus aureus ATCC 25923 and Pseudomonas aeruginosa ATCC 15442 Biofilms. *International journal of molecular sciences, 2020. 21(9): p. 3034.*

75. *Andrews, P., J. Thyssen, and D. Lorke,* The biology and toxicology of molluscicides, Bayluscide. *Pharmacology & therapeutics, 1982. 19(2): p. 245-295.*

76. *Pearson, R.D. and E.L. HEWLETT,* Niclosamide therapy for tapeworm infections. *1985, American College of Physicians.*

77. *Organization, W.H.,* World Health Organization model list of essential medicines: 21st list 2019. *2019, World Health Organization.*

78. *Whitesell, J.K.,* The Merck Index, CD-ROM (Macintosh): An Encyclopedia of Chemicals, Drugs & Biologicals Edited by S. Budavari, M. O'Neill, A. Smith, P. Heckelman, and J. Kinneary (Merck & Co., Inc.). Chapman & Hall: New York. 1997. $250.00. ISBN 0-412-75940-3. *1998, ACS Publications.*

79. *Copp, J.N., et al.,* Mechanistic understanding enables the rational design of salicylanilide combination therapies for Gram-negative infections. *Mbio, 2020. 11(5): p. e02068-20.*

80. *Mohammad, H., et al.,* Repurposing niclosamide for intestinal decolonization of vancomycin-resistant enterococci. *International journal of antimicrobial agents, 2018. 51(6): p. 897-904.*

81. *Gooyit, M. and K.D. Janda,* Reprofiled anthelmintics abate hypervirulent stationary-phase Clostridium difficile. *Scientific reports, 2016. 6(1): p. 1-8.*

82. *Tam, J., et al.,* Host-targeted niclosamide inhibits C. difficile virulence and prevents disease in mice without disrupting the gut microbiota. *Nature communications, 2018. 9(1): p. 1-11.*

83. *Berube, B.J., et al.,* Novel screen to assess bactericidal activity of compounds against non-replicating Mycobacterium abscessus. *Frontiers in microbiology, 2018. 9: p. 2417.*

84. *Piccaro, G., et al.,* Activities of drug combinations against Mycobacterium tuberculosis grown in aerobic and hypoxic acidic conditions. *Antimicrobial agents and chemotherapy, 2013. 57(3): p. 1428-1433.*

85. *Tharmalingam, N., et al.,* Repurposing the anthelmintic drug niclosamide to combat Helicobacter pylori. *Scientific reports, 2018. 8(1): p. 1-12.*

86. *Early, J.V., S. Mullen, and T. Parish,* A rapid, low pH, nutrient stress, assay to determine the bactericidal activity of compounds against non-replicating Mycobacterium tuberculosis. *PloS one, 2019. 14(10): p. e0222970.*

87. *Sun, Z. and Y. Zhang,* Antituberculosis activity of certain antifungal and antihelmintic drugs. *Tubercle and Lung Disease, 1999. 79(5): p. 319-320.*

88. *Zhurina, M., et al.,* Niclosamide as a promising antibiofilm agent. *Microbiology, 2017. 86(4): p. 455-462.*

89. *Chen, W., et al.,* Niclosamide: Beyond an antihelminthic drug. *Cellular signalling, 2018. 41: p. 89-96.*

CHAPTER II

IN VITRO EVALUATION OF THE REPURPOSED ANTIBACTERIAL DRUG NICLOSAMIDE AGAINST *S. AUREUS* AND *S. EPIDERMIDIS*

INTRODUCTION

The emergence of antimicrobial resistance represents a critical global health problem. According to data provided by the Center for Disease Control and Prevention (CDC) from the United States, drug-resistant bacteria cause at least 2.8 million of infections leading to approximately 35,000 deaths annually[1]. Similarly, each year in Europe, approximately 670, 000 people get infected with drug-resistant bacteria. As a consequence, 33 000 people die of these infections[2].

Excessive and inappropriate usage of classical antibiotics in the clinic has greatly increased the incidence of resistant-bacterial infections which most often result in treatment failure. Concomitant with the unstoppable increase in antimicrobial resistance (AMR), there is a lack of effective therapeutic solutions due to the suspension of antibacterial discovery research programs of major pharmaceutical companies. Difficulties in the drug discovery and development process and unfavourable economic profits have driven away the commercial launching of novel antibiotics by major pharmaceutical companies[3, 4].

In this context, drug repurposing, defined as the identification of a novel therapeutic indication for an already approved drug, offers a cost-effective strategy to develop new effective antimicrobial treatments in a short period of time[5, 6]. Niclosamide, a world health organization essential medicine and widely used anthelmintic drug, has recently been identified as one of the most promising candidates to combat Gram-positive bacteria namely *S. aureus* and *S. epidermidis* [7-9]. Remarkably, niclosamide displays overall low toxicity and inhibits bacterial growth of the aforementioned bacterial species at very low concentrations[10-12].

In this connection, we further characterized the *in vitro* antibacterial activity of niclosamide against a panel of relevant bacterial pathogens. The minimum inhibitory concentration (MIC), minimum bactericidal concentration (MBC) and time-killing profile of niclosamide was determined against these panel of bacteria. Moreover, the mode of action of niclosamide and the development of resistance to this drug was

systematically assessed. Finally, the antibiofilm activity and *in vitro* cytotoxic effect of niclosamide was further evaluated

MATERIAL AND METHODS

BACTERIAL SPECIES

All bacterial strains used in this project were taken from an in-house strain collection (Table 1). Bacterial strains were maintained in glycerol stocks at – 80 °C prior to be used in the different antimicrobial studies described in this chapter.

Bacteria	Strain	Phenotype
S.aureus	ATCC 33591	MRSA
S.aureus	ATCC 43300	MRSA
S.aureus	WGH29	MRSA
S.aureus	ATCC 25923	MSSA
S.aureus	7280	MRSA
S.aureus	BAA1556	MRSA
S.aureus	Xen 29	MSSA
S.epidermidis	ATCC 35984	MRSE
S.epidermidis	ATCC 155	MRSE
S.epidermidis	Alpha99	MRSE
S.epidermidis	G220	MRSE
P.aeruginosa	PAO1	WT
E.coli	AG100	WT

Table 1. List of different Gram-positive and Gram-negative strains used for *in vitro* antibacterial evaluation of niclosamide

DETERMINATION OF MINIMUM INHIBITORY CONCENTRATION AND MINIMUM BACTERICIDAL CONCENTRATION VALUES BY THE BROTH MICRODILUTION METHOD

In order to assess the ability of niclosamide to inhibit bacterial growth, the *minimum inhibitory concentration (MIC) and minimum bactericidal concentration* (MBC) values were determined using the microdilution broth method following the CLSI guidelines with small modifications [13].

Briefly, each bacterial strain was grown from glycerol stocks onto TSA agar plates (Sigma Aldrich, Germany) at 37 °C for 24 h. After 24-h incubation, 2-3 colonies were selected from grown-bacteria TSA agar plates and suspended in 0.9 % saline solution. Subsequently, bacterial suspensions in saline solution were adjusted to obtain a McFarland standard value of 0.5 (equivalent to ~$5x10^7$ CFU/mL). Finally, the inoculum was prepared by diluting 0.5-MacFarland suspensions (1:200) in tryptic soy broth media (TSB) (Oxoid, United Kingdom), getting an equivalent bacterial concentration of ~2 x 10^5 CFU/mL.

For MIC determination, corresponding volumes of niclosamide (Sigma Aldrich, Germany) stocks solutions were added into each well of a 96-well microtiter plate (MTP) to get 2-fold serial decreasing concentrations (32, 16, 8, 4, 2, 1, 0.5, 0.250, 0.125, 0.0625 and 0.0315 µg/mL) in the final total volume of 100 µL of bacterial inoculum. For all the experiments, rifampicin (Sigma Aldrich, Germany) was used as the reference standard antibiotic. Afterwards, bacterial seeded MTPs were incubated at 37 °C for 18-20 h under static conditions. After incubation, MIC was measured as the lowest concentration of niclosamide preventing bacterial growth by visual inspection. MBC determination was performed by subculturing 50 µL of broth from wells with non-visible bacterial growth onto TSA plates. Then, TSA plates were incubated for 24 h at 37 °C. After the incubation step, MBC was defined as the lowest concentration that prevents bacterial growth on the agar plate.

DETERMINATION OF MIC VALUE BY THE AGAR DILUTION METHOD

The MIC values in niclosamide-containing agar plates were accordingly determined for each of the Gram-positive strains listed in Table 1.

Niclosamide-containing agar plates for MIC were prepared as follows: 1 mL of 20x niclosamide stock solutions (40, 20, 10, 5, 2.5, 1.25 µg/mL) was added into sterile petri dishes and immediately after 19 mL of molten tryptone soy agar (TS) (Sigma Aldrich, Germany) were poured. Molten agar-niclosamide mixtures were let solidify and then dry for 30 min. TS agar plates supplemented with niclosamide were stored at 4 °C until their utilization.

For MIC experiments, bacterial inoculum was prepared as follows: briefly different staphylococcal bacterial strains (Table 1), taken from glycerol stocks, were streaked on TSA plates. The next day, colonies were selected and resuspended in physiological 0.9 % saline solution. Immediately after, bacterial suspensions were adjusted at a value of 0.5 McFarland and diluted 1:10 in physiological saline solution, getting an equivalent bacterial concentration of approx. $1x10^7$ CFU/mL.

Inmeadiatly after, 2 µl of bacterial suspensions were spotted onto niclosamide-containing agar plates and incubated at 37 °C for 20-24 hours. TS agar plates without niclosamide served as negative controls. In this method the MIC was regarded as the lowest concentration of the antimicrobial agent that completely inhibited bacterial growth in the form of colonies.

DETERMINATION OF TIME-KILLING KINETICS OF NICLOSAMIDE

Time killing curve experiments were performed using *S. aureus* ATCC 25923 and *S. epidermidis* ATCC 25984 as these strains are regarded as the most common pathogens in device associated infections[14].

Each bacterial strain was grown from glycerol stocks onto TSA agar plates at 37 °C for 24 h. After 24-h incubation, 4 colonies were taken from an overnight inoculated plate

were cultured in TSB and incubated at 37 °C for 4 h to reach mid-log phase. Immediately after, bacterial suspensions (~10^6 CFU/mL) were seeded into 96-well microtiterplate and exposed to final concentrations of niclosamide of 0.125, 0.25,1,8,16, and 32 μg/mL. As untreated control, bacteria were incubated in phosphate buffered saline (PBS) solution (Sigma Aldrich, Germany). Inoculated plates were incubated at 37 °C, 120 rpm for 24 h. Then, at determined time points (0.25, 0.5, 1, 3, 5 and 24 h), samples were taken from the wells, 10-fold serially diluted, and spot plated in TSA plates to determine the number of viable bacterial cells as means of LogCFU/mL.

IN VITRO EVALUATION OF THE POTENTIAL FOR RESISTANCE DEVELOPMENT TO NICLOSAMIDE

In vitro development of resistance to niclosamide and rifampicin (Sigma Aldrich, Germany) (reference compound) was determined over 20 consecutive days. Briefly, *S. aureus* ATCC 2923 and *S. epidermidis* ATCC 35984 were seeded from glycerol stocks into TSA plates and incubated overnight at 37 °C. After incubation, 3-4 colonies were selected from TSA plates and resuspended in 5 mL of TSB and incubated overnight at 37 °C under shaking of 200 rpm. The following day, 50 μL of the overnight culture was transferred into in 5 mL of fresh pre-warmed TSB and incubated at 37 °C at 200 rpm for 3h. The bacterial inoculum obtained after this incubation was adjusted to an OD_{600} value of 0.3 which is equivalent to approximately 10^7 CFU/mL.

Ten μL of the bacterial inoculum was added to a mixture of 40 μL of PBS, 40 μL of TSB and 10 μL of niclosamide stock solutions, to obtain a a final volume of 100 μL per MTP well. 0.125, 0.25,1,8,16, and 32 μg/mL were the final concentrations of niclosamide/well tested. Seeded MTPs were incubated for 20 h at 37 °C under shaking (120 rpm). The next day, the MIC, the lowest concentration of antibiotic that caused lack of visible bacterial growth, was determined for each bacterial species. Thereafter, 5 μL of media with bacterial growth at ½ MIC was added to a 96-well microtiter plate replenish with fresh medium containing the same niclosamide concentrations per well and these mixtures were incubated as described before. This procedure was repeated over 20 passages[15].

DETERMINATION OF MINIMUN BIOFILM INHIBITORY CONCENTRATION BY THE CRYSTAL VIOLET STAINING ASSAY

In order to examine the efficacy of niclosamide to prevent biofilm formation of *staphylococcus* spp. a crystal violet (CV) biofilm assay was carried out as described by George O'Toole with minor modifications[16].

Bacterial strains were streaked out from frozen glycerol stocks onto agar plates and incubated at 37 °C for 24 h. After 24h incubation, colonies were taken and suspended into saline solution in order to get a bacterial suspension equivalent to a value of 0.5 McFarland standard. Immediately after, bacterial suspensions were further diluted (1:20) in fresh TSB supplemented with 1 % of Glucose (1M) (Sigma Aldrich, Germany), obtaining a bacterial inoculum of ~2 x 10^6 CFU/mL.

Bacterial inoculum (~10^6 CFU/mL) were seeded into 96-well MTP and exposed to final concentrations of niclosamide of 0.125, 0.25,1,8,16, and 32 µg/mL. in a final volume of 200 µl per well. Bacterial biofilms were formed by incubating the plates at 37 °C for 24h under static conditions. For all the experiments, rifampicin was used as a reference antibiotic at a biofilm inhibitory concentration of 0.5 µg/mL. After the incubation period, planktonic cells suspended in broth media were aspired from each well of the plate, and wells were rinsed twice carefully with 200 µL of Milli-Q water. Then, plates were air dried at room temperature for at least 1 h to fix formed biofilms. For staining individual biofilms, 200 µL of 0.1 % CV stain (Sigma Aldrich, Germany) were added per well, incubating for 15 min. Exceeding Crystal Violet stain in the wells was removed by washing twice with 200 µL of Milli-Q water, and then MTPs were dried for at least 3 h at room temperature (RT). Cristal violet from stained biofilms was solubilized by adding 200 µL of a 96 % ethanol solution and incubating for 20 min. After the incubation step, 130 µL of solubilized CV solutions were transferred to a new MTP and biofilm formation was determined by measuring the absorbance at 595 nm using a spectrophotometer (SPECTROstar Nano, Germany). Data are presented as the average of the absorbance values from each biofilm tested with treatments (6 replicates). The minimum biofilm inhibitory concentration (MBIC) value was regarded as the lowest concentration exerting at least 95 % inhibition of biofilm growth.

DETERMINATION OF NICLOSAMIDE DISRUPTION ACTIVITY AGAINST PRE-FORMED BIOFILMS BY CRYSTAL VIOLET STAINNING ASSAY

Niclosamide ability to disrupt bacterial biofilms was evaluated following a crystal violet staining assay[16].Bacterial strains were taken from frozen glycerol stocks, streaked onto TSA plates, and incubated at 37 °C overnight. After the incubation step, 3-4 colonies were selected and resuspended into 5 mL of physiological saline solution and adjusted to a value of 0.5 McFarland standard (~10^7 CFU/mL). Immediately after, bacterial suspensions were further diluted (1:20) in fresh TSB supplemented with 1 % of Glucose (1M), obtaining a bacterial inoculum of ~2 x 10^6 CFU/mL.

Subsequently, MTPs were seeded with 200 µL/well of the bacterial inoculum and incubated at 37 °C for 24 h (under static conditions) in order to establish a biofilm per well. After obtaining established biofilms, planktonic cells were discarded, and individual biofilms were rinsed twice with 200 µL/well of sterile Milli-Q water. Plates were let dry for 10 minutes and immediately after niclosamide treatments were added to obtain final concentrations of 32, 16, 8, 4, 2, 1, 0.5, 0.250, 0.125, 0.0625 and 0.0315 µg/mL, respectively in a total volume of 200 µL of TSB supplemented with 1 % (v/v) of 1M Glucose. Biofilms were incubated for additional 24 h at 37 °C.

After incubation with niclosamide treatments, broth media was aspired, and individual biofilms were washed 2 times with sterile Milli-Q water. Then, plates were dried for at least 1 h at Room Temperature. After the drying step, individual biofilms were stained with 200 µL of 0.1 % Crystal Violet (CV) solution and incubated for 15 min. Afterwards, wells were rinsed twice with sterile MQ water and let drying for 3 h at room temperature. Cristal Violet was solubilized by incubating stained biofilms with 200 µL of 96 % ethanol for 20 min. Immediately after, 130 µL of solubilized CV solutions were transferred to a new MTPs. Disruption of biofilms by niclosamide was analyzed by measuring spectrophotometrically the absorbance of solubilized crystal violet solutions at 595 nm (SPECTROstar Nano, Germany).

EVALUATION OF THE ANTIBACTERIAL MECHANISM OF ACTION OF NICLOSAMIDE BY THE MACROMOLECULE SYNTHESIS ASSAY

In order to identify bacterial metabolic pathways affected by niclosamide, the macromolecule synthesis assay was carried out with *S.aureus* ATCC 25923

The day before the experiment, the initial inoculum was prepared as follows: 1 Bead from MicroBank aliquot was transferred to 20 mL of 100% MHB (Sigma Aldrich, Germany) and incubated at 37°C, for 24h under orbital shaking (100rpm). After incubation time, 1.2 mL from the over-night culture were transferred into 55 mL of pre-warmed (at 37 °C for about 30-45 min) 20% (v/v) MHB media and incubated at 37°C until reaching a OD_{530} value of 0.500.

The MMS assay on *S. aureus* ATCC 25923 was performed in the presence or absence of increasing concentrations of Niclosamide (0.03, 0.06, 0.125, 0.25, 0.5, 1, 2, 4 µg/mL) and a fixed concentration of radiolabeled precursors, [3H]Thymidine, [3H]Uridine, [3H]L-Leucine, [3H]N-Acetyl-D-glucosamine and [3H]Acetic Acid for DNA, RNA, Protein, Cell-wall peptidoglycan and Fatty Acids synthesis, respectively. The following antibiotics were used in the assay as reference compounds: Ciprofloxacin (8 µg/mL), rifampicin (0.25 µg/mL), tetracycline (8 µg/mL), vancomycin (64 µg/mL) and triclosan (2 µg/mL) for DNA, RNA, Protein, Cell-wall Peptidoglycan and Fatty Acids synthesis inhibition, respectively.

One hundred twenty µL of the bacterial culture suspension were dispensed into the test plate. Incorporation of radiolabelled precursors was started by adding 15µL/well of the reaction mixes and then plates were incubated at 37°C under shaking. After 5, 10 and 20 minutes, the incorporation was stopped by adding 20µL/well of 50% (w/v) trichloroacetic acid (TCA) (Sigma Aldrich, Germany). Plates were kept at 4°C for 1 hour to allow cell lysis and macromolecule precipitation and then, filtered through a 96-well Packard UniFilter® GF/C® plates using the Packard FilterMate™ Harvester system under vacuum condition.

The filter plates were washed twice (200 µL/well) with 5% ice-cold TCA, twice with ice-cold MQ water and twice with ice-cold 96% Ethanol and incubated for 15-20 minutes at 37°C to allow filter drying. Afterwards, a back-seal was fixed on the plate and 50µL of

Microscint-20 (PerkinElmer, USA) were added to each well. The plates were sealed, and radioactivity counted on the MicroBeta2 Microplate Counter for Radiometric Detection.

ASSESSMENT OF THE *IN VITRO* CYTOTOXICITY ACTIVITY OF NICLOSAMIDE

In vitro cytotoxicity test was carried out on L929 murine derived fibroblast cell line by MTT assay in order to analyze how niclosamide could affect the viability of murine cells. L929 fibroblast cell line was cultured in Dulbecco's modified Eagle's medium (DMEM, Thermofisher, USA) supplemented with 10% fetal bovine serum (FBS) (Sigma Aldrich, Germany) and penicillin streptomycin (Sigma Aldrich, Germany) in cell culture dish. Cells were incubated at 37 degrees, 5% CO_2, and 99% relative humidity for 24h. After incubation, cells were detached with 1x trypsin-EDTA (0.25%, 1mM EDTA Na) (Sigma Aldrich, Germany). For cytotoxicity experiments, 96-well plates were cultivated with 5000 cells/ 100 uL and incubated for 24h at 37 degrees and 5% CO2. After incubation, the medium (containing non-attached cells) was removed from each well of the plate and niclosamide was added to get final concentrations of 2, 6 and 10uM in a final volume of 200 µL of DMEM media. DMSO at 10% was used as positive control and DMEM with penicillin (Sigma Aldrich, Germany) and streptomycin was used for negative control. The cells were then incubated for 24, 48 and 72 hours at 37 degrees and 5% CO_2. At each time point, the medium with the drug was withdrawn and cells were washed with 200 ul of PBS. To confirm the number of viable cells, MTT assay was performed according to Sigma Aldrich manufacturer instructions.

RESULTS

DETERMINATION OF MIC/MBC VALUES BY BROTH MICRODILUTION METHOD

The antibacterial activity of niclosamide was evaluated against a panel of collection and clinical strains by means of MIC and MBC. Niclosamide MIC and MBC values for each strain are reported in Figure 1-A. MIC values of niclosamide ranged from 0.25 to 0.5 for all of the staphylococcal strains tested in the current project. Similarly, an MBC value of 32 µg/mL was observed for all the staphylococcal strains. On the other hand, MIC values

couldn’t be determined for Gram-negative bacteria as they would be high above of the solubility limit of Niclosamide under these experimental conditions. For this reason, these bacterial species were not used for further characterization.

DETERMINATION OF MIC VALUE BY AGAR DILUTION METHOD

Given the fact that niclosamide was at its limit of solubility and didn’t inhibit the bacterial growth of *P. aeruginosa* and *E. coli* in the previous assay, we decided to assess only the MIC for *S. aureus* and *S. epidermidis* by the agar dilution method. A niclosamide concentration of 0.5 µg/mL was found to be effective at inhibiting bacterial growth of all the staphylococcal strains tested (Figure 1-B).

A

		Niclosamide (µg/mL)	
Bacteria	**Strain**	**MIC**	**MBC**
S.aureus	ATCC 33591	0.25	32
S.aureus	ATCC 43300	0.25	>32
S.aureus	WCUH29	0.25	>32
S.aureus	ATCC 25923	0.25	32
S.aureus	7280	0.25	>32
S.aureus	BAA1556	0.25	32
S.aureus	Xen 29	0.25	32
S.epidermidis	ATCC 35984	0.25	32
S.epidermidis	ATCC 155	0.25	32
S.epidermidis	Alpha99	0.25	32
S.epidermidis	G220	0.25	32

B

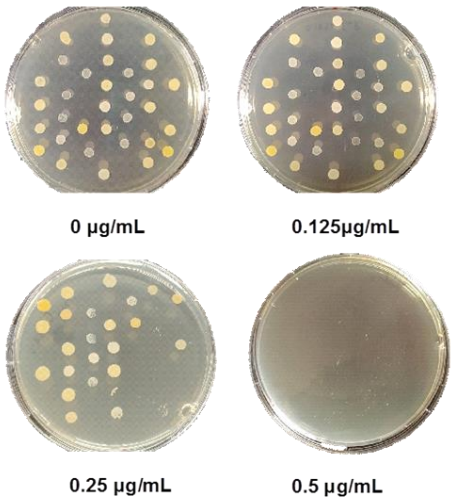

Figure 1. Determination of the Minimum inhibitory concentration (MIC) of niclosamide against different bacterial strains by (Panel A) broth microdilution method and (Panel B) agar dilution method.

DETERMINATION OF TIME-KILLING KINETICS OF NICLOSAMIDE AGAINST *S. aureus* AND *S. epidermidis*

To investigate the bactericidal effects of niclosamide a time-killing assay with *Staphylococcus aureus* ATCC 25923 and *S. epidermidis* ATCC 35984 performed. The strains were exposed to increasing concentrations of niclosamide over period of 24 h. At fixed time points, samples were taken, and viable bacterial cells were enumerated. Results from the time-killing assay against both pathogens are shown in Figure 2. Niclosamide at concentrations above 1 µg/mL reduced completely the cell viability (LogCFU reduction of ~ 7.4) of both *S. aureus* ATCC 25923 and S. epidermidis ATCC 25984 during an exposure time of 24 h.

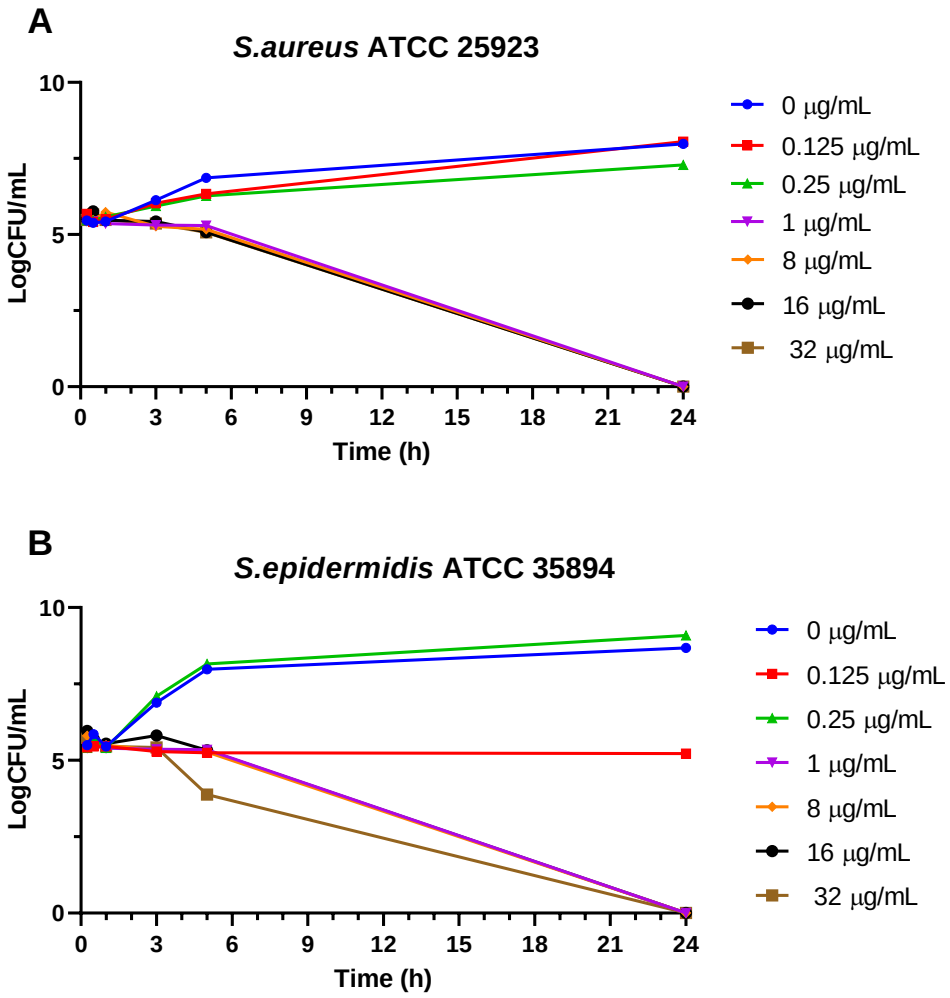

Figure 2. Time killing analysis of different concentrations of niclosamide in killing (Panel A) *S. aureus* ATCC 25923 and (Panel B) *S. epidermidis* ATCC 35984.

IN VITRO EVALUATION OF THE POTENTIAL FOR RESISTANCE DEVELOPMENT TO NICLOSAMIDE

To evaluate potential development of resistance to niclosamide, a serial passage assay was performed using the 2 most commons pathogens involved in medical-device associated infections, namely staphylococcus aureus and staphylococcus epidermidis[14].

As shown in Figure 3, neither *S. aureus* ATCC 25923 nor *S. epidermidis* ATCC 35984 developed resistance to niclosamide after being exposed to the drug for 20 consecutive days. In contrast, the aforementioned strains developed a high-level resistance to Rifampicin after 2 passages.

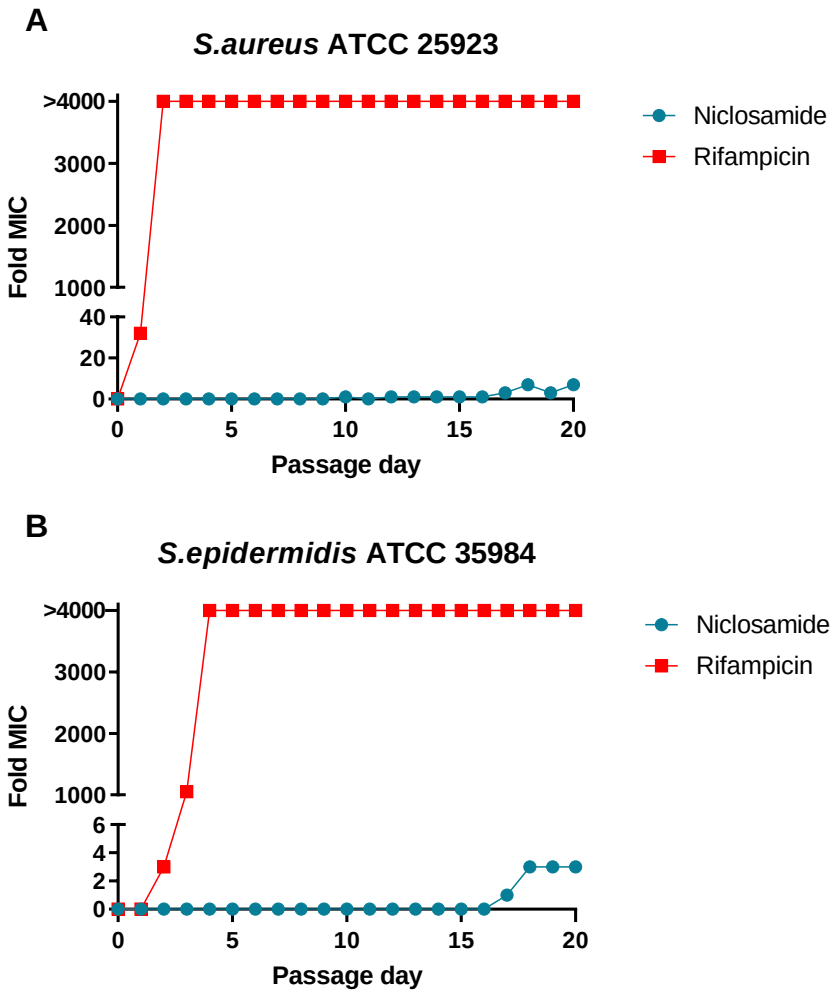

Figure 3. Development of *in vitro* resistance to niclosamide and rifampicin. Panel A): *S. aureus* ATCC 25923. Panel B) :S. *epidermidis* ATCC 35984.

DETERMINATION OF MBIC BY THE CRYSTAL VIOLET STAINING ASSAY

Niclosamide has previously reported as a novel antibacterial compound with the ability of reducing biofilm formation of different clinically relevant pathogens such as *Staphylococcus aureus* and *S. epidermidis*[9, 10, 12, 17]. Antibiofilm activity of Niclosamide was confirmed using a MTP-based biofilm formation assay in which different strains of *Staphylococcus aureus* and *S. epidermidis* growing biofilms were treated with increasing concentrations of Niclosamide. The inhibitory effect of niclosamide on biofilm biomass growth is shown in figure 4. Overall, the MBIC value concentration for most of the tested strains ranged from 0.0625 to 0.25 µg/mL.

DETERMINATION OF NICLOSAMIDE DISRUPTION ACTIVITY AGAINST PRE-FORMED BACTERIAL BIOFILMS BY THE CRYSTAL VIOLET STAINNING ASSAY

The ability of niclosamide to disrupt pre-stablished biofilms was analysed by the Cristal Violet staining method which allow us to quantify changes in the amount of biofilm biomass after incubating biofilms with different concentrations of niclosamide (Figure 5). Results showed that compared to non-treated control, niclosamide displayed significant reduction of the biofilm mass for all of the preformed biofilms at concentrations as low as 0.0625 µg/mL. We also observed that the biofilm disruption activity of niclosamide was not dependent of the concentration as the reduction of biofilm biomass in preformed biofilms was comparable independently of the niclosamide treatments.

EVALUATION OF THE ANTIBACTERIAL MECHANISM OF ACTION OF NICLOSAMIDE BY THE MACROMOLECULAR SYNTHESIS ASSAY

In order to investigate the potential antibacterial mechanism of action of niclosamide, we incubated S. aureus bacterial cells with increasing concentrations of niclosamide in presence of radio-labeled precursors of 5 main macromolecular synthesis pathways (DNA, RNA, fatty acids, peptidoglycan and protein synthesis). The assay was performed

at different time points (5, 10 and 20 min) which were always less than the doubling time of S. aureus.

The Figure 6 illustrates how niclosamide inhibited the 5 major metabolic pathways after an incubation time of 5 minutes. As seen from the data, we observed that all of the metabolic pathways were inhibited at the concentrations tested. Interestingly at 0.03 ug/mL niclosamide inhibited by almost 60 % of the synthesis of fatty acids while the other metabolic pathways presented a reduction of less than 25 %. Correspondingly, after an incubation time of 10 minutes, fatty acid biosynthesis was considerably affected yielding a 43 % inhibition rate at a concentration as low as 0.03 ug/mL. Moreover, the incorporation rate of DNA, RNA, Peptidoglycan, and protein precursors were reduced by less than 16 %. At the last time point, both fatty acid and RNA biosynthesis presented greater inhibition rates at 0.03 and 0.6 ug/mL.

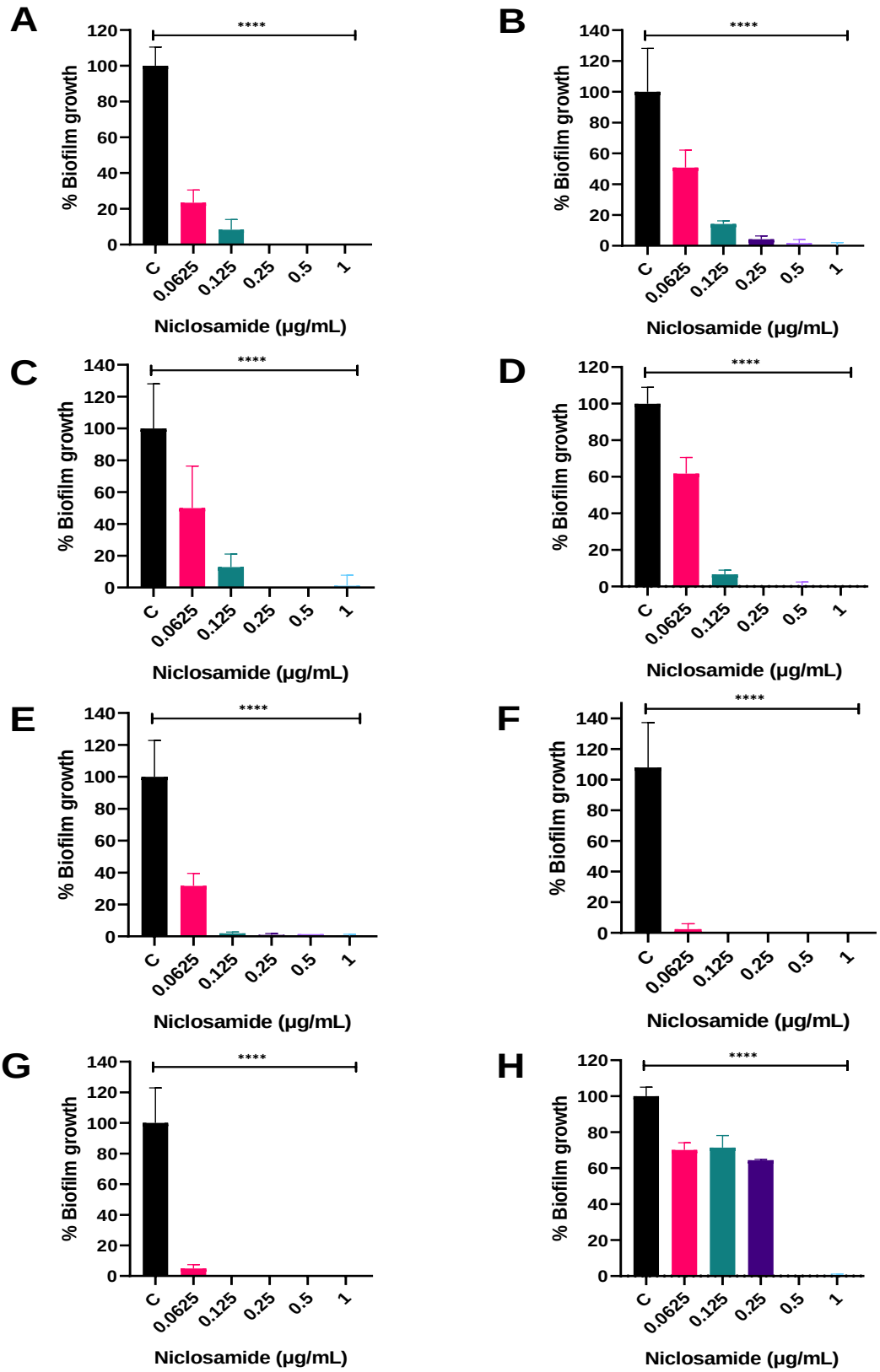

Figure 4. Biofilm growth (%) of A) *S. aureus* ATCC 43300 B) *S. aureus* 7280 C) *S. aureus* BAA1556 D) *S. aureus* WCUH29 E) *S. aureus* ATCC 25923 F) *S. aureus* ATCC 33591 G) *S. aureus* Xen29 H) *S. aureus* ATCC 35984 after niclosamide treatment

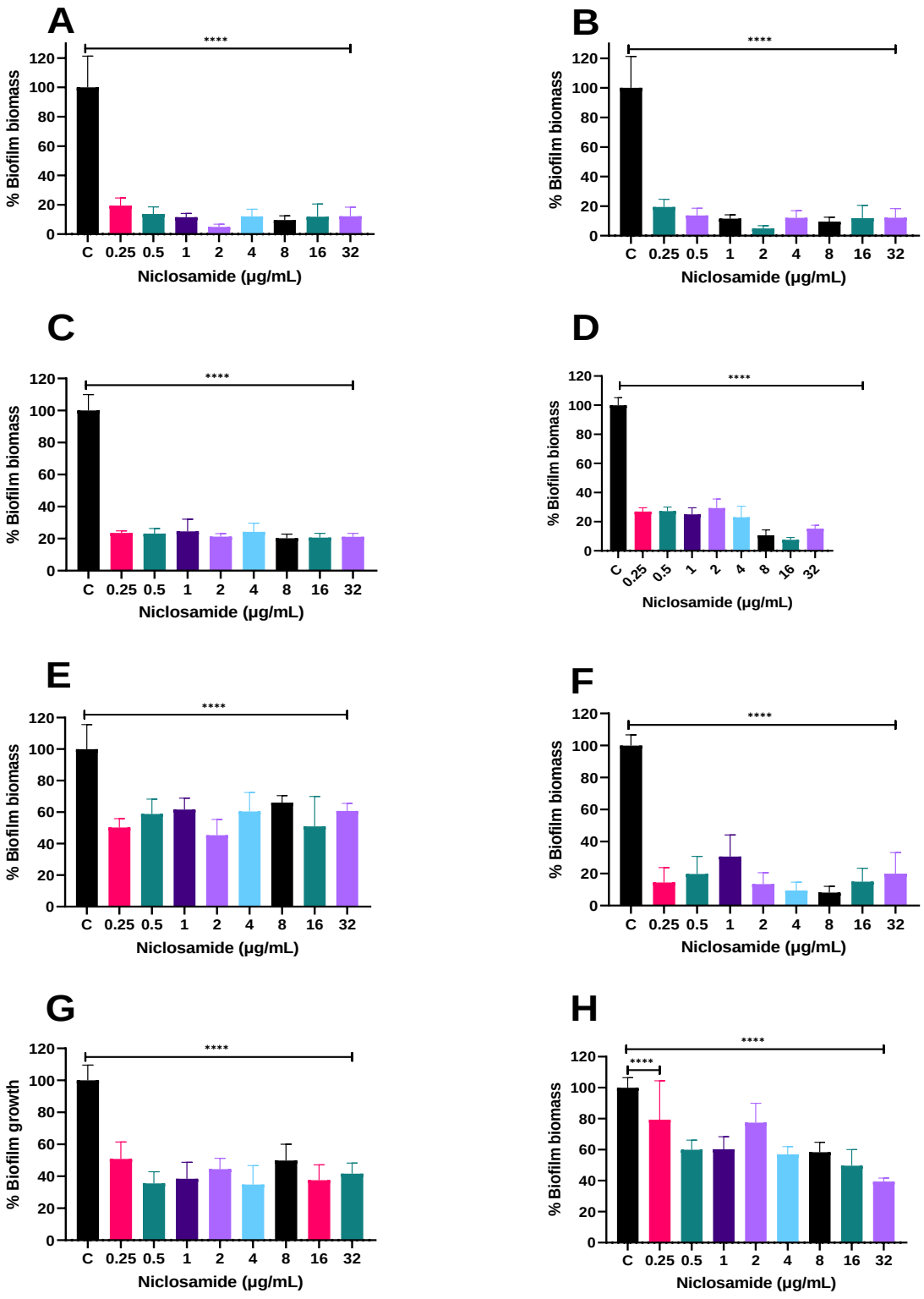

Figure 5. % Of remanent biofilm biomass of different staphylococcal strains after exposing preformed biofilms to increasing concentrations of niclosamide. A) *S. aureus* ATCC 43300 B) *S. aureus* 7280 C) *S. aureus* BAA1556 D) *S. aureus* WCUH29 E) *S. aureus* ATCC 25923 F) *S. aureus* ATCC 33591 G) *S. aureus* ATCC 35984 H) *S. aureus* Xen29

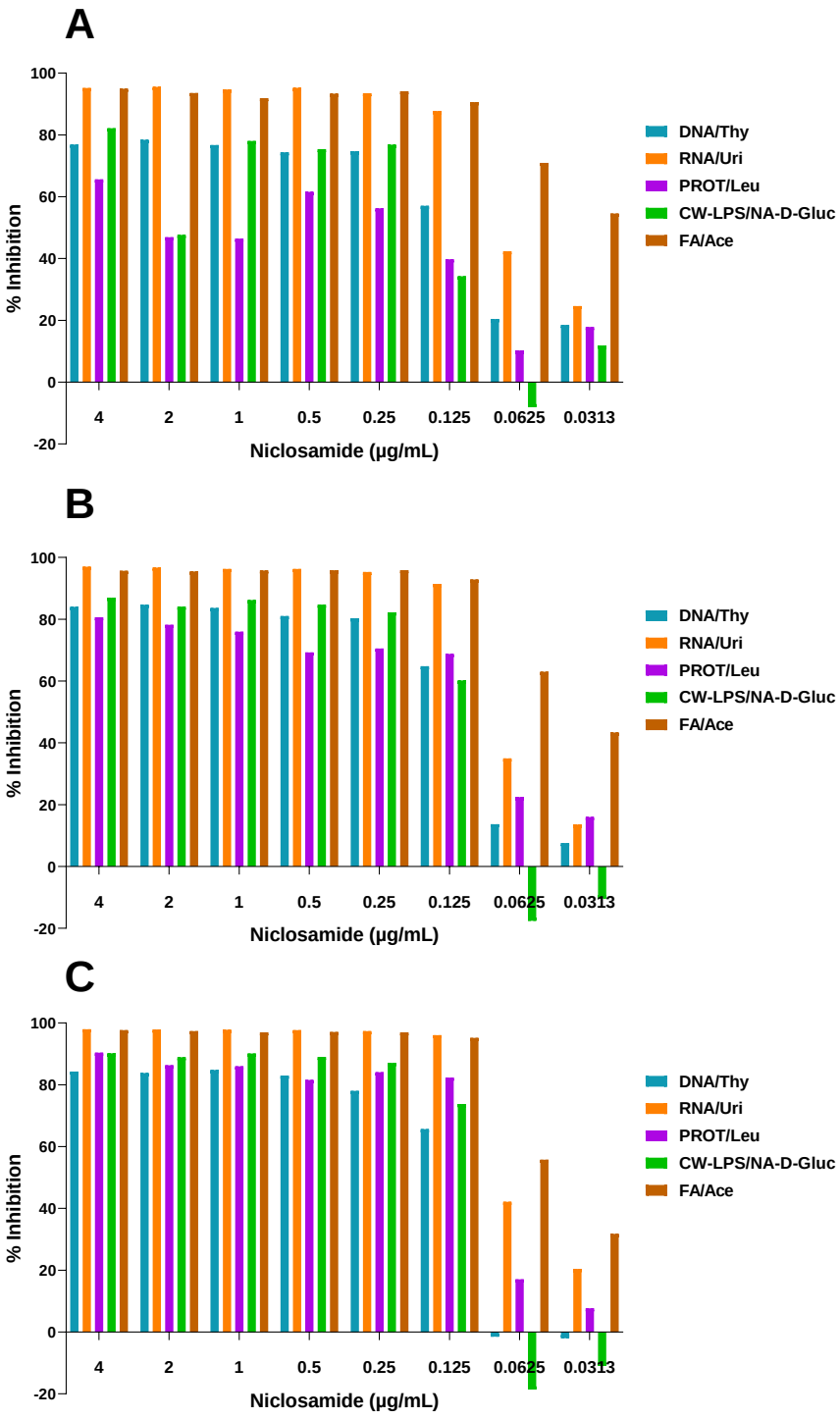

Figure 6. Macromolecular synthesis assay conducted in *S. aureus* ATCC 25923 in the presence of increasing concentrations of niclosamide. Percent of inhibition in the cellular incorporation of radiolabeled precursors after an incubation time with niclosamide of A) 5 , B) 10 and C) 30 minutes.

ASSESSMENT OF THE *IN VITRO* CYTOTOXICITY ACTIVITY OF NICLOSAMIDE

To assess a possible *in vitro* cytotoxic effect of niclosamide on eukaryotic cells, the viability of L229 fibroblast derived cells was measured by the MTT assay. Briefly, L229 cells were exposed to niclosamide final concentrations of 2, 6 and 10 µM and incubated for 24, 48 and 72 hours.

As shown in Figure 7, niclosamide affected to varying degrees the viability of L229 cells, which was affected by the drug concentration and the drug exposure time. After 24 h of treatment, niclosamide at both 2 and 6 µM did not reduce the cell viability whereas a significant reduction in cell viability was observed for niclosamide treatments of 10 µM. At 48 h, it wasn't found an inhibitory effect on cell viability in groups treated with both 2 and 6 µM, however niclosamide at 10 µM exerted a cytotoxic effect on L229 cells, inhibiting completely cell viability. Furthermore, we observed a similar inhibitory effect of niclosamide on L229 cells after an exposure time of 72 h.

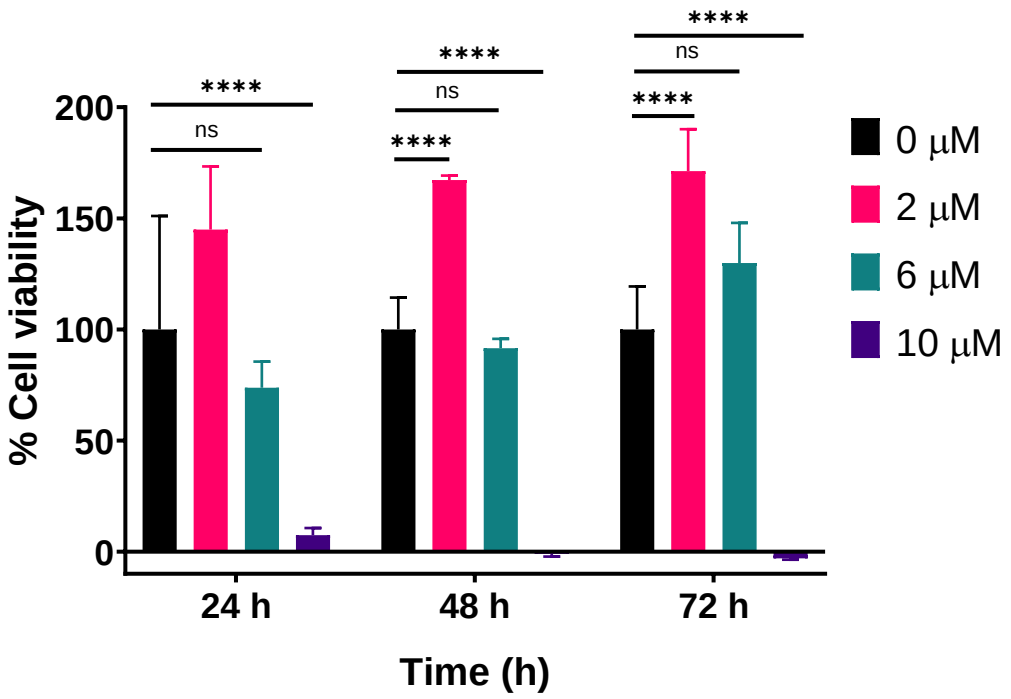

Figure 7. Percentage of cell viability of L229 fibroblast derived cells after exposure with different concentrations of niclosamide.

DISCUSSION AND CONCLUSION

There is an unrelenting spreading of drug-resistant bacteria in medical and non-medical settings which underscore the necessity of developing novel antibacterial agents to tackle this overwhelming health threat. Methicillin-Resistant *Staphylococcus aureus (*MRSA) is one of the most serious pathogens causing difficult-to-threat infections, leading to an estimated of 10 600 deaths in USA alone [18]. Moreover, in USA alone, MRSA represents an annual economic burden of $478 million to 2.2 billion[19]. MRSA strains have become endemic], predominantly causing skin and soft tissue infections, device-associated infections as well as necrotizing pneumonia and other conditions such as necrotizing fasciitis, osteomyelitis, septic thrombophlebitis, bacteremia, and severe sepsis[20].

Drug repurposing efforts have identified an increasing number of promising anti-infectious candidates, of which niclosamide has been proved to be highly effective against *Staphylococcus aureus* not only in its planktonic mode but also in biofilms [7, 9, 10, 21]. In this chapter we we evaluated the antibacterial profile of niclosamide against different strains of *S. aureus*, *S. epidermidis*.Through the microdilution and agar dilution method, we confirmed the remarkable antibacterial activity of niclosamide against a panel of sensitive and Methicillin resistant strains of *S. aureus* and *S. epidermidis.* Observed MIC (ranging from 0.06 to 0.5 μg/mL) and MBC (≥ 32 μg/mL) values are well in agreement with previous literature [12, 21]. On the other hand, niclosamide failed at inhibiting the growth of *P. aeruginosa* and *E. coli*; these results are in accordance with recent published data in which Gram-negative bacteria were found to be resistant to niclosamide via intrinsic efflux pumps and nitroreductases [22, 23]. Despite of the limited efficacy of niclosamide against Gram-negative bacteria, combinatorial formulations of this anthelmintic with antibiotics/repurposed drugs have been proved efficacious to circumvent this inherent drawback [24-26]. Given our main scope, we did not further analyze the antibacterial properties of niclosamide against Gram-negative bacteria.

Interestingly, the analysis of the time-killing data revealed that the bactericidal effect of niclosamide is mainly concentration-dependent, yielding a maximum killing rate at 24-h exposure time, this time-killing profile for staphylococcal strains has also reported by

other authors[9, 10]. Moreover, from our assays we have proven that niclosamide doesn't trigger in *vitro* development of resistance in *S. aureus* and *S. epidermidis* over 21 days, which renders this molecule suitable to be applied in the clinic as there is an alarming emergence of antimicrobial resistant bacterial strains. From our results we also confirm that Rifampicin, which is used to treat staphylococcal infections, drives to the emergence of antibacterial resistance in *S. aureus* and *S. epidermidis*, leading to an increase of more than 1000-fold in the value of the original MIC which agrees with published data[15].
Our findings confirmed the effective antibacterial activity of niclosamide, however it does not necessarily imply an efficacy against biofilms. As more than 80 % of chronic infections are caused by biofilms[27], we decided to evaluate whether niclosamide is able to either prevent or disrupt staphylococcal biofilms. We found that niclosamide was able to prevent biofilm formation of different strains of *S. aureus* and *S. epidermidis*. In agreement with our results, several studies have proposed niclosamide as a novel antimicrobial therapy to overcome the lack of antibiofilm therapeutic agents due to its outstanding activity *in vitro*[7, 12].

Given the intrinsic biological properties of mature biofilms leading to emergent resistance mechanisms, biofilms are highly tolerant to the action of antibiotics[28]. In fact, biofilms can withstand concentrations of more than 1000-fold the MIC of their planktonic counterpart[14]. Interestingly, we observed that niclosamide is still active against mature staphylococcal biofilms, disrupting biofilm mass by more than 60 % when compared with untreated biofilms. Even though biofilms weren't destroyed completely, combinatorial formulations could be applied to further disrupt and eradicate staphylococcal biofilms. These results are well in line with previous reports, in which niclosamide partially destroyed pre-formed biofilms of *S. aureus*[7, 10].

Understanding the mode of action of a given antibiotic provides vital information of potential resistance mechanisms that may occur in bacterial cells which give us valuable insight of how the molecule in question could be modified to outmaneuver bacterial resistance emergence. In this regard, niclosamide has been demonstrated to affect mainly bacterial cells by uncoupling the electron chain transport, dissipating the Proton Motive force (PMF), increasing oxygen consumption, and decreasing ATP production[24] .As

far as we are concerned there are few studies in the literature, examining how niclosamide impacts the metabolic activity of bacterial cells and the synthesis of macromolecules[29]. Therefore, we approached this matter by performing a Macromolecular Synthesis assay using *S. aureus* ATCC 25923. It was found that independently of the incubation time, niclosamide inhibited the synthesis of DNA, RNA, Fatty acids, proteins and peptidoglycan below the MIC. Additionally, fatty acid and RNA synthesis were inhibited by more than 40 % at Sub-MIC values which may indicate that these cellular processes are primarily affected by niclosamide. The ability of niclosamide to disturb multiple macromolecular synthesis pathways indicates that niclosamide may in fact have a complex mode of action that involves inhibition of multiple targets in *S. aureus,* or it may disrupt general cellular energy metabolism. For instance, several reports link the disruption of the PMF, the decrease in both ATP production and oxidative phosphorylation (all of these changes occur at the bacterial surface level) to a huge impact in central carbon metabolism and TCA cycle, leading to a progressive cellular death[6, 24]. Taken all together we hypothesize that niclosamide first impacts the bacterial surface of *S. aureus* and related physiological processes, triggering changes in the central carbon metabolism and fatty acid synthesis which may eventually diminish the synthesis of other macromolecules along with cellular death.

Additionally, we observed that niclosamide affected the cell viability of the L229 cell line with concentrations above 10 μM, Jain *et al* reported a similar cytotoxicity values for niclosamide using the same cell line. [30]. It is worth highlighting that despite the inhibitory activity of niclosamide upon different cell lines, there are several studies reporting the almost null *in vivo* toxicity of this drug[31-34], which in fact renders it promising for treating different medical conditions, such as psoriasis, endometriosis, cancer, fibrosis, viral and bacterial infections[8, 34-37].

In conclusion, the data presented in this chapter provides further experimental information on the potential of niclosamide for treating bacterial infections, especially those caused by *S. aureus* and *S. epidermidis*. In fact, the later bacterial species are the most common pathogens causing medical-device associated infections, for which we

decided to develop novel anti-infective medical devices using additive manufacturing and using niclosamide as the antibacterial active agent.

SUPPLEMENTARY INFORMATION

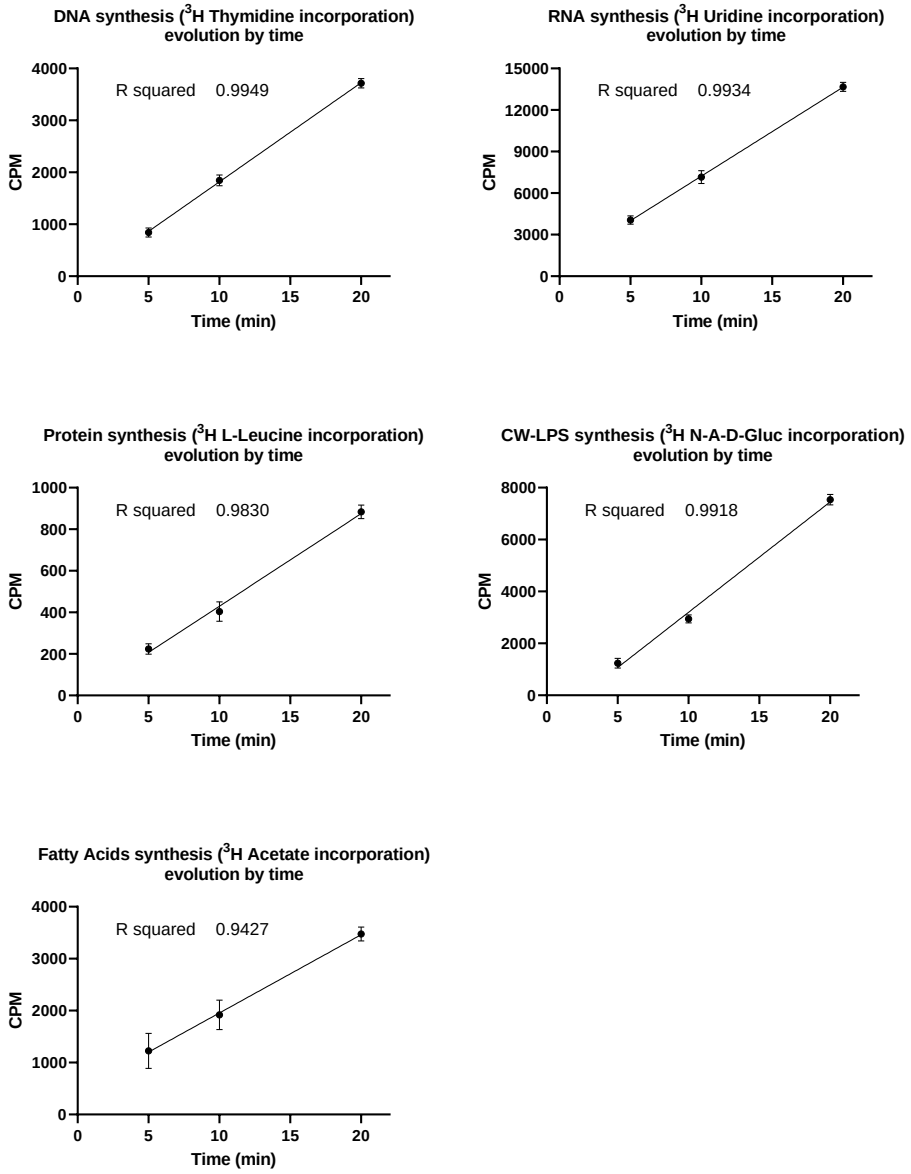

Supplementary figure 1. Macro molecular synthesis assay with *S. aureus* ATCC 25923: Calibration curve of the incorporation of radiolabelled precursors overtime.

REFERENCES

1. Control, C.f.D. and Prevention, *Antibiotic: antimicrobial Resistance*. http://www. cdc. gov/drugresistance/index. html, 2011.
2. Co-operation, O.f.E. and Development, *Antimicrobial Resistance–Tackling the Burden in the European Union*. 2019, OECD Paris, France.
3. Durand, G.A., D. Raoult, and G. Dubourg, *Antibiotic discovery: history, methods and perspectives.* Int J Antimicrob Agents, 2019. **53**(4): p. 371-382.
4. Lewis, K., *Platforms for antibiotic discovery.* Nature Reviews Drug Discovery, 2013. **12**(5): p. 371-387.
5. Das, S., A. Dasgupta, and S. Chopra, *Drug repurposing: a new front in the war against Staphylococcus aureus.* Future microbiology, 2016. **11**(8): p. 1091-1099.
6. Farha, M.A. and E.D. Brown, *Drug repurposing for antimicrobial discovery.* Nature Microbiology, 2019. **4**(4): p. 565-577.
7. Zhurina, M., et al., *Niclosamide as a promising antibiofilm agent.* Microbiology, 2017. **86**(4): p. 455-462.
8. Whitesell, J.K., *The Merck Index, CD-ROM (Macintosh): An Encyclopedia of Chemicals, Drugs & Biologicals Edited by S. Budavari, M. O'Neill, A. Smith, P. Heckelman, and J. Kinneary (Merck & Co., Inc.). Chapman & Hall: New York. 1997. $250.00. ISBN 0-412-75940-3.* 1998.
9. Torres, N.S., et al., *Screening a commercial library of pharmacologically active small molecules against Staphylococcus aureus biofilms.* Antimicrobial agents and chemotherapy, 2016. **60**(10): p. 5663-5672.
10. Rajamuthiah, R., et al., *Repurposing salicylanilide anthelmintic drugs to combat drug resistant Staphylococcus aureus.* PloS one, 2015. **10**(4): p. e0124595.
11. Kadri, H., O.A. Lambourne, and Y. Mehellou, *Niclosamide, a Drug with Many (Re)purposes.* ChemMedChem, 2018. **13**(11): p. 1088-1091.
12. Gwisai, T., et al., *Repurposing niclosamide as a versatile antimicrobial surface coating against device-associated, hospital-acquired bacterial infections.* Biomedical Materials, 2017. **12**(4): p. 045010.
13. Espinel-Ingroff, A., et al., *Quality control and reference guidelines for CLSI broth microdilution susceptibility method (M38-A document) for amphotericin B, itraconazole, posaconazole, and voriconazole.* Journal of clinical microbiology, 2005. **43**(10): p. 5243-5246.

14. Arciola, C.R., D. Campoccia, and L. Montanaro, *Implant infections: adhesion, biofilm formation and immune evasion.* Nature Reviews Microbiology, 2018. **16**(7): p. 397.
15. de Breij, A., et al., *The antimicrobial peptide SAAP-148 combats drug-resistant bacteria and biofilms.* Science translational medicine, 2018. **10**(423).
16. O'Toole, G.A., *Microtiter dish biofilm formation assay.* Journal of visualized experiments: JoVE, 2011(47).
17. Gilbert-Girard, S., et al., *Optimization of a High-Throughput 384-Well Plate-Based Screening Platform with Staphylococcus aureus ATCC 25923 and Pseudomonas aeruginosa ATCC 15442 Biofilms.* International journal of molecular sciences, 2020. **21**(9): p. 3034.
18. Dantes, R., et al., *National burden of invasive methicillin-resistant Staphylococcus aureus infections, United States, 2011*. JAMA Intern Med, 2013. **173**(21): p. 1970-8.
19. Lee, B.Y., et al., *The economic burden of community-associated methicillin-resistant Staphylococcus aureus (CA-MRSA).* Clinical microbiology and infection : the official publication of the European Society of Clinical Microbiology and Infectious Diseases, 2013. **19**(6): p. 528-536.
20. Turner, N.A., et al., *Methicillin-resistant Staphylococcus aureus: an overview of basic and clinical research.* 2019. **17**(4): p. 203-218.
21. Xu, J., et al., *Discovery of niclosamide and its O-alkylamino-tethered derivatives as potent antibacterial agents against carbapenemase-producing and/or colistin resistant Enterobacteriaceae isolates.* Bioorganic & medicinal chemistry letters, 2019. **29**(11): p. 1399-1402.
22. Mohammad, H., et al., *Repurposing niclosamide for intestinal decolonization of vancomycin-resistant enterococci.* International journal of antimicrobial agents, 2018. **51**(6): p. 897-904.
23. Domalaon, R., et al., *The anthelmintic drug niclosamide synergizes with colistin and reverses colistin resistance in Gram-negative bacilli.* Antimicrobial agents and chemotherapy, 2019. **63**(4).
24. Copp, J.N., et al., *Mechanistic understanding enables the rational design of salicylanilide combination therapies for Gram-negative infections.* Mbio, 2020. **11**(5).

25. Imperi, F., et al., *New life for an old drug: the anthelmintic drug niclosamide inhibits Pseudomonas aeruginosa quorum sensing.* Antimicrobial agents and chemotherapy, 2013. **57**(2): p. 996-1005.
26. Ayerbe-Algaba, R., et al., *Synergistic activity of niclosamide in combination with colistin against colistin-susceptible and colistin-resistant Acinetobacter baumannii and Klebsiella pneumoniae.* Frontiers in cellular and infection microbiology, 2018. **8**: p. 348.
27. Jamal, M., et al., *Bacterial biofilm and associated infections.* J Chin Med Assoc, 2018. **81**(1): p. 7-11.
28. Mah, T.-F.C. and G.A. O'Toole, *Mechanisms of biofilm resistance to antimicrobial agents.* Trends in microbiology, 2001. **9**(1): p. 34-39.
29. Matias, C.S.S., *Antibiotic drug development*. 2020, Technical University of Denmark. p. 200
30. Jain, N.K., et al., *Niclosamide encapsulated polymeric nanocarriers for targeted cancer therapy.* RSC Advances, 2019. **9**(46): p. 26572-26581.
31. Sanphui, P., S.S. Kumar, and A. Nangia, *Pharmaceutical Cocrystals of Niclosamide.* Crystal Growth & Design, 2012. **12**(9): p. 4588-4599.
32. Chang, Y.-W., et al., *Pharmacokinetics of anti-SARS-CoV agent niclosamide and its analogs in rats.* Journal of Food and Drug Analysis, 2006. **14**(4).
33. Parikh, M., et al., *Phase Ib trial of reformulated niclosamide with abiraterone/prednisone in men with castration-resistant prostate cancer.* Scientific reports, 2021. **11**(1): p. 1-7.
34. Barbosa, E.J., et al., *Niclosamide repositioning for treating cancer: Challenges and nano-based drug delivery opportunities.* European Journal of Pharmaceutics and Biopharmaceutics, 2019. **141**: p. 58-69.
35. Boyapally, R., et al., *Niclosamide alleviates pulmonary fibrosis in vitro and in vivo by attenuation of epithelial-to-mesenchymal transition, matrix proteins & Wnt/β-catenin signaling: A drug repurposing study.* 2019. **220**: p. 8-20.
36. Yilmaz, B., *Nifedipine, Niclosamide and Furosemid Release of A Biocompatible and Protective Hydrogel for Cancer Therapy.* 2021.
37. Zhu, Y., et al., *Repurposing of the anti-helminthic drug niclosamide to treat melanoma and pulmonary metastasis via the STAT3 signaling pathway.* 2019. **169**: p. 113610.

CHAPTER 3

A NICLOSAMIDE-RELEASING HOT-MELT EXTRUDED CATHETER PREVENTS STAPHYLOCOCCUS AUREUS IN EXPERIMENTAL BIOMATERIAL-ASSOCIATED INFECTION

A NICLOSAMIDE-RELEASING HOT-MELT EXTRUDED CATHETER PREVENTS *STAPHYLOCOCCUS AUREUS* IN EXPERIMENTAL BIOMATERIAL-ASSOCIATED INFECTION

Augusto Vazquez-Rodriguez[1*#], Bahaa Shaqour[2,3#], Clara Guarch-Pérez[4], Emilia Choińska[5], Martijn Riool[4], Bart Verleije[6], Koen Beyers[6], Vivian Costantini[1], Wojciech Święszkowski[5], Sebastian A. J. Zaat[4], Paul Cos[2], Livia Ferrari[1], Antonio Felici[1]

[1]Discovery Microbiology, Aptuit S.r.l., an Evotec Company, via A. Fleming 4, 37135, Verona, Italy

[2]Laboratory for Microbiology, Parasitology and Hygiene (LMPH), Faculty of Pharmaceutical, Biomedical and Veterinary Sciences, University of Antwerp, Universiteitsplein 1 S.7, 2610 Antwerp, Belgium

[3]Mechanical and Mechatronics Engineering Department, Faculty of Engineering & Information Technology, An-Najah National University, P.O. Box 7, Nablus, Palestine

[4]Department of Medical Microbiology and Infection Prevention, Amsterdam institute for Infection and Immunity, Amsterdam UMC, University of Amsterdam, 1105 AZ Amsterdam, The Netherlands

[5]Faculty of Materials Sciences and Engineering, Warsaw University of Technology, Wołoska 141,
02-507 Warsaw, Poland

[6]Voxdale BV, Bijkhoevelaan 32C, 2110 Wijnegem, Belgium

[#]These authors contributed equally to this work.

*Corresponding author

Keywords: central venous catheter; infection; antimicrobial catheter; niclosamide; hot melt extrusion; *in vivo*; murine model; drug repurposing

ABSTRACT

Medical device related infections are a major healthcare challenge as they are responsible for high disease burden in critically ill patients. In this study, we have developed non-antibiotic drug-eluting antibacterial catheters to prevent catheter associated infections. Niclosamide (NIC), originally a well-studied antiparasitic drug, was incorporated into the polymeric matrix of thermoplastic polyurethane (TPU) via solvent casting, and catheters were fabricated using hot-melt extrusion technology. The mechanical and physicochemical properties of TPU polymers loaded with NIC were studied as well. NIC was released in a sustained manner from the catheters and exhibited antibacterial activity against *Staphylococcus aureus* and *Staphylococcus epidermidis* in different *in vitro* models. Moreover, the antibacterial efficacy of NIC-loaded catheters was validated in an *in vivo* biomaterial-associated infection mouse model using a methicillin-susceptible and methicillin-resistant strain of *S. aureus.* The released NIC from the produced catheters reduced bacterial colonization of the catheter as well as of the surrounding tissue. Additionally, a sustained *in vivo* release of NIC from the catheters for at least 14 days was observed. In summary, the NIC-releasing hot-melt extruded catheters prevented implant colonization and reduced the bacterial colonization of peri-catheter tissue by methicillin sensitive as well as resistant *S. aureus* in a biomaterial-associated infection mouse model and has good prospects for clinical development.

INTRODUCTION

Catheters represent an indispensable medical tool to improve the health quality and medical care of patients. The demand for catheters has increased due to the wide use of such devices in the administration of medications, nutritional support, blood sampling and performing dialysis in critically or chronically ill patients [1]. At least 150 million intravascular catheters are used annually in North America alone [2]. However, 3.5 % of these catheters are colonized by bacterial or fungal pathogens causing serious and costly bloodstream infections [3]. Catheter-related bloodstream infections (CRBSIs) increase the morbidity and mortality of intensive care patients with a mortality ranging from 19 to 34 % [4]. These infections are mainly caused by Gram-positive bacteria, mostly *Staphylococcus aureus* and *Staphylococcus epidermidis* [5, 6]. CRBSIs are primarily due to bacterial colonization of the catheter surface during insertion leading to a biofilm infection [5]. Bacterial cells encased in biofilm structures are very difficult to be eradicated by the immune defenses and antimicrobial agents [7, 8]. Hence, catheters must be removed and replaced to prevent further medical complications. Preventing bacterial attachment and subsequent biofilm formation on catheter surfaces would be the most cost-effective strategy to prevent CRBSIs [9].

There are many strategies described in the literature to address this increasing problem. These can be categorized as: 1) antifouling strategies such as hydration and steric repulsion, specific protein interactions, or low surface energy, and 2) antimicrobial mechanisms such as the release of biocidal agents, or surface microbicidal activity [10]. The release of biocidal agents' approach has been extensively investigated over the past years via incorporating or coating medical devices with biocidal compounds such as antibiotics or other active compounds, for instance compounds identified in "repurposing" studies.

Antibacterial drug repurposing entails the use of already approved drugs for novel applications, such as antibacterial indications [11]. Niclosamide (NIC), an anthelmintic drug declared by the WHO as an essential medicine [12], has been identified as one of the most promising candidates to combat Gram-positive

infections, especially those caused by *S. aureus* and *S. epidermidis*, being effective at relatively low concentrations (between 0.0625-0.5 µg/mL) [13-20]. However, given its poor solubility in water and low bioavailability, it may be less suitable for treating systemic infections [21-23]. Nevertheless, NIC has the potential to be applied to treat localized infections such as wound, soft tissue, gastrointestinal, skin and medical-device related infections [14, 15, 23-27].

Based on this rationale, the aim of this research work was to develop an antibacterial catheter releasing NIC to prevent catheter related infections. Specifically, we developed a local drug delivery system by incorporating NIC into the polymeric matrix of thermoplastic polyurethane (TPU) via solvent casting. Furthermore, the resulting material was used to fabricate antibacterial catheters by hot-melt extrusion (HME) technology. The produced catheters were characterized to study the effect of NIC loading on the mechanical and thermal properties of the TPU. Moreover, the antimicrobial efficacy of the catheters was tested *in vitro* and then *in vivo* in a murine biomaterial associated infection (BAI) model.

METHOD AND MATERIALS

REAGENTS

Thermoplastic polyurethane (TPU; Tecoflex EG-60D) was obtained from Lubrizol, VELOX, The Netherlands. The polymer contains a soft and hard segment in a ratio of 3:1. The glass transition temperature is 23°C and the melting temperature is 63°C [28]. Niclosamide (NIC; N3510, ≥98 % purity) and all other reagents and materials were purchased from Sigma-Aldrich (USA) unless indicated otherwise.

BACTERIAL STRAINS

For *in vitro* microbiological evaluation, the bacterial strains used were the methicillin susceptible *S. aureus* ATCC 25923 (MSSA), the methicillin resistant *S. aureus* ATCC 33591 (MRSA), the methicillin susceptible *S. epidermidis* O47 (MSSE) and the methicillin resistant *S. epidermidis* ATCC 35984 (MRSE). For *in vivo* microbiological evaluation the pathogens used were MSSA and MRSA.

Bacterial strains were grown in tryptic soy broth (TSB); Difco Laboratories Inc, USA) at 37°C. Specific growth conditions for each experiment are described in the respective section.

MATERIAL PREPARATION

TPU was loaded with NIC at 2, 5 and 10 % (*w/w*) using the solvent casting approach adopted from the work of Shaqour *et al.* [29], as shown in Figure 1A. First, the required amount of NIC was suspended in chloroform and sonicated for 30 min. Then, a magnetic stirrer was used to homogeneously distribute the NIC particles for 30 min. Subsequently, the TPU was added to the system while stirring and the suspension was left overnight to dissolve the polymer. The ratio between TPU and chloroform was 12.5 % (*w/v*). The polymer solution with suspended NIC was then poured into a petri dish with a diameter of 200 mm to allow the chloroform to evaporate through the fume hood. Finally, the casted films were vacuum dried for 3 days at 25°C and 50 mbar.

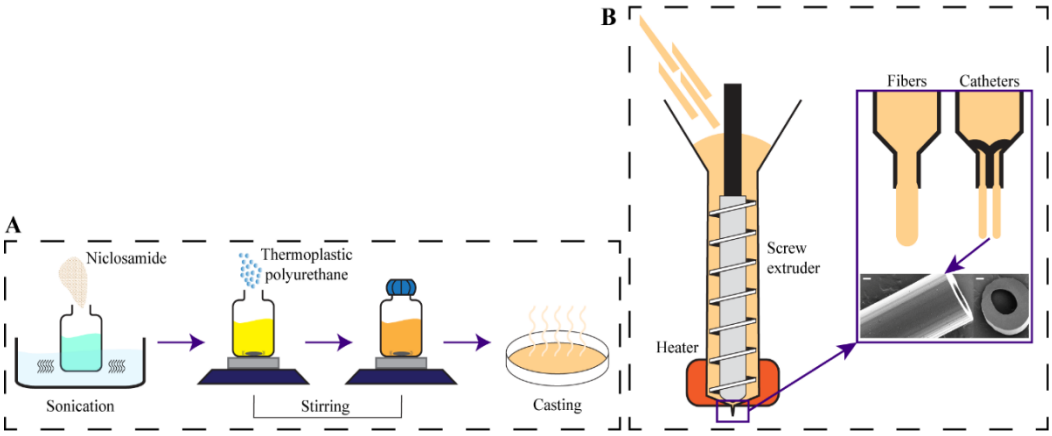

Figure 1. Process for A) incorporating NIC into the polymeric matrix of TPU using solvent casting and B) for producing fibers and catheters using HME technology. Scale bar in B is 200 μm.

Fibers and catheters were extruded using an in-house single screw extrusion setup attached with a specially in house designed an e3d v6 stainless steel nozzle (E3D-Online, United Kingdom) with a diameter of 0.8 mm and or 3D-printed coaxial nozzle (Figure 1B). In order to extrude the fibers and catheters, first, cast films (with or without NIC) were cut into stripes and directly fed into the extruder. Subsequently, fibers and catheters were extruded at a temperature of 180°C with a

screw extrusion speed of 75 rpm. The extruded fibers were cut into 4 cm segments and used to evaluate the effect of NIC loading on the mechanical properties of the TPU, while the extruded catheters segments (0.5 and 1 cm length) were used for material characterization and for microbiological characterization. Catheter segments for microbiological testing were further sterilized by incubation in ethanol 70 % for 2 min followed by air-drying for 30 min [29].

MICROSCOPY

Catheter segments were inspected using an s9i microscope (Leica, Belgium). Catheters from each group were imaged and then analysed using ImageJ software (v 1.52a; US National Institutes of Health, USA) by calculating the equivalent diameter $\left(\sqrt{\frac{4*Area}{\pi}}\right)$ of the measured area for the inner and outer circles for each catheter (n = 6 for each group) [29].

MECHANICAL TESTING

Tensile tests were performed on an AGS 5 kND machine (Shimadzu, Germany). The tensile rate was set to 20 mm/min and the distance between grips was 20 mm. Extruded fibers (n = 5 per group) were used for this test. The tensile elastic modulus (EM) was calculated from the force-displacement curve generated by the machine's software. A Matlab (v.R2020b; The Mathworks Inc.,USA) code was written to calculate the stress-strain curve and the slope of the best fit line between 50 % and 150 % strain.

THERMAL ANALYSIS

Thermogravimetric analysis was conducted on a Q5000 analyser (TA Instruments, USA). Samples of around 10 mg were placed on a platinum pan and then a dynamic heating ramp of 20°C/min with resolution of 3.00°C to 500°C under nitrogen flow of 60 mL/min was applied.

CONTACT ANGLE

The water contact angle measurements were done at room temperature using demineralized water and an OCA20 goniometer (Dataphysics, Germany). For each sample, the left and the right contact angles of at least 10 droplets with a volume of 2 µL were measured and averaged.

FOURIER-TRANSFORM INFRARED SPECTROSCOPY

NIC powder before and after heating to 180°C was examined using Fourier-transform infrared (FTIR) spectroscopy in order to study the effect of heat on NIC molecules. Moreover, to study the interactions between NIC and the TPU molecules, FTIR analysis was conducted on the produced catheters. The FTIR spectrometer used (Nicolet 8700, ThermoScientific, USA) was equipped with a diamond attenuated total reflectance (ATR) accessory. All ATR-FTIR spectra were recorded at room temperature in the 400–4,000 cm^{-1} range. The spectral resolution and accuracy were 4 cm^{-1} and ±1 cm^{-1}, respectively.

X-RAY POWDER DIFFRACTION

X-ray powder diffraction (XRPD) analysis was performed in order to analyse the solid-state characteristics of NIC pure powder, non-loaded TPU, and NIC-loaded TPU catheters. The XRPD analyses were run in transmission mode on PANalytical X'Pert Pro X-Ray Diffractometer (PANalytical B.V., The Netherlands) equipped with an X'Celerator detector using a standard XRPD method. The instrumental parameters used are listed in the supplementary Table 1.

IN VITRO DRUG RELEASE ASSAY

Catheter segments loaded with NIC (2, 5 and 10 % (*w/w*)) and non-loaded, with a length of 1 cm were weighted using a microbalance (Sartorius, Germany). Then, each catheter segment was placed in 1 mL of phosphate buffered saline (PBS; ThermoFisher, USA) with 2 % of Tween 80 (ThermoFisher) and incubated at 37°C with an agitation of 120 rpm (n = 3 per group). The buffer solution was exchanged for fresh solution at every time point (1, 3, 4, 6 and 24 h, daily on days 2 – 10, and

at 13, 16, 20 and 27 days). The aliquots were stored at -20°C for later use. The concentration of NIC released at every time point was calculated by measuring the absorbance at 340 nm of 300 µL of each aliquot in 96 well plates in flat bottom microtiter plates (Greiner Bio-One, USA) with a multi-well plate reader (Synergy H1, BioTek, USA). A calibration curve was plotted for NIC to estimate the concentration of drug released from the catheter segments. This curve ranged from 1 to 50 µg/mL with R^2 equal to 0.9998.

IN VITRO ANTIMICROBIAL SUSCEPTIBILITY TEST

To evaluate the minimal inhibitory concentration (MIC) and quantitatively assess the minimal bactericidal concentration (MBC) of NIC after heating at 180°C to mimic the extrusion process, MSSA was grown in TSB at 37°C and 120 rpm until reaching mid-logarithmic growth phase, and a bacterial inoculum of 1×10^6 CFU/mL was prepared by dilution in fresh TSB, based on the optical density at 620 nm (OD_{620}). Ninety microliters of TSB containing either untreated NIC control or NIC heated at 180°C were 2-fold serially diluted in TSB from 128 µg/mL to 0.125 µg/mL in a flat bottom microtiter plate (Greiner Bio-One, USA). Immediately after, 10 µL of bacterial inoculum was added to the solution and incubated overnight at 37°C 120 rpm. As a control for bacterial growth, 10 µL of the inoculum was incubated in TSB without NIC. The MIC was defined as the lowest NIC concentration without visible bacterial growth. For the MBC, 2 droplets of 10 µL of the undiluted samples from the wells without visible growth and from the well with the lowest NIC concentration where visible growth had occurred, were plated at blood agar plates (Oxoid, United Kingdom) and incubated at 37°C overnight. The MBC was assessed the next day as the lowest concentration of NIC which had caused ≥99.9 % reduction in numbers of CFU compared to the inoculum.

CELL VIABILITY ASSAY

A cell viability assay was performed to investigate the possible cytotoxic effect of NIC after heating. The L929 mouse fibroblasts cell line was purchased from the European Collection of Authenticated Cell Cultures (ECACC; United Kingdom) and cultured in Dulbecco's modified Eagle's medium (DMEM; ThermoFisher,

USA) supplemented with 10 % of fetal bovine serum (FBS; ThermoFisher, USA) and 1 % of both penicillin and streptomycin (Pen/Strep; ThermoFisher, USA) in cell culture flasks of 75 mL. Cells from passage no. 5-8 were incubated at 37°C, 5 % CO_2 and 99 % relative humidity. Cells were detached with trypsin-EDTA (0.25 %, 1 mM EDTA, ThermoFisher, USA) and counted. One hundred microliters containing approximately 10^3 cells were seeded per well of three 96 well cell culture plates and incubated at 37°C and 5 % CO_2 for 24 hours.

The next day the medium was removed and 200 µL of DMEM containing 10 µg/mL of either non-heated or 180°C heated NIC were added. DMSO at 10 % was used as positive control and DMEM with 1 % pen/strep was used as a negative control for cytotoxicity. The cells were incubated at 37°C and 5 % CO_2 for 24, 48 or 72 hours. At each time point, the medium from wells containing NIC-treated cells and untreated cells was removed and cells were washed with 200 µL of PBS. To assess cell viability, 100 µL/well of DMEM and 20 µL of the reagent of Cell Titer 96 Aqueous One Solution Cell Proliferation Assay (Promega, USA) were added. The plates were incubated for 2 h at 37°C and then absorbance was measured at 490 nm with the spectrophotometer (BMG Labtech, The Netherlands). A potential cytotoxicity effect was considered when the cell viability was reduced to ≤ 70 % of the untreated control group [30].

EVALUATION OF ANTIMICROBIAL PROPERTIES OF TPU-CATHETERS LOADED WITH NIC

Catheter segments loaded with 2, 5, and 10 % (*w/w*) NIC and non-loaded catheter segments were analysed for antibacterial activity (release) and prevention of biofilm formation using the MSSA, MRSA, MSSE and MRSE strains.

Firstly, a modified Kirby-Bauer disk diffusion assay [31] was performed to determine the zone of inhibition (ZOI) of 0.5 cm catheter segments loaded with NIC and non-loaded catheters. Briefly, 1 to 3 colonies of each strain were incubated in 5 mL of TSB overnight at 37°C and 120 rpm. Two hundred microliters of an inoculum of 1×10^6 CFU/mL was spread on blood agar plates with a cotton swab. The catheter segments were inserted vertically into the blood agar plates, which

were then incubated at 37°C for 24 h. The next day, the catheter segments were transferred to freshly inoculated blood agar plates and this step was repeated for 10 days. Each day the resulting zones of growth inhibition (including catheter diameter) were measured in mm.

Secondly, 1 cm catheter segments were placed in tubes containing suspensions of each of the 4 aforementioned bacterial strains (approx. 5×10^6 CFU/mL) in 1 mL of TSB. Catheter segments were incubated in the bacterial suspensions at 37°C and 120 rpm for 24 hours. After the incubation, 2 measures of bacterial growth were quantified: 1) planktonic bacterial growth in the medium; and 2) biofilm formation on the catheter surfaces. To assess the antibacterial activity, planktonic cells in the medium were enumerated by quantitative culture, performed as follows: aliquots of the bacterial suspensions were taken, 10-fold serially diluted, and the dilutions and undiluted suspensions plated on tryptic soy agar (TSA) plates; these plates were incubated at 37°C for 24 hours and CFUs were determined. Similarly, biofilm formation was quantitatively measured by enumerating the viable cells attached to the surface. In brief, catheter segments were removed from the medium and washed 3 times in PBS to remove planktonic cells. Immediately thereafter, catheter segments were transferred to 1 mL of PBS, vortexed for 30 seconds, and sonicated for 15 min using an ultrasonic bath (Branson CPX2800-E, 40 kHz) to detach and disperse adherent-biofilm cells. This procedure does not affect viability of the bacteria. The bacteria recovered from the catheter segments were quantitatively cultured. For each experiment, triplicates were analysed for each sample (NIC-loaded and non-loaded catheter segments).

Finally, scanning electron microscopy (SEM) was performed to visualize the morphological changes of MSSA bacterial cells adhered to NIC loaded and non-loaded catheter segments. As previously described in this section, bacterial suspensions were incubated with NIC loaded and non-loaded catheter segments until washing steps with PBS. Prior to SEM imaging, samples were fixed in a solution of 4 % (*v/v*) paraformaldehyde supplemented with 1 % (*v/v*) glutaraldehyde (Merck, USA) overnight at room temperature. Samples were rinsed twice with demi water for 10 min and dehydrated in a graded ethanol concentration

series from 50 % to 100 % of ethanol. To reduce the sample surface tension, samples were immersed in hexamethyldisilane (Polysciences Inc., USA) overnight and air-dried. Before imaging, samples were mounted on aluminum SEM stubs and sputter-coated with a 4 nm platinum–palladium layer using a Leica EM ACE600 sputter coater (Microsystems, Germany). Images were acquired at 8 kV using a Zeiss Sigma 300 SEM (Zeiss, Germany) at the Electron Microscopy Center Amsterdam (ECMA; Amsterdam UMC, Amsterdam, The Netherlands). Of each tube, 6-8 fields were inspected and photographed at magnifications of 100× and 500×. Catheter segments loaded with 10 % of NIC were not included in the results as the material was partially degraded by the fixation procedure for SEM visualization.

IN VIVO EVALUATION OF TPU-CATHETERS LOADED WITH NIC USING A MURINE BAI MODEL.

The efficacy of NIC-loaded catheters to prevent infection was evaluated *in vivo* using a murine BAI model. As *S. aureus* is one of the most frequent pathogens in medical device related infection [5, 6], the MSSA and MRSA strains were used for the *in vivo* evaluation of the NIC loaded catheters.

All studies were conducted in accordance with national Italian legislation, under approval of the internal Aptuit Committee on Animal Research and Ethics and under authorization issued by the Italian Ministry of Health (Italian Ministry of Health Authorization Project – Internal Code No. 21205). General procedures for animal care and housing were in accordance with the current recommendations of the Association for Assessment and Accreditation of Laboratory Animal Care.

Male CD-1 mice (Charles River, Italy), weighing between 18-20 g, were housed in solid bottomed plastic cages with sawdust litter at a temperature of 20-22°C, a relative humidity range of 45-65 %, and lighting from approximately 06:00 to 18:00 hours daily. Mice were fed a standard maintenance diet (A. Rieper SpA, Italy) and drinking water was filtered from normal domestic supply. Regimen diet was *ad*

libitum. A period of acclimatization of 5 days was implemented before any experimental procedure.

Briefly, the mice were anesthetized using inhaled isoflurane at 2.5 % and the back of the mice was shaved using an electric razor and cleansed using a solution of benzalkonium chloride 0.175 % (*v/v*). A small incision was made in both flanks of the mice and two subcutaneous pockets were created using forceps, a 1 cm catheter segment was inserted into each pocket and the incisions were closed using surgical staples (AUTOCLIP™ wound closing system, Clay Adams, USA) under sterile conditions. Each mouse received two catheter segments with the same concentration of NIC, either non-loaded, 2 or 5 % (*w/w*) NIC loaded catheters (n = 7 mice per group, so n = 14 catheter segments per group). Three additional mice were added to each experimental group and dedicated to histological analysis on day 3 post-infection.

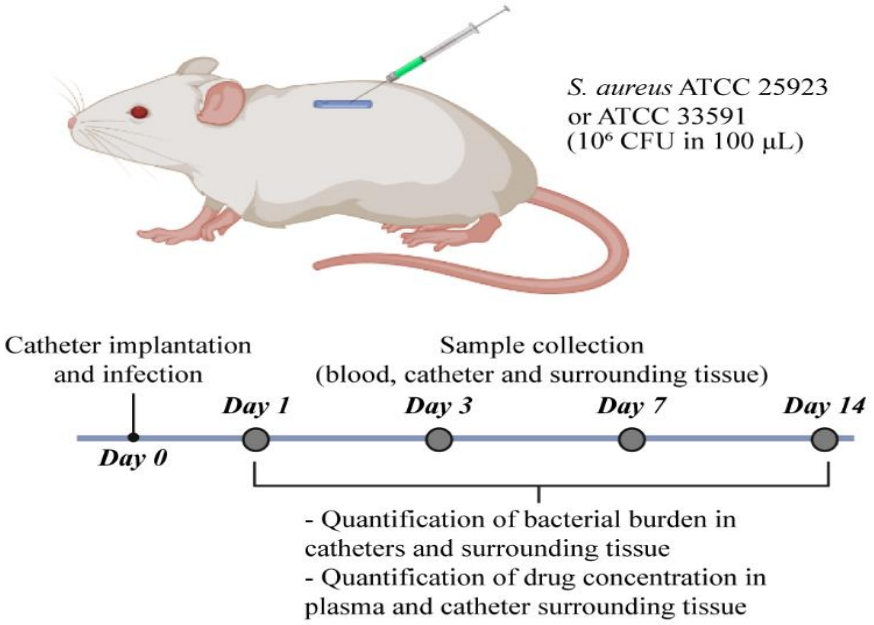

Figure 2. *In vivo* efficacy evaluation of non-loaded, 2 and 5 % (*w/w*) NIC loaded TPU catheters using a murine BAI model. Two 1 cm catheters segments were implanted subcutaneously in the mice and a bacterial challenge (10^6 CFU in 100 µL) of either MSSA or MRSA was injected intraluminally into each catheter. Blood, catheter segments, and the surrounding tissue were collected of mice sacrificed on day 1, 3, 7 and 14 after challenge. Bacterial colonization of the catheter and the surrounding tissue, and the NIC concentration in plasma and in the tissue surrounding the catheter were quantified.

Immediately following catheter implantation, 100 µL containing 10^6 CFU of either MSSA or MRSA were injected intraluminally into the catheter segments (Figure 2). Animals were anesthetized using inhaled isoflurane (2.5 %) and the blood collected by terminal cardiac puncture at 1-, 3-, 7- or 14-days post-infection. Blood, catheter segments and the respective surrounding tissue were collected. Biopsies were aseptically retrieved using a 12 mm diameter biopsy punch and accordingly processed for bacterial load determination: catheter segments were separated from their surrounding tissue and washed 3 times in 0.9 % saline solution to remove non-adherent bacteria. Next, catheter segments were transferred into tubes containing 1 mL of sterile PBS, vortexed for 30 seconds and sonicated for 15 min using an ultrasonic bath (Branson CPX2800-E, 40 kHz) to detach and disperse biofilm cells from the catheter surfaces. Recovered bacteria from the catheters were then quantitively cultured. Surrounding tissue was homogenized in 1 mL of PBS using a Precelys tissue homogenizer device (Bertin Technologies, France). Tissue homogenates were quantitatively cultured to enumerate viable bacterial cells residing in the tissue. In case of bacterial growth on day 14 post-infection, *S. aureus* colonies were retrieved and the MIC for NIC was determined for all single retrieved colonies following the CLSI guidelines[32, 33].

For histopathology analysis, biopsies were retrieved from histology dedicated mice and preserved in 10 % neutral buffered formalin. Following fixation, samples were embedded in paraffin, sectioned at a nominal thickness of 3-5 µm and stained with hematoxylin-eosin for histological analysis.

The NIC *in vivo* release profile in animals carrying NIC-loaded catheters was determined in plasma and in the tissue surrounding the catheter segments collected on day 1, 3, 7 and 14 post infection. First plasma was collected as follows: 1 mL of blood was placed in K3-EDTA collection tubes (Greiner Bio-One, USA) and centrifuged at 3,000 RCF, 4°C for 10 min. Fifty microliters of supernatant-containing plasma was then retrieved and mixed with 150 µL of HEPES 0.1 N and stored at -20°C until analysis.

Second, catheter surrounding tissue was processed as previously described and resulting tissue homogenates were further homogenized by enzymatical digestion: 1 mL of a solution of collagenase type 1 (8 mg/mL in PBS) and incubated for 3 hours at 37°C with agitation. Digested tissue homogenates were kept at -20°C until analysis. Prior to the analytical procedure, plasma and tissue homogenate samples were deproteinized with 2 volumes of acetonitrile containing diclofenac (200 ng/mL) as internal standard, vortexed and then centrifuged at 3,000 rpm for 10 min. After centrifugation, supernatants were diluted (160 µL ultrapure water + 200 µL of supernatant) using a Hamilton Microlab STARlet small liquid handler (Hamilton Company, Switzerland). Levels of NIC in supernatants were determined by analyzing 2 µL of the supernatants using a Waters ultrahigh performance liquid chromatography system (UPLC; Milford, USA) coupled with an API400 (Applied Biosystems/MDS Sciex, USA)) in tandem mass spectrometry mode. Chromatographic separation was performed using a Waters Acquity UPLC BEH C18 30x2.1mm,1.7 µm analytical column. Mobile Phase A consisted of 0.1 % (*v/v*) formic acid in water; mobile phase B was 0.1% (*v/v*) formic acid in acetonitrile.

STATISTICAL ANALYSIS

Quantitative data was expressed as the average ± standard deviation, with the number of samples stated in each experiment. The statistical analysis of all the *in vitro* and *in vivo* characterization experiments was performed using a one-way analysis of variance (ANOVA) with Dunnet's comparison test to evaluate post-hoc differences between the test groups with respect to the control group. Alpha was set at 0.05 for all analyses. Statistical analysis was performed using Prism8 (GraphPad Software, San Diego, CA, USA). * Indicates a *p*-value of 0.01 to 0.05, ** indicates a *p*-value of 0.001 to 0.01, *** *p*-value of 0.0001 to 0.001, **** indicates a *p* value < 0.0001.

RESULTS

TPU FILMS LOADED WITH NIC AND CATHETER/FIBER EXTRUSION

The NIC loaded and non-loaded TPU films were successfully produced. The non-loaded TPU films were transparent while the NIC-loaded ones were yellowish and opaque. TPU is highly soluble in chloroform. The level of colouring and opaqueness increased with increasing NIC content. However, the NIC distribution was homogeneous as no agglomerates were spotted in the films.

The tensile elastic modulus was used to assess the mechanical properties of the produced fibers and whether the addition of NIC affected TPU's mechanical properties. The extruded fibers from the 0.8 mm nozzle had a diameter of 0.91 ± 0.08 mm. There were no significant differences between the NIC-loaded and non-loaded fibers and tubes in term of dimensions. The tensile elastic modulus was 4.8 ± 0.2, 5.1 ± 0.3, 5.6 ± 1.0 and 6.0 ± 0.3 MPa for the non-loaded and 2, 5 and 10 % (*w/w*) NIC loaded TPU fibers, respectively (Figure 3A). Only the 10 % (*w/w*) NIC loaded fibers showed a slight but significant (p =0.027) increase in the elastic modulus which may affect the mechanical properties of extruded catheters.

The produced catheters had an average outer and inner diameter of 1.24 ± 0.62 mm and 0.62 ± 0.01 mm, respectively, with no differences between the different types of catheters (Figure 3B). Water contact angle measurements from non-loaded and NIC-loaded TPU catheters are shown in Figure 3C. All catheters were hydrophobic (*i.e.* contact angle higher than 90°) [34], with a contact angle of 106.5 ±1.9°, 106.8 ± 1.5°, 116.3 ± 5.0° and 118.4 ± 2.5° for non-loaded, 2, 5 and 10 % NIC loaded TPU catheters, respectively. The hydrophobicity of the NIC-loaded catheters increased with higher NIC loading, which is expected since NIC is considered a hydrophobic molecule [35]. However, only the 5 and 10 % (*w/w*) NIC-loaded catheters (p = < 0.0001) showed a significant increase in the contact angle when compared to non-loaded catheters.

Thermogravimetric analysis (Figure 3D and E) showed the thermal degradation behavior for NIC powder, non-loaded and NIC-loaded TPU catheter segments. NIC and TPU had an onset degradation temperature (T_{onset}) of 260°C and 295°C, respectively. However, measurements of the NIC loaded catheters showed that the T_{onset} for NIC-loaded TPU was slightly higher than that of non-loaded catheters. T_{onset} for 2, 5 and 10 % NIC loaded TPU were 315°C, 313°C and 311°C, respectively. Such increase in T_{onset} was also reported when TPU was loaded with ciprofloxacin [29] or tetracycline hydrochloride [36], which indicates that, like NIC, the presence of these antibiotics improved the thermal stability of the polymer.

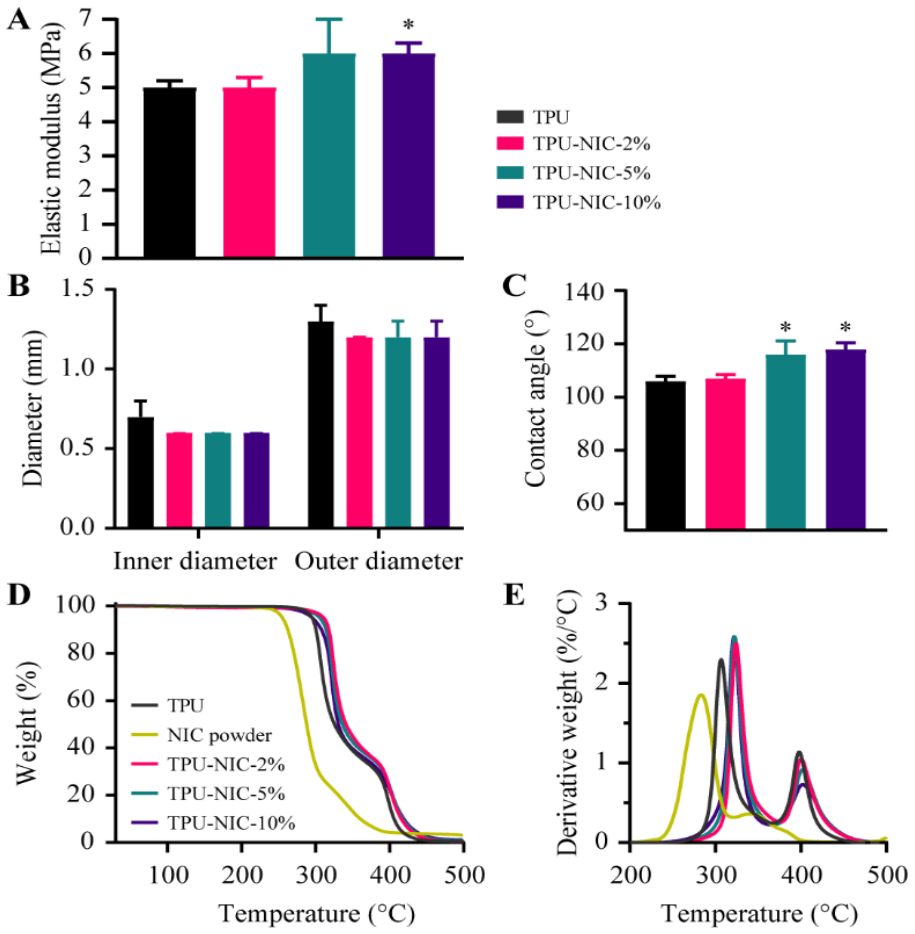

Figure 3. (A) Tensile elastic modulus of produced TPU fibers (n = 5), (B) Inner and outer diameter of produced TPU tubes (n = 6), (C) Water contact angle measurements of produced TPU catheters (n = 10). (D) Percentage weight loss vs. temperature and (E) Derivative of percentage weight loss vs. temperature in produced TPU fibers. Note: In section B, some error bars cannot be displayed as the SD is minimal.

FOURIER-TRANSFORM INFRARED SPECTROSCOPY AND X-RAY POWDER DIFFRACTION ANALYSIS

The FTIR analysis for the untreated NIC powder and NIC heated at 180°C revealed no major changes in the spectra due to the heating (supplementary figure 1). The FTIR spectra of NIC powder, non-loaded and NIC loaded TPU are shown in Figure 4A. The NIC spectrum showed characteristic bands at 3,576.34 cm^{-1}, 3,088.44 cm^{-1} and 1,679.69 cm^{-1} corresponding to -OH, -NH, and C=O groups, respectively (Figure 4B) [37]. The non-loaded TPU tubes exhibited a typical distribution of absorption bands for this type of material. The vibrational band at 3,330 cm^{-1} corresponds to NH stretching vibrations. The peaks in the range from 3,000 to 2,800 cm^{-1} relate to CH asymmetrical and symmetrical stretching vibrations [38]. The double peak in the region of 1,680 to 1,740 cm^{-1} (C=O stretching vibrations), the bands above 1,500 cm^{-1} (probably N-H bending vibrations and C-N stretching vibrations), and the strong bands in the region of 1,300 to 1,000 cm^{-1} (asymmetrical and symmetrical O-C-O stretching vibrations) are associated with the bonds of urethane groups [38]. The FTIR spectrum of NIC-loaded TPU tubes have characteristic peaks similar to those of the spectrum of non-loaded TPU tubes (Figure 4A). However, new specific peaks due to the presence of NIC appeared in the spectrum of the loaded tubes. The FTIR spectra of the TPU tubes loaded with 10 % of NIC showed the NIC characteristic peaks at 3,576 cm^{-1}, 3,088 cm^{-1} and 1,679 cm^{-1} corresponding to the –OH, -NH and C=O stretching vibration of the NIC molecule, respectively [37]. The peak at 3,576 cm^{-1} and the peak at 1,679 cm^{-1} were also present with lower intensity in the catheter loaded with 5 % of NIC. The absence of the peak at 3,088 cm^{-1} may indicate a chemical interaction between NIC and the polymer, and the possible presence of the drug as molecular dispersion[39].

The XRPD patterns of the non-loaded and NIC-loaded TPU tubes and pure NIC powder are reported in the Figure 4C and D. NIC powder exhibited the characteristic peaks corresponding to the crystal form of the molecule [40]. On the contrary, the XRPD pattern of TPU indicated its amorphous nature [41]. The TPU tubes loaded with NIC showed an XRPD pattern without the sharp NIC diffraction peaks, which suggest a transformation of crystalline NIC to its amorphous form,

this phase change was also reported by Jara *et al.* when hot-melt extruding NIC with the polymer poly(1-vinylpyrrolidone-co-vinyl acetate) (PVP–VA) at 180°C for the production of enteric formulations with increased bioavailability [42].

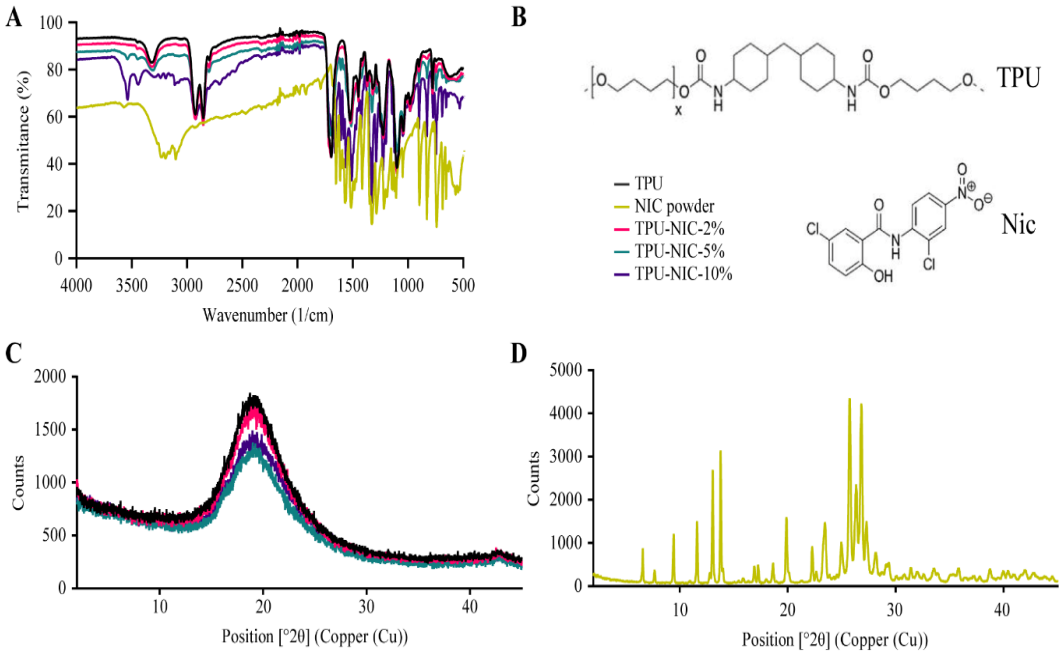

Figure 4. (A) FTIR spectra shown as the transmittance (%) of NIC, NIC-loaded and non-loaded TPU catheters (n = 3), (B) Molecular structure of TPU and NIC used in this study, (C) X ray powder diffraction pattern of non-loaded TPU catheters and TPU catheters loaded with 2, 5 and 10 % (w/w) NIC and (D) NIC plain drug.

NIC THERMOSTABILITY AND CYTOTOXICITY

Heating of NIC at 180°C did not affect the antibacterial activity of the drug as judged from the MIC and MBC against MSSA and MRSE strains (Figure 5A). This indicates that NIC is thermally stable at the processing temperature and is expected not to lose its antimicrobial activity during extrusion at 180°C. To evaluate the cytotoxicity of heated NIC, the L929 mouse fibroblast cell line was exposed to different concentrations of NIC powder either or not heated to 180°C. Heating NIC minimally impacted on the effect of NIC on the viability of the L929 cells. NIC did show a concentration dependent effect on cell viability as can be seen in figure 5B. The lowest tested concentration of NIC, 0.67 µg/mL, did not inhibit the fibroblast growth after 24 hours incubation, but the highest tested concentration, 3.27 µg/mL,

reduced the L929 cell metabolic activity by >50 %. After 48 hours the cell viability was reduced by >50 % by all NIC treatments. (Figure 5B).

A

	Niclosamide (µg/mL)			
	Non heated		180ºC	
Bacteria	MIC	MBC	MIC	MBC
MSSA	0.0625	0.125	0.0625	0.125
MSRA	0.125	0.125	0.125	0.125

B

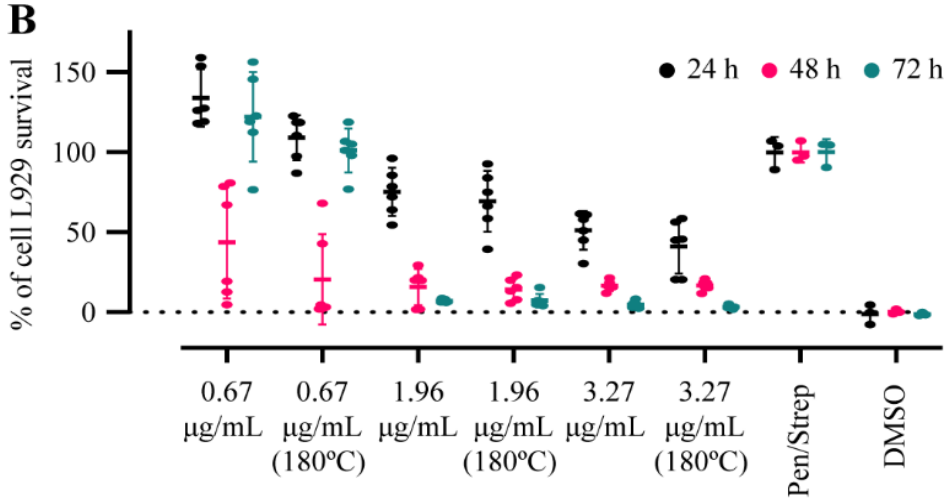

Figure 5. (A) MIC and MBC of non-heated NIC, and heated NIC at 180°C and (B) Mean percentage (± SD) of L929 cell mouse fibroblast cell viability, after 24, 48 and 72 hours of exposure to non-heated NIC and heated NIC at 180°C as determined by the Cell Titer 96 Aqueous One Solution Cell Proliferation Assay. Medium with 1 % penicillin and streptomycin (Pen/Strep) was used as a positive growth control and medium with 10 % DMSO as a negative growth control (n = 6).

IN VITRO DRUG RELEASE

The estimated amount of NIC (µg) loaded per 1 cm catheter segment was 258 ± 3, 573 ± 5 and 1110 µg ± 7, for tubes loaded with 2, 5 and 10 % NIC, respectively. All NIC loaded catheter segments showed an initial burst release of NIC in the first 24 h, followed by a gradual and sustained release over 27 days (Figure 6A). Overall, the 2, 5 and 10 % NIC-loaded catheters showed similar drug release kinetics over time (Figure 6A-B). During the first 10 days, about 70 % of NIC was released from the catheter segments loaded with 10 % of NIC, while around 80 % of the drug was released from catheter segments loaded with 2 and 5 % of NIC. After 20 days,

catheters loaded with 10 % of NIC released 80 % of the drug whereas a release of 90 % was achieved for catheters with 2 and 5 % of NIC (Figure 6A-B).

ANTIMICROBIAL ACTIVITY OF NIC OVER TIME

All catheter segments loaded with 2, 5 and 10 % NIC showed a detectable zone of inhibition (ZOI) of bacterial growth for MSSA, MRSA, MSSE and MRSE for 10 consecutive days (Figure 6C-F). As expected, non-loaded catheter segments did not produce any ZOI. For the first 5 days, catheters segments loaded with 2 % of NIC produced a ZOI between 4 and 8 mm depending on the bacterial strain. On subsequent days, the ZOI was gradually reduced reaching in some strains a minimum diameter of 2 mm at 10 days. Catheter segments loaded with 5 % of NIC exhibited a larger ZOI, ranging from 8 to 12 mm during the first 5 days. The ZOI was between 10 and 6 mm reaching a minimum ZOI of 5 mm on the last day. Compared to catheters with other loading percentage, catheter segments loaded with 10 % of NIC showed the largest inhibition zones after 10 days.

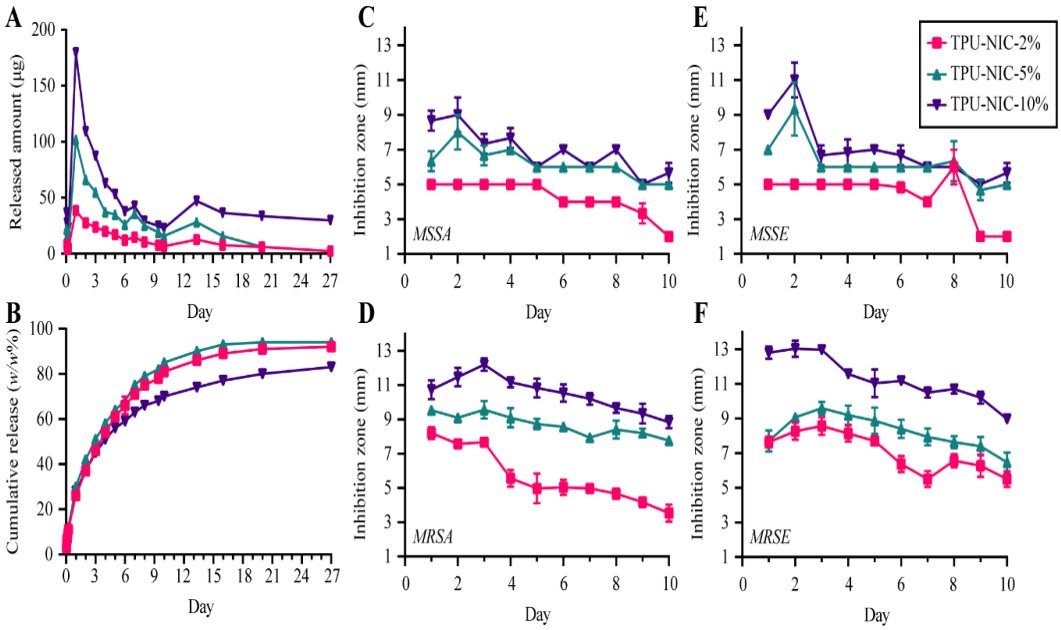

Figure 6. (A) Amount of NIC released (in µg) and (B) cumulative release (in *w/w*% of original NIC loading) over time up to 27 days, ZOI diameter (in mm) of (C) MSSA, (D) MRSA, (E) MSSE and (F) MRSE around NIC-loaded catheter segments transferred to fresh plates each day for 10 consecutive days. (n = 3)

EVALUATION OF ANTIMICROBIAL PROPERTIES OF TPU-CATHETERS LOADED WITH NIC

The *in vitro* antibacterial activity of NIC-loaded catheters was assessed using MSSA, MRSA, MSSE, MRSE strains (Figure 7A-H).

Biofilm formation was significantly reduced on the surface of all NIC-loaded catheter segments, with reductions higher than 2 LogCFU for both tested *S. aureus* strains (Figure 7A-B). Planktonic growth around all NIC-loaded catheters was reduced when compared against the non-loaded group (Figure 7E-F). However, similar reductions on the bacterial load were observed for all the drug loadings, indicating a possible bacteriostatic effect of released NIC. The biofilm formation for both *S. epidermidis* strains on all NIC-loaded catheters segments was significantly reduced (> 1.6 LogCFU reductions) (Figure 7C-D) whereas corresponding planktonic bacterial growth was only reduced by catheter segments loaded with NIC at 5 and 10 % (Figure 7G-H). The reduction of the bacterial burden on catheter segments challenged with MSSA was confirmed by visualization with SEM (Figure 8A-C). In non-loaded catheter segments, a high number of bacterial cells were attached to the intraluminal surface forming a biofilm structure. In contrast, the catheter segments loaded with 2 and 5 % of NIC showed only few bacteria adhered to the surface.

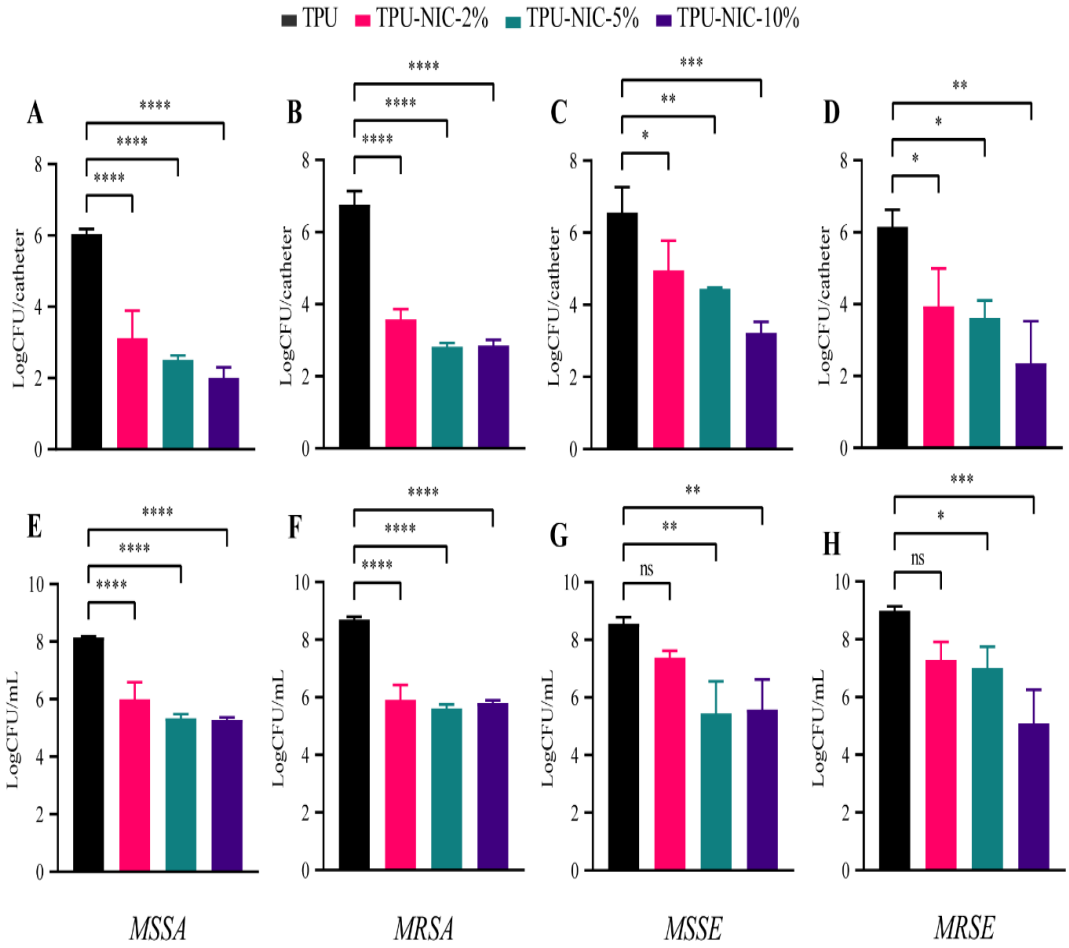

Figure 7. *In vitro* activity of NIC-loaded catheters against biofilm formation and planktonic growth in the surrounding medium after inoculation with 5×10^6 CFU of different *S. aureus* and *S. epidermidis* strains. Top row: biofilm growth (24 h) on catheters segments and bottom row: Planktonic bacterial growth in surrounding media (24 h) of A, E) MSSA; B, F) MRSA; C, G) MSSE and D, H) MRSE. Each group was analyzed in triplicate and data expressed as mean LogCFU with SD.

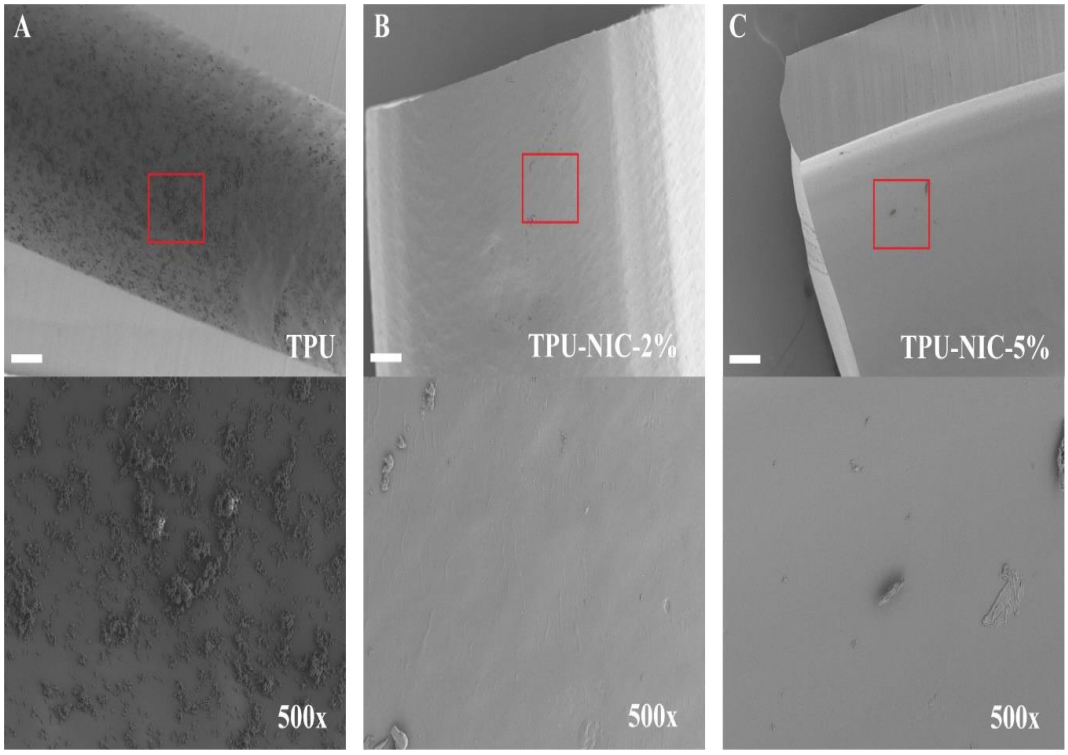

Figure *8.* (A-C) Representative SEM images of 24 h biofilm formation of MSSA on catheter surfaces. Low magnification (top row, 100×) and higher magnification views (bottom row, 500×) of longitudinally sectioned catheter segments showing intraluminal bacterial colonization of TPU (A) and TPU loaded with 2 and 5 % of NIC (B and C).

IN VIVO EVALUATION OF TPU-CATHETERS LOADED WITH NIC IN A BAI MODEL.

Due to significantly changes in the mechanical properties of catheters loaded with 10 % which could compromise the structural integrity and to avoid potential adverse effects *in vivo*, we assessed the *in vivo* efficacy of catheters loaded with 2 and 5 % of NIC against the MSSA (Figure 9A-B). On day 1, the retrieved catheter segments loaded with 2 and 5 % NIC exhibited a significantly lower bacterial load than non-loaded catheter segments (for both loadings, $p = < 0.0001$). On day 3 and 7 post infection a further reduction was observed in the bacterial burden of the NIC-loaded catheters and the respective surrounding tissues than the corresponding unloaded control. Finally, after 14 days, bacterial load was greatly reduced (LogCFU reduction of ~5.7, $p = < 0.0001$) on NIC loaded catheters which was in

line with further bacterial reduction in surrounding tissue (LogCFU reduction of ~4.2, $p = < 0.0001$) (Figure 9A-B).

As the NIC-loaded catheters were effective against MSSA, in a subsequent experiment we challenged them with the MRSA (Figure 9C-D). On day 1 after infection, mice carrying catheter segments with 2 and 5 % of NIC had significantly lower bacterial numbers on their catheters than mice with unloaded catheters (p= .001 and $p = < 0.0001$, respectively). The bacterial load of surrounding tissue of catheters with NIC was significantly reduced as well. On the following days, the bacterial burden on catheter segments and in the surrounding tissue from animals carrying NIC-loaded catheter segments was observed to gradually decrease over time, registering the lowest bacterial numbers on day 14 (for both NIC loadings $p = < 0.0001$) (Figure 9C-D). A few colonies isolated at day 14 presented increased MIC values for NIC (MIC of 1 (2 colonies), 2 and 8 µg/mL (1 colony each), but most of the colonies tested had the same MIC as that of the original strain (0.25 µg/mL; 56 colonies)

Histology of tissue surrounding the catheters was performed on tissue samples from mice infected with MSSA and sacrificed on day 3 (Figure 9E). In mice carrying non-loaded catheter segments without infection, the inflammation reaction was characterized by a small number of neutrophils and macrophages, with minimal fibrin deposition restricted to peri-catheter tissue. In addition, no necrosis was observed in this group (Figure 9E). On the other hand, in biopsies from mice with infected non-NIC-loaded catheter segments, the inflammation was characterized by the presence of abundant neutrophils and less macrophages which were embedded in abundant edema and fibrin. Extensive necrosis was observed around the catheter segments, variably extending into the surrounding tissues. Moreover, a full-thickness coagulative skin necrosis was observed in this group (Figure 9E). Intralesional bacterial biofilm formation was observed within the necrotic debris that surrounded the catheter segment. Additionally, features such as epidermal hyperplasia, furunculosis and skin ulceration were registered in the tissue. Animals with NIC-loaded catheter segments showed morphological changes similar to those present in the infected mice with non-loaded catheters, however the severity was

not as marked. Additionally in the same biopsies, we observed a moderate number of neutrophils and macrophages with moderate fibrin deposition. Furthermore, a minimal number of necrotic debris was found in the surrounding tissue and no bacterial aggregates were observed.

The NIC distribution *in-situ* in the surrounding tissue is shown in Figure 9F. An initial NIC level of 407 and 932 ng/g of tissue was recorded in mice bearing catheter segments with 2 and 5 % NIC, respectively. After 3 days, NIC levels of 781 ng/g and 312 ng/g were recorded in the surrounding tissue of catheter segments loaded with 2 and 5% NIC, respectively. On the following experimental days, the *in situ* NIC concentration decreased in the surrounding tissue, reaching the lowest values of 65 ng/g (NIC 2 %) and 135 ng/g (NIC 5 %) on day 14. The *in vivo* level of NIC in plasma is shown in Figure 9G. After 1 day, NIC plasma levels of 20 and 47 ng/mL were measured for catheters with 2 and 5 % of NIC, respectively. On the consecutive time points, the NIC plasma levels for both NIC loadings gradually dropped over time, reaching levels at the limit of detection on day 14.

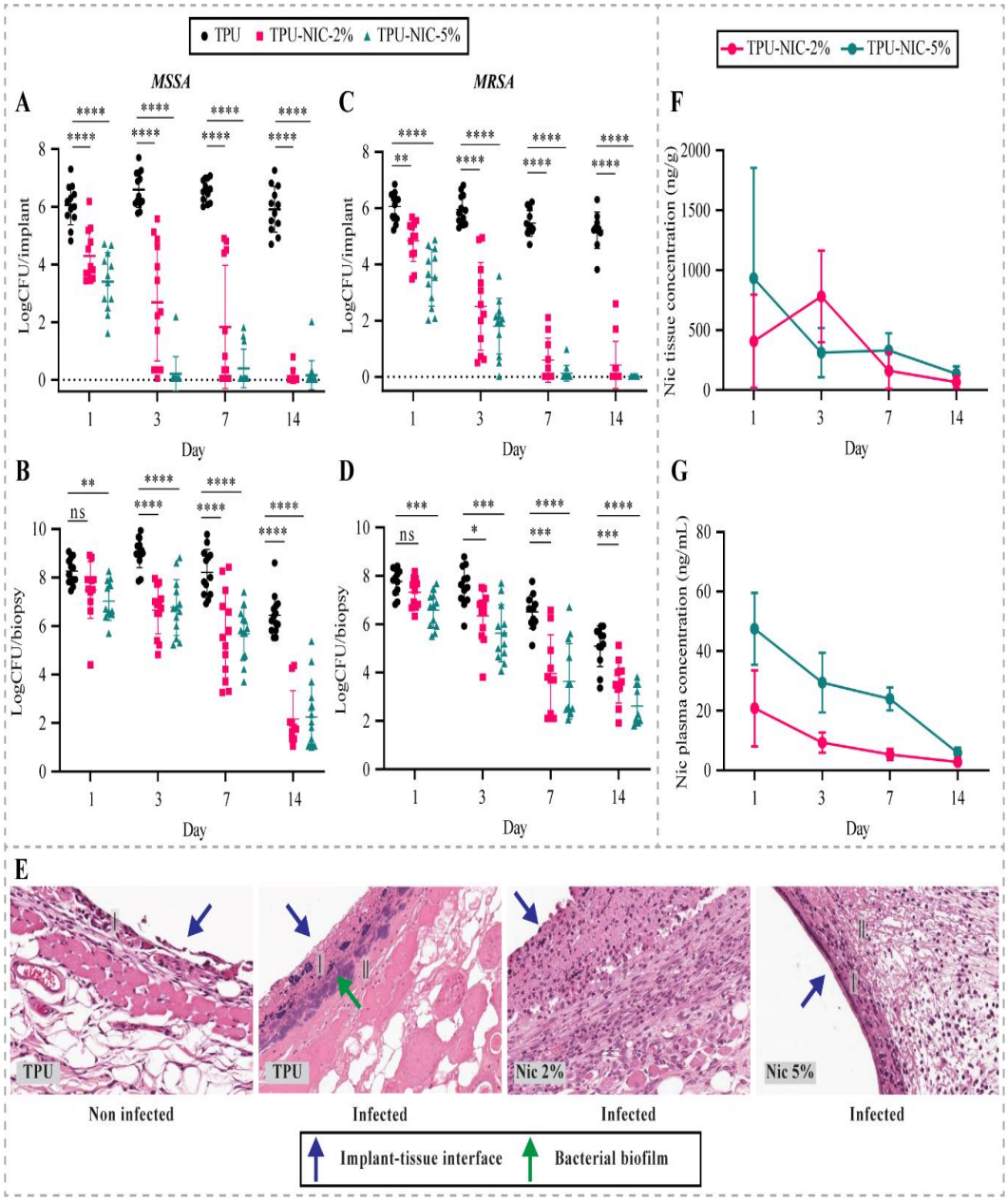

Figure 9. Antibacterial evaluation of TPU catheters loaded with 2 and 5 % of NIC at 1, 3, 7 and 14 days after implantation and infection using a BAI model. *In vivo* efficacy of NIC-loaded catheters on MSSA colonization of A) catheters and B) peri-catheter tissue. Efficacy of NIC-loaded catheters on MRSA colonization of C) catheter and D) peri-catheter tissue. E) Histological analysis of MSSA subcutaneous biofilm infections in peri-catheter tissue sections of animals implanted with non-loaded and NIC-loaded catheters (I) Infiltration of neutrophiles/macrophages, (II) Fibrin deposition. Mice carrying non-loaded catheter segments without infection were used for baseline histological observations. Pharmacokinetic profiles of NIC released from catheters loaded with 2 and 5 % NIC over 14 days. Concentration of NIC F) in peri-catheter tissue and G) in plasma. * Indicates a p-value of 0.01 to 0.05, ** indicates a p-value of 0.001 to 0.01, *** p-value of 0.0001 to 0.001, **** indicates a p value < 0.0001

DISCUSSION AND CONCLUSION

Catheters are essential medical devices which are mainly used for diagnosis, prevention, and treatment of many diseases and health conditions [1]. Catheters are mainly fabricated by HME process in which medical grade polymers are fed into an extrusion machine, then heated up to melting and finally extruded through a nozzle [43]. Anti-infective catheters can be produced by loading the active pharmaceutical ingredient (API) within the polymeric matrix of the catheter. This can be done via HME processes, however, the thermal stability of the loaded API should be taken into consideration to avoid any possible degradation [44].

We developed a novel NIC eluting catheter adapting the methodology previously described by Shaqour *et al.* [29] to prevent catheter related infections. We used NIC, as a repurposed antibacterial drug, to minimize the potential development of antibiotic resistance which currently is a rising global health issue [45]. Moreover, the potential antibacterial activity of NIC has been tested against multi-drug resistant bacteria such as methicillin-resistant *S. aureus* and *S. epidermidis*, two of the most prominent device-related pathogens [13, 14]. Furthermore, NIC has not only been proven biologically active in different preclinical models but also not toxic in clinical trials [15, 21, 46-49].

We confirmed that NIC can withstand processing temperatures (up to 180°C) without undergoing degradation [42] and any detrimental changes in its *in vitro* antibacterial and *in vitro* cytotoxic activity. Under the present *in vitro* experimental conditions non-heated and heated NIC similarly affected the viability of the L929 cells which indicates no change in the biological effect of NIC after heating treatment. Moreover, It has been reported that NIC is active in varying degrees against cell lines from different origin[24, 50-52]. Considered together, these results prove NIC's suitability to fabricate anti-infective medical devices by using not only HME but also different processes involving temperatures at least up to 180°C such as melt extrusion 3D-printing technologies. After proving the suitability of NIC for HME applications, NIC-loaded TPU catheters were fabricated at loadings of 2, 5 and 10 % NIC (*w/w*). Overall, the addition of NIC at 2 and 5 % (*w/w*) did not alter

the mechanical properties of the TPU fibers which would likely be the same for NIC-loaded catheters. A NIC loading of 10 % significantly affected the mechanical properties which may affect the mechanical stability of such catheters. The incorporation of NIC into the polymeric matrix of TPU catheters was confirmed by the appearance of new functional groups in the FTIR spectra. These changes in NIC-loaded TPU likely are due to covalent modifications, while the shift of spectral bands characteristic of the TPU or the immobilized NIC may indicate non-covalent interaction [53, 54]. Moreover, NIC underwent a phase transition from crystalline to an amorphous form within the NIC-loaded catheters. This drug phase transition is likely caused by the combined effect of solvent casting and the HME process during catheter production [42, 55]. The amorphous form of NIC improves the drug's bioavailability, which in turn is pivotal for a successful delivery of the drug within a host and to exert the intended antibacterial effect [55].

Catheters loaded with NIC presented a steady drug release over 27 days. In similar drug-loaded implants, the drug release is mainly mediated by passive diffusion, which governs how the drug migrates towards the external media [56]. In drug delivery systems governed by diffusion, the release kinetics relies on the solubility of the drug in the polymer, the diffusion coefficient of the drug, the drug loading, and the degradation of the polymer[57]. In fact, we observed that the total amount of released NIC to the media was dependent on the drug loading.The *in vitro* antibacterial properties of NIC-loaded catheter segments were demonstrated by both a disc diffusion assay and the quantification of biofilm-forming bacteria on catheter surfaces and planktonic bacterial growth in liquid media [58]. Not only did the NIC prevent/reduce biofilm formation, the apparent release of NIC in the medium inhibited the bacteria to grow. The released concentrations of NIC however did not kill the planktonic bacteria, since their numbers did not significantly decrease relative to the inoculum, suggesting a bacteriostatic activity of released NIC.

Based on the *in vitro* studies, we next investigated whether the protective activity of NIC-loaded catheters with 2 and 5 % of NIC would translate to *in vivo* efficacy

using a BAI model. In prior studies, this *in vivo* model has been proven useful to fast track the development of new antimicrobials and anti-infective medical devices to combat device related infections [59]. In this *in vivo* model, the NIC-loaded catheters exhibited a similar antibacterial efficacy against both MSSA and MRSA strains for at least 14 days. The *in vivo* activity was reflected in significantly reduced bacterial colonization of both the catheter segments and the peri-catheter tissue. Several colonies re-cultured from the tissue of mice with 2 % or 5 % NIC-loaded catheter segments displayed elevated MIC values. As the antibacterial indication is not approved for NIC, there are no data available of resistance concentration breakpoints for clinical susceptibility. The shifts in the MIC of NIC could be due to either emergence of resistance or tolerance, and in case of the later, it could be circumvented by delivering therapeutically attainable NIC concentrations to the infection site. Apparently, the elevated MIC had not resulted in dominance of this trait in the bacteria in the tissue since most of the retrieved colonies had lower MIC values. Resistance development of Gram-positive bacteria to NIC has to the best of our knowledge not been reported until now but should be kept in mind as a possibility of prolonged *in vivo* exposure to concentrations released, which are decreasing over time. Therefore, we strongly suggest performing NIC susceptibility assays with bacteria re-cultured from *in vivo* models with NIC as the antimicrobial agent. On the other hand, Gram-negative bacteria possess inherent resistance to NIC, mediated by efflux pumps and nitro-reduction [60]. Interestingly, it has been reported that co-administration of NIC and colistin exerted *in vivo* synergistic antibacterial efficacy against resistant *Pseudomonas aeruginosa* in a skin abscess infection model, which is a difficult to treat infection with standard antibiotics alone [60]. Therefore, the development of catheters containing NIC and synergistic antibiotics holds potential to decrease the likelihood of emergence of newly NIC tolerance/resistance while increasing the antibacterial efficacy against Gram positive and Gram-negative bacteria.

The reduction of bacterial colonization in surrounding tissue was also confirmed by histological analysis, which is relevant since peri-catheter tissue is a niche allowing infecting bacteria to survive in device related infections [61, 62]. Also, NIC-loaded

catheters hold the potential to elicit a complete anti-infective protection against bacteria coming from the skin or emanating from contaminated hubs [5, 63, 64]. In addition, our data suggest that NIC is rapidly released and retained into peri-catheter tissue, since the local tissue concentration was several folds higher than in plasma. Importantly these NIC plasma levels have been reported to not exert systemic toxicity [21, 46, 47]. The higher NIC levels in tissue indicate that NIC likely slowly diffuses through the tissue and into the blood vessels. From similar reported *in vivo* release kinetics, we can hypothesize that once in blood NIC undergoes a rapid systemic clearance which in fact will minimize the systemic concentrations of NIC [65]. In addition, considering the amount of NIC in the loadings of 2 and 5 % per 1 cm catheter, and the initial mean weight of the mice (~20 g) at the beginning of the experiments, we approximately administered to the mice a NIC dose of 12.5 mg/kg and 31.25 mg/kg per a NIC loading of 2 and 5 % respectively. Different preclinical studies have reported that daily subcutaneous NIC doses of 1 and 10 mg/kg and intraperitoneal NIC doses of 10, 20 ,30 and 50 mg/kg did not exert any toxic effect in mice after several days of treatment [60, 66-70]. Moreover, the acute oral toxicity LD_{50} value for mice is 1500 mg/kg while the subcutaneous LD_{50} value is >1000 mg/kg[71]. In its anthelmintic indication NIC is administered orally at a dose of 2000 mg/patient and is well tolerated by human patients[72]. Furthermore, the amount of NIC loaded in the catheters is gradually released into the peri-catheter tissue which modulates the real concentration of bioavailable NIC overtime and therefore minimizes the exposure to potential systemic toxic NIC levels.

Although the BAI model does not completely mimic a catheterization in mice, this model offers relevant valid *in vivo* information on the functionality of NIC-loaded catheters to resist *S. aureus* infection in potential clinical conditions [59]. Moreover, our results suggest a potential clinical application for NIC-loaded TPU catheters, as NIC was able to combat infection by the MRSA strain tested, and MRSA strains are known to cause most of the life-threatening staphylococcal infections [53, 54]. Furthermore, the approach followed in this research work could be applied for developing novel NIC-functionalized medical devices to prevent or treat

staphylococcal infections such as those associated with wounds, heart valves, urinary catheters, intra-uterine devices, voice prostheses, endotracheal tubes, and prosthetic implants. In future studies it would be interesting to use combinations of NIC and other antibacterial agents to generate broad-spectrum antibacterial catheters. In conclusion, this research work serves as a proof of concept of the potential use of NIC to develop medical devices using high-temperature manufacturing technologies, for preventing device related infections.

ACKNOWLEDGMENT

This research was funded by the research project PRINTAID, the EU Framework Programme for Research and Innovation within Horizon 2020—Marie kłodowska-Curie Innovative Training Networks under grant agreement No. 722467.The authors would like to thank Prof. Christophe Vande Velde from the Intelligence in Processes, Advanced Catalysts and Solvents (iPRACS) research group, Antwerp University for allowing researchers to use the thermogravimetric analysis machine in his lab. Additionally, Mr. Jean-Pierre Smet from the Material Science department for allowing researchers to use the tensile machine in his lab. We would also like to thank Edwin Scholl and Dr. Nicole van der Wel (Electron Microscopy Center Amsterdam (EMCA), Amsterdam UMC) for their technical assistance in the collection of the SEM images. We would also like to thank Dr. Bartłomiej Wysocki and Agnieszka Chmielewska for producing the coaxial nozzle that were used to extrude the catheters.

AUTHOR CONTRIBUTIONS

Conceptualization A.V., B.S., C.G.-P., A.F., L.F., M.R., P.C., S.A.J.Z., B.V, K.B, V.C. and W.S.; investigation A.V., B.S., C.G.-P and E.C.; writing—original draft preparation A.V., B.S. and C.G.-P.; writing—review and editing A.F., L.F., V.C., M.R.,P.C., S.A.J.Z., E.C. and P.C.; supervision A.F., L.F., P.C., M.R., S.A.J.Z., B.V., K.B., V.C. and W.S.; funding acquisition A.F., L.F., B.V., K.B., P.C., S.A.J.Z., W.S. and P.C. All authors have read and agreed to the published version of the manuscript.

REFERENCES

1. French, P., D. Tanase, and J. Goosen, *Sensors for catheter applications.* Sensors Update, 2003. **13**(1): p. 107-153.
2. O'grady, N.P., et al., *Guidelines for the prevention of intravascular catheter–related infections.* Clinical infectious diseases, 2002. **35**(11): p. 1281-1307.
3. Dudeck, M.A., et al., *National Healthcare Safety Network (NHSN) Report, data summary for 2010, device-associated module.* American journal of infection control, 2011. **39**(10): p. 798.
4. Lee, Y.-M., et al., *Clinical impact of early reinsertion of a central venous catheter after catheter removal in patients with catheter-related bloodstream infections.* Infection Control & Hospital Epidemiology, 2021. **42**(2): p. 162-168.
5. O'Grady, N.P. and S.S. Kadri, *Central venous catheter failures: nowhere near zero.* Critical care medicine, 2018. **46**(12): p. 2054.
6. Katneni, R. and S.S. Hedayati, *Central venous catheter-related bacteremia in chronic hemodialysis patients: epidemiology and evidence-based management.* Nature Clinical Practice Nephrology, 2007. **3**(5): p. 256-266.
7. Mah, T.-F.C. and G.A. O'Toole, *Mechanisms of biofilm resistance to antimicrobial agents.* Trends in microbiology, 2001. **9**(1): p. 34-39.
8. Arciola, C.R., D. Campoccia, and L. Montanaro, *Implant infections: adhesion, biofilm formation and immune evasion.* Nature Reviews Microbiology, 2018. **16**(7): p. 397.
9. Saint, S., D.L. Veenstra, and B.A. Lipsky, *The clinical and economic consequences of nosocomial central venous catheter-related infection: are antimicrobial catheters useful?* Infection Control & Hospital Epidemiology, 2000. **21**(6): p. 375-380.
10. Zander, Z.K. and M.L. Becker, *Antimicrobial and antifouling strategies for polymeric medical devices*. 2018, ACS Publications.
11. Farha, M.A. and E.D. Brown, *Drug repurposing for antimicrobial discovery*. Nature Microbiology, 2019. **4**(4): p. 565-577.
12. Organization, W.H., *World Health Organization model list of essential medicines: 21st list 2019*. 2019, World Health Organization.
13. Rajamuthiah, R., et al., *Repurposing salicylanilide anthelmintic drugs to combat drug resistant Staphylococcus aureus.* PloS one, 2015. **10**(4): p. e0124595.

14. Gwisai, T., et al., *Repurposing niclosamide as a versatile antimicrobial surface coating against device-associated, hospital-acquired bacterial infections.* Biomedical Materials, 2017. **12**(4): p. 045010.
15. Brunaugh, A.D., et al., *Development and evaluation of inhalable composite niclosamide-lysozyme particles: A broad-spectrum, patient-adaptable treatment for coronavirus infections and sequalae.* PloS one, 2021. **16**(2): p. e0246803.
16. Xu, J., et al., *Discovery of niclosamide and its O-alkylamino-tethered derivatives as potent antibacterial agents against carbapenemase-producing and/or colistin resistant Enterobacteriaceae isolates.* Bioorganic & medicinal chemistry letters, 2019. **29**(11): p. 1399-1402.
17. Das, S., A. Dasgupta, and S. Chopra, *Drug repurposing: a new front in the war against Staphylococcus aureus.* Future microbiology, 2016. **11**(8): p. 1091-1099.
18. Torres, N.S., et al., *Screening a commercial library of pharmacologically active small molecules against Staphylococcus aureus biofilms.* Antimicrobial agents and chemotherapy, 2016. **60**(10): p. 5663-5672.
19. Zhurina, M., et al., *Niclosamide as a promising antibiofilm agent.* Microbiology, 2017. **86**(4): p. 455-462.
20. Gilbert-Girard, S., et al., *Optimization of a High-Throughput 384-Well Plate-Based Screening Platform with Staphylococcus aureus ATCC 25923 and Pseudomonas aeruginosa ATCC 15442 Biofilms.* International journal of molecular sciences, 2020. **21**(9): p. 3034.
21. Whitesell, J.K., *The Merck Index, CD-ROM (Macintosh): An Encyclopedia of Chemicals, Drugs & Biologicals Edited by S. Budavari, M. O'Neill, A. Smith, P. Heckelman, and J. Kinneary (Merck & Co., Inc.). Chapman & Hall: New York. 1997. $250.00. ISBN 0-412-75940-3.* 1998.
22. Chen, W., et al., *Niclosamide: Beyond an antihelminthic drug.* Cellular signalling, 2018. **41**: p. 89-96.
23. Kadri, H., O.A. Lambourne, and Y. Mehellou, *Niclosamide, a Drug with Many (Re)purposes.* ChemMedChem, 2018. **13**(11): p. 1088-1091.
24. Tharmalingam, N., et al., *Repurposing the anthelmintic drug niclosamide to combat Helicobacter pylori.* Scientific reports, 2018. **8**(1): p. 3701.
25. Mohammad, H., et al., *Repurposing niclosamide for intestinal decolonization of vancomycin-resistant enterococci.* International journal of antimicrobial agents, 2018. **51**(6): p. 897-904.

26. Domalaon, R., et al., *The anthelmintic drug niclosamide synergizes with colistin and reverses colistin resistance in Gram-negative bacilli.* Antimicrobial agents and chemotherapy, 2019. **63**(4).
27. Copp, J.N., et al., *Mechanistic understanding enables the rational design of salicylanilide combination therapies for Gram-negative infections.* Mbio, 2020. **11**(5).
28. Verstraete, G., et al., *Thermoplastic polyurethane-based intravaginal rings for prophylaxis and treatment of (recurrent) bacterial vaginosis.* International Journal of Pharmaceutics, 2017. **529**(1): p. 218-226.
29. Shaqour, B., et al., *Coupling Additive Manufacturing with Hot Melt Extrusion Technologies to Validate a Ventilator-Associated Pneumonia Mouse Model.* Pharmaceutics, 2021. **13**(6): p. 772.
30. Iso, I., *10993–5: 2009 Biological evaluation of medical devices—part 5: tests for in vitro cytotoxicity*. International Organization for Standardization, Geneva, 2009.
31. Sabee, M.M., et al. *Gentamicin loaded PLA microspheres susceptibility against Staphylococcus aureus and Escherichia coli by Kirby-Bauer and micro-dilution methods*. in *AIP Conference Proceedings*. 2020. AIP Publishing LLC.
32. Weinstein, M.P., *Methods for dilution antimicrobial susceptibility tests for bacteria that grow aerobically. M07* 11 ed. 2018: Clinical and Laboratoy Standards Institute.
33. Mandel, S., et al., *OMN6 a novel bioengineered peptide for the treatment of multidrug resistant Gram negative bacteria.* Scientific Reports, 2021. **11**(1): p. 6603.
34. Law, K.-Y., *Definitions for Hydrophilicity, Hydrophobicity, and Superhydrophobicity: Getting the Basics Right.* The Journal of Physical Chemistry Letters, 2014. **5**(4): p. 686-688.
35. Naqvi, S., S. Mohiyuddin, and P. Gopinath, *Niclosamide loaded biodegradable chitosan nanocargoes: an in vitro study for potential application in cancer therapy.* Royal Society Open Science, 2017. **4**(11): p. 170611.
36. Mathew, E., et al., *Fused deposition modeling as an effective tool for anti-infective dialysis catheter fabrication.* ACS Biomaterials Science & Engineering, 2019. **5**(11): p. 6300-6310.
37. Zaazaa, H.E., et al., *Kinetic study and mechanism of Niclosamide degradation.* Spectrochimica Acta Part A: Molecular and Biomolecular Spectroscopy, 2014. **132**: p. 655-662.

38. Jiang, L., et al., *Electrospun nanofibrous thermoplastic polyurethane/poly (glycerol sebacate) hybrid scaffolds for vocal fold tissue engineering applications.* Materials Science and Engineering: C, 2019. **94**: p. 740-749.
39. Kowalczuk, D. and M.J.M. Pitucha, *Application of FTIR method for the assessment of immobilization of active substances in the matrix of biomedical materials.* 2019. **12**(18): p. 2972.
40. Sanphui, P., S.S. Kumar, and A. Nangia, *Pharmaceutical Cocrystals of Niclosamide*. Crystal Growth & Design, 2012. **12**(9): p. 4588-4599.
41. Witzleben, S.T., et al., *Investigation of temperature dependency of morphological properties of thermoplastic polyurethane using WAXS and SAXS monitoring.* 2015.
42. Jara, M.O., Z.N. Warnken, and R.O. Williams, *Amorphous Solid Dispersions and the Contribution of Nanoparticles to In Vitro Dissolution and In Vivo Testing: Niclosamide as a Case Study.* Pharmaceutics, 2021. **13**(1): p. 97.
43. Cho, S., et al., *Extrusion Characteristics of Thin Walled Tubes for Catheters Using Thermoplastic Elastomer.* Polymers, 2020. **12**(8): p. 1628.
44. Shaqour, B., et al., *Production of Drug Delivery Systems Using Fused Filament Fabrication: A Systematic Review.* Pharmaceutics, 2020. **12**(6): p. 517.
45. Organization, W.H., *Antimicrobial resistance: global report on surveillance*. 2014: World Health Organization.
46. Chang, Y.-W., et al., *Pharmacokinetics of anti-SARS-CoV agent niclosamide and its analogs in rats.* Journal of Food and Drug Analysis, 2006. **14**(4).
47. Barbosa, E.J., et al., *Niclosamide repositioning for treating cancer: Challenges and nano-based drug delivery opportunities.* European Journal of Pharmaceutics and Biopharmaceutics, 2019. **141**: p. 58-69.
48. Backer, V., et al., *A randomized, double-blind, placebo-controlled phase 1 trial of inhaled and intranasal niclosamide: A broad spectrum antiviral candidate for treatment of COVID-19.* The Lancet Regional Health-Europe, 2021: p. 100084.
49. Parikh, M., et al., *Phase Ib trial of reformulated niclosamide with abiraterone/prednisone in men with castration-resistant prostate cancer.* Scientific reports, 2021. **11**(1): p. 1-7.
50. Hamdoun, S., P. Jung, and T. Efferth, *Drug Repurposing of the Anthelmintic Niclosamide to Treat Multidrug-Resistant Leukemia.* Frontiers in pharmacology, 2017. **8**: p. 110-110.

51. Zhang, J.L., et al., *New life for an old drug: in vitro and in vivo effects of the anthelmintic drug niclosamide against Toxoplasma gondii RH strain.* 2019. **9**: p. 27-34.
52. Hochmair, M., et al., *Effects of salinomycin and niclosamide on small cell lung cancer and small cell lung cancer circulating tumor cell lines.* 2020. **38**(4): p. 946-955.
53. Kowalczuk, D. and M. Pitucha, *Application of FTIR Method for the Assessment of Immobilization of Active Substances in the Matrix of Biomedical Materials.* Materials, 2019. **12**(18): p. 2972.
54. Kowalczuk, D., *FTIR Characterization of the Development of Antimicrobial Catheter Coatings Loaded with Fluoroquinolones.* Coatings, 2020. **10**(9): p. 818.
55. Baghel, S., H. Cathcart, and N.J. O'Reilly, *Polymeric amorphous solid dispersions: a review of amorphization, crystallization, stabilization, solid-state characterization, and aqueous solubilization of biopharmaceutical classification system class II drugs.* Journal of pharmaceutical sciences, 2016. **105**(9): p. 2527-2544.
56. Stewart, S.A., et al., *Implantable polymeric drug delivery devices: Classification, manufacture, materials, and clinical applications.* 2018. **10**(12): p. 1379.
57. Pillai, O. and R.J.C.o.i.c.b. Panchagnula, *Polymers in drug delivery.* 2001. **5**(4): p. 447-451.
58. Amin Yavari, S., et al., *Combating Implant Infections: Shifting Focus from Bacteria to Host.* Advanced Materials, 2020. **32**(43): p. 2002962.
59. Nowakowska, J., R. Landmann, and N. Khanna, *Foreign Body Infection Models to Study Host-Pathogen Response and Antimicrobial Tolerance of Bacterial Biofilm.* Antibiotics (Basel, Switzerland), 2014. **3**(3): p. 378-397.
60. Copp, J.N., et al., *Mechanistic understanding enables the rational design of salicylanilide combination therapies for Gram-negative infections.* 2020. **11**(5): p. e02068-20.
61. Zaat, S.A.J., C.A.N. Broekhuizen, and M. Riool, *Host tissue as a niche for biomaterial-associated infection.* Future microbiology, 2010. **5**(8): p. 1149-1151.
62. Zaat, S.A.J., *Tissue colonization in biomaterial-associated infection*, in *Biomaterials associated infection*. 2013, Springer. p. 175-207.
63. Mermel, L.A., *What is the predominant source of intravascular catheter infections?* Clinical Infectious Diseases, 2011. **52**(2): p. 211-212.

64. Casimero, C., et al., *Minimising Blood Stream Infection: Developing New Materials for Intravascular Catheters.* Medicines, 2020. **7**(9): p. 49.
65. Zhang, D., et al., *Drug concentration asymmetry in tissues and plasma for small molecule–related therapeutic modalities.* Drug Metabolism and Disposition, 2019. **47**(10): p. 1122-1135.
66. Thatikonda, S., V. Pooladanda, and C.J.J.o.c.p. Godugu, *Repurposing an old drug for new use: Niclosamide in psoriasis-like skin inflammation.* 2020. **235**(6): p. 5270-5283.
67. Boyapally, R., et al., *Niclosamide alleviates pulmonary fibrosis in vitro and in vivo by attenuation of epithelial-to-mesenchymal transition, matrix proteins & Wnt/β-catenin signaling: A drug repurposing study.* 2019. **220**: p. 8-20.
68. Liang, L., et al., *Inhibitory effects of niclosamide on inflammation and migration of fibroblast-like synoviocytes from patients with rheumatoid arthritis.* 2015. **64**(3): p. 225-233.
69. Londoño-Joshi, A.I., et al., *Effect of niclosamide on basal-like breast cancers.* 2014. **13**(4): p. 800-811.
70. Zhu, Y., et al., *Repurposing of the anti-helminthic drug niclosamide to treat melanoma and pulmonary metastasis via the STAT3 signaling pathway.* 2019. **169**: p. 113610.
71. Hayes, W.J. and E.R. Laws, *Handbook of pesticide toxicology.* 1991.
72. Organization, W.H., *WHO specifications and evaluations for public health pesticides: niclosamide.* 2002.

CHAPTER 4

DEVELOPMENT OF NICLOSAMIDE-RELEASING COATINGS BY INK JET PRINTING FOR PREVENTING DEVICE-RELATED INFECTIONS

INTRODUCTION

The tremendous impact of health care-associated infections (HAIs) is demonstrated by the high number of deaths as well as the huge economic burden worldwide. In USA alone, annually there are about 2 million cases of HAIs and around 90,000 deaths, whilst an estimated of 4.5 million HAIs cases occur in Europe each year with an impact of around 37 000 deaths [1-3]. Since the management of HAIs are both challenging and expensive, the development of prevention technologies represents a cost-effective strategy to combat device-associated infections.

Medical devices are prone to bacterial colonization which in most of the cases leads to biofilm formation and the subsequent infection[4]. Once a device-associated infection is produced within the host, the functionality of the related medical device might be negatively affected, leading to the removal and substitution of the device[5]. However, the removal and substitution of an infected device does not ensure infections clearing, as bacterial cells may reside in device surrounding tissue[6]. Thus, the most promising antimicrobial-based strategies are those based on the prevention of bacterial colonization on the device and/or reducing the number of bacterial cells in the vicinity of the device; among such strategies, coatings releasing antibacterial agents are rapidly emerging as the most promising strategy to prevent device-associated infections[7]. Coating releasing antibacterial, can be formulated with biocompatible carrier polymers, and loaded with a broad range of active agents such as metals, antibiotics, biocides, phages, peptides and experimental drugs[8, 9]. Moreover, the release kinetics of the antibacterial agent can be tuned according to specific applications, offering the possibility to release the antibacterial agent in a controlled manner over the time[10]. Additionally, the antibacterial agent is delivered locally, achieving high local concentrations without triggering systemic toxicity[7].

Additive manufacturing (AM) technologies allow for the fabrication of complex structures and geometries from 3D model data by depositing layers of materials on the top of each other, to produce specific structures[11]. Among the different AM technologies, *Ink jet printing* (IJP) allows for the deposition of polymeric solutions (inks) on different surfaces to produce 2D and 3D structures[12]. Interestingly, this technology

has been adapted to deposit polymer coating films on medical device surfaces[13]. The polymeric ink coatings can be formulated with different antimicrobials and then deposited with specific and regular deposition patterns on medical devices to exert a pharmacological effect[14]. By using this approach, manufacturing-related costs can be significantly reduced as an exact amount of coating (and thus of drug) can be deposited on the device surface[13]. IJP technology has been utilized to coat different devices such as microneedles, and bone implants[15]. For example, Boehm et al developed an IJP method to coat accurately microneedles with a polymeric ink containing the antimycotic miconazole to treat fungal infections[16]. Gu et al, developed poly (lactic-co-glycolic acid) (PLGA) inks containing rifampicin which was then printed on TiAI6V4 surfaces. Interestingly, Rifampicin-containing coatings prevented the *in vitro* biofilm formation of *S. epidermidis[17]*. In a different study, Chen *et al*, deposited PLGA-rifampicin solutions onto polycaprolactone (PCL) chitosan nanofiber meshes via IJP. These coated meshes prevented the attachment of *S. epidermidis* cells while promoting osteoblasts adhesion[18].

Based on IJP technology, polymeric inks containing niclosamide, a repurposed drug with anti-staphylococcal activity, were developed to coat polyethylene catheters. This polymeric coating will release niclosamide in a controlled and sustained way, thus exerting its antimicrobial effect leading to the prevention device-associated infections.

MATERIALS AND METHODS

PREPARATION OF NICLOSAMIDE-POLYMER INK COATING FORMULATIONS

~~First,~~ Low density polyethylene (LDPE) tubing (Smiths Medical ASD, USA) was cut in 2-cm segments and treated to modify their surface by low pressure oxygen/argon plasma etching. The catheter segments were treated with oxygen/argon plasma (0.5 Torr) at a potency setting of 40 % (200 W) for 60 s.

In order to prepare the ink coating formulations, poly (DL-lactide), (PDLA), (PDL02A Purasorb, Corbion, Netherlands) or PDLA with different increasing concentrations of

Polyethylene glycol (PEG), (Sigma Aldrich, USA) were dissolved in 3:1 (V/V) ratio of Chloroform/Anisole (Sigma Aldrich, USA). The inks were sonicated for 15 minutes at room temperature (RT) and then transferred into syringe printer cartridges, which were set on the 3D printer (Table 1).

Coating	PDLA (mg/mL)	PEG (mg/mL)	Niclosamide (mg/mL)
PDLA-Nic	4.00	0.00	2.00
PDLA-PEG15-Nic	3.40	0.60	6.00
PDLA-PEG30-Nic	2.80	1.20	6.00
PDLA-PEG50-Nic	2.00	2.00	6.00

Table 1. Drug-polymer ink formulations for coating LDPE catheters.

INK DEPOSITION ON CATHETER SURFACE

Due to the cylindrical structure of the catheters and because their rotation during the coating process, a stepper motor rotating device coupled with a metallic shaft was designed. The catheter segments were set on the stepped shaft characterised by a diameter smaller than that of the catheter segments.

All the printings were performed using a commercial 3D Printer (3DDiscovery, regenHU, Switzerland) with a drop on demand print head set within a BSL2 flow cabinet permitting working under sterile conditions. Polymeric inks containing niclosamide were directly printed on catheter segments through a pressure-assisted microvalve print-head in the form of droplets of around 5 µL with a spatial resolution of approximately 0.225 mm. The nozzle used had a diameter of 150 µM and the printing parameters set were: dispensing pressure (1 bar), valve opening time (150 µs), valve closing time (127 µs), dosing distance (4 mm) and printing temperature (22 °C)

A coating pattern was defined by an algorithm in which the print-head dispenses polymeric inks longitudinally on the catheter and then the print-head moves longitudinally and vertically forming a rectangular shape over the catheter, returning to the starting point and printing again. At the end of each coating pattern the shaft rotates

at 90° to coat the next part of the surface. After depositing a cycle of 4 coating patterns a layer was completed (a whole rotation of 360°) (Fig.1). In total, 4 layers were printed on the catheter segments. After the printing process, to evaporate the remaining organic solvents in the coating, coated catheter segments were left under a laminar hood for 18 hours and then transferred to a low pressure (50 mbar) chamber for 24 hours. After the drying process, coated catheter segments were weighted to gravimetrically determine the amount of coating.

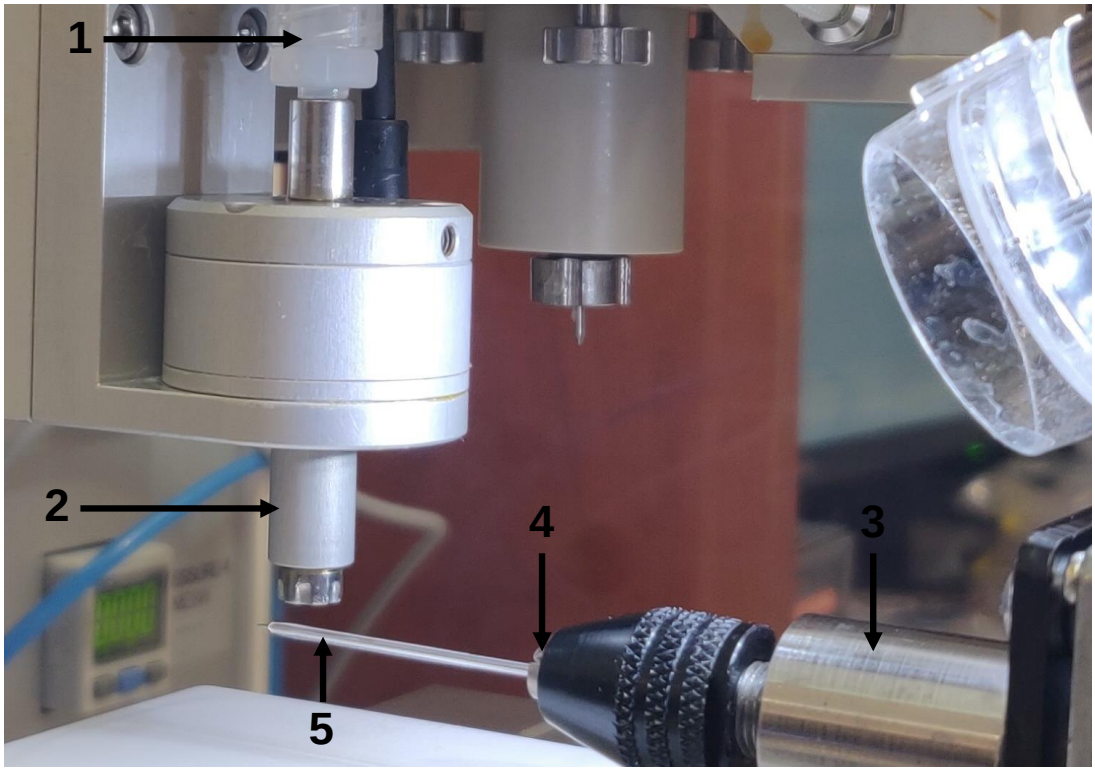

Figure 1. Customized drop on demand printing set up for controlled deposition of niclosamide-polymer coatings on LDPE catheters. 1) Printer cartridge loaded with ink; 2) printer head; 3) stepper motor; 4) metallic shaft; 5) catheter segment

IN VITRO DRUG RELEASE STUDY OF NIC-POLYMER COATINGS

To determine the drug release kinetics, titanium coupons were coated with the same printing parameters and the coating pattern was accordingly adapted to deposit the ink coatings on the circular surface of the coupons. Coated coupons were then immersed in induvial wells of a 6-well microtiterplate containing 1 ml of release media, phosphate buffered saline (PBS) with 2% of Tween 80 (v/v) (Sigma Aldrich, USA) per well, and

incubated at 37 °C with an agitation of 120 rpm. At specific intervals of time, the incubated release media was collected and the OD_{332mm} was measured in a spectrophotometer to calculate the amount of released niclosamide by extrapolating the values of a niclosamide calibration curve (Sup. Figure 1).

CHARACTERIZATION OF NICLOSAMIDE-POLYMER COATINGS

In order to confirm the correct incorporation of niclosamide and functionalization of the polymeric coatings, a Fourier-transform infrared spectroscopy (FTIR) analysis was performed on coated catheters. The catheters were analysed using a FTIR spectrophotometer (Nicolet 8700, ThermoScientific, Madison, WI, USA). The FTIR spectra were recorded in the spectral range of 4,000–600 cm^{-1} at 4 cm^{-1} spectral resolution.

In order to analyse changes in the hydrophobicity of catheter surfaces, the water contact angle of coated catheters was measured using demineralized water and OCA20 goniometer (Dataphysics, Germany). For each sample, the left and the right contact angles of at least 10 droplets with a volume of 2 µL were measured and averaged.

Scanning Electron Microscopy (SEM) was used to characterize the ultrastructural morphology of the polymeric coatings. Before imaging, samples were mounted on aluminium SEM stubs and sputter-coated with a 4 nm platinum–palladium layer using a Leica EM ACE600 sputter coater (Microsystems, Wetzlar, Germany). Images were acquired at 3 kV using a Zeiss Sigma 300 SEM (Zeiss, Oberkochen, Germany). Of each tube, 3-6 fields were viewed and photographed at 1000X magnification.

IN VITRO ANTIBACTERIAL ACTIVITY OF CATHETERS COATED WITH PDLA-NIC and PDLA-PEG50-NIC AND SEM VISUALIZATION

The antibacterial efficacy of the PDLA-Nic and PDLA-PEG50-Nic coatings against the Gram-positive bacteria *S. aureus* ATCC 25923 and *S. aureus* ATCC33591 was assessed using bacterial counts. Briefly, bacterial suspensions of *S. aureus* ATCC 25923 and *S. aureus* ATCC 33591(10^6 CFU/mL) were prepared in tryptic soy broth (TSB) (Sigma-Aldrich, USA).1-cm catheter segments coated with either PDLA-Nic or PDLA-PEG50-

Nic were immersed in 1 mL of the prepared bacterial suspensions and incubated at 37 °C, under shaking (120 rpm) for 24 hours.

After the incubation step, biofilm-forming bacteria attached to the catheter surface and remaining bacterial cells suspended in the TSB incubation media were enumerated by the drop plate method. Briefly, catheter segments were removed from incubation suspensions and washed 3 times in physiological saline solution to remove unbound bacteria. After that, catheter segments were placed in tubes containing 1 ml of PBS, vortexed for 30 seconds and sonicated for 15 minutes (40 kHz, RT). Resulting bacterial suspensions were then 10-fold serially diluted and spotted on tryptone soy agar (TSA) plates (Sigma Aldrich, USA) and incubated at 37 °C for 24 h. Colonies on TSA plates were enumerated, and the bacterial load (LogCFU/catheter) was calculated. In parallel, incubation suspensions containing planktonic bacterial cells were 10-fold serially diluted and plated onto TSA plates. TSA plates were incubated at 37 °C for 24 hours and the bacterial load was determined as mentioned before. All catheter segments were tested independently, and catheter segments coated with PDLA or PDLA-PEG50 were used as the controls.

SEM microscopy was performed in order to visualize *S. aureus* ATCC 25923 cells attached to catheter segments coated with either PDLA, PDLA-Nic, PDLA-PEG50-Nic or PDLA-PEG50 coatings. Briefly, coated catheter segments were incubated with *S. aureus* ATCC 25923 as aforementioned in this section until the third washing step with PBS. Subsequently, catheter segments were fixed in a solution of 4 % (v/v) paraformaldehyde added with 1 % (v/v) glutaraldehyde (Sigma Aldrich, USA) and incubated overnight at room temperature. Catheter segments were then rinsed with demi water and dehydrated in increasing ethanol concentrations, ranging from 50 to 100 % (v/v). After the dehydration step, catheter segments were immersed in hexamethyldisilane (Sigma Aldrich, USA) overnight and air dried. Finally, catheter segments were sputter coated and visualized using a Zeiss Sigma 300 SEM (Zeiss, Germany).

DISK DIFFUSION ASSAY

TSA plates were seeded with 10^7 CFU bacterial cells contained in 200 μL of PBS and immediately after 0.5-cm catheter segments coated with either PDLA, PDLA-Nic, PDLA-PEG50 or PDLA-PEG50-Nic were inserted vertically into the agar. Catheter

segments coated with PDLA and PDLA-PEG50 were used as the negative controls. TSA Plates were then incubated at 37 °C for 24 hours. The next day, the inhibition zone was measured, and catheter segments were transferred to freshly inoculated TSA plates. A daily serial passage to newly inoculated TSA plates was performed over 9 days.

EVALUATION OF THE ANTIBACTERIAL EFFICACY OF PDLA-NIC AND PDLA-PEG50-NIC COATINGS USING A SUBCUTANEOUS FOREIGN BODY INFECTION MODEL

To determine the *in vivo* efficacy to prevent material-associated infection of PDLA-NIC and PDLA-PEG50-NIC coatings, a subcutaneous foreign body infection model was used as described earlier in this dissertation (Chapter 3). of this thesis. As an *in vivo* proof of principle study, we challenged our antibacterial Nic-polymer coatings against *S. aureus* since this pathogen causes most of the device-associated infections[19]. For our *in vivo* studies the Methicillin sensitive *S. aureus* ATCC 25923 strain was used.

Animal experiments were conducted in accordance with Italian legislation, under approval of the internal Aptuit Committee on Animal Research and Ethics and under authorization issued by the Italian Ministry of Health (Italian Ministry of Health Authorization Project – Internal Code No. 21205). General procedures for animal care and housing were in accordance with the current Association for Assessment and Accreditation of Laboratory Animal Care recommendations. All the animals were subjected to an acclimation process and were kept as described in Chapter 3.

In order to conduct the foreign body infection model (Figure 2), animals were first anesthetized by inhalation of isoflurane (2.5 %, v/v) and immediately shaved with an electric razor. Subsequently, shaved skin was disinfected using a solution of Benzalkonium Chloride 0.175 % (Citrosil, Manetti and Roberts, Italy). A small incision was made in both flanks of the mice, after which a subcutaneous tunnel was created using sterile scissors. Immediately after, one catheter segment coated with either PDLA-Nic, PDLA-PEG50-Nic, PDLA or PDLA-PEG50-Nic coatings was accordingly implanted in each subcutaneous pocket. After catheter implantation, mice got infected by a subcutaneous injection of 10^6 CFU of *S. aureus* ATCCC25923 in 100 µL of saline

physiological solution. On day 3 and 7 post-infection, catheters and corresponding surrounding tissue were collected and processed as detailed in Chapter 3. Quantification of bacterial load in both catheters and surrounding tissue was performed by plating 10-fold serial dilutions in TSA plates. Bacterial load was expressed as the mean value LogCFU/catheter and LogCFU/biopsy ± standard deviation (SD)

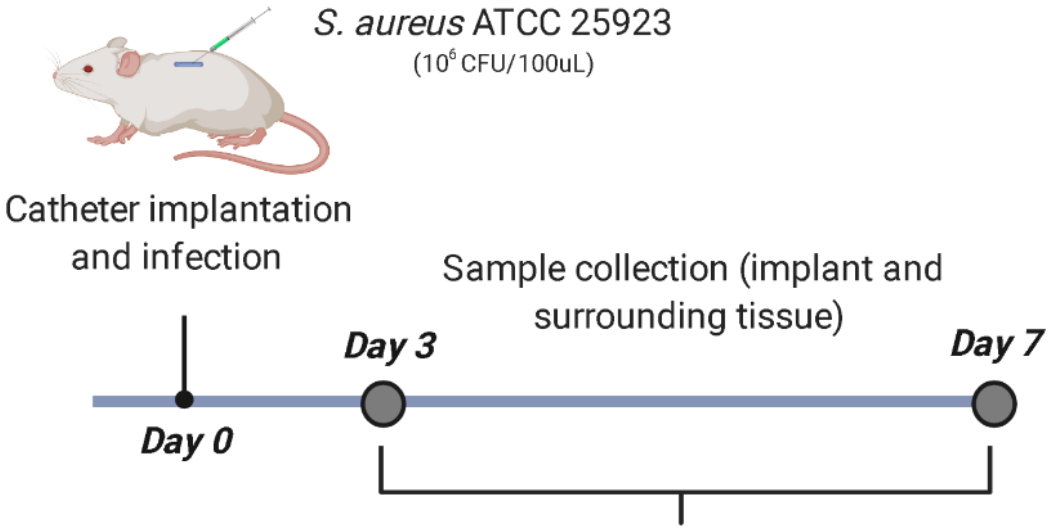

Figure 2. Antibacterial *In vivo* evaluation of catheters coated with PDLA-Nic and PDLA-PEG50-Nic using a foreign body infection model.

RESULTS

IN VITRO RELEASE STUDIES OF NIC-POLYMER COATINGS

All the different coating formulations were evaluated for drug release to select those exhibiting the most suitable niclosamide release pattern to be further characterized.
PDLA-Nic coating presented a drug burst release of 25.23 µg at 24 h, releasing niclosamide in a steady manner over 456 h (Figure 3). The addition of different concentrations of PEG to the PDLA formulation increased the drug release rate from the coatings. A drug burst release of 69.6, 67.5 and 118.2 µg at 24 h was registered for PDLA-PEG15-Nic, PDLA-PEG30-Nic and PDLA-PEG50-Nic coating, respectively.

As reported in the Figure 3, the cumulative release ratio of niclosamide from PDLA-Nic coatings was slow and steady as it was around 22 % at the end of the experiment (456 h).

The cumulative release ratio of Nic from PDLA-PEG15-Nic and PDLA-PEG30-Nic coatings was gradual during the first 192 h, registering a % of 53 and 66, respectively; after which the cumulative release reached a plateau for both coatings. On the other hand, niclosamide was almost released from PDLA-PEG50 coatings at 96 h as the cumulative release radio reached 79.6 %, immediately after this time point the release kinetics reached a plateau.

Given that PDLA formulations containing 50 % (w/w) of PEG showed the highest peak of niclosamide concentration during the first 96 h and over the consecutive 19 days, it was selected for further *in vitro* and *in vivo* characterization. Non- loaded PDLA and PDLA-PEG50 and PDLA-Nic formulations were tested as well for comparison purposes.

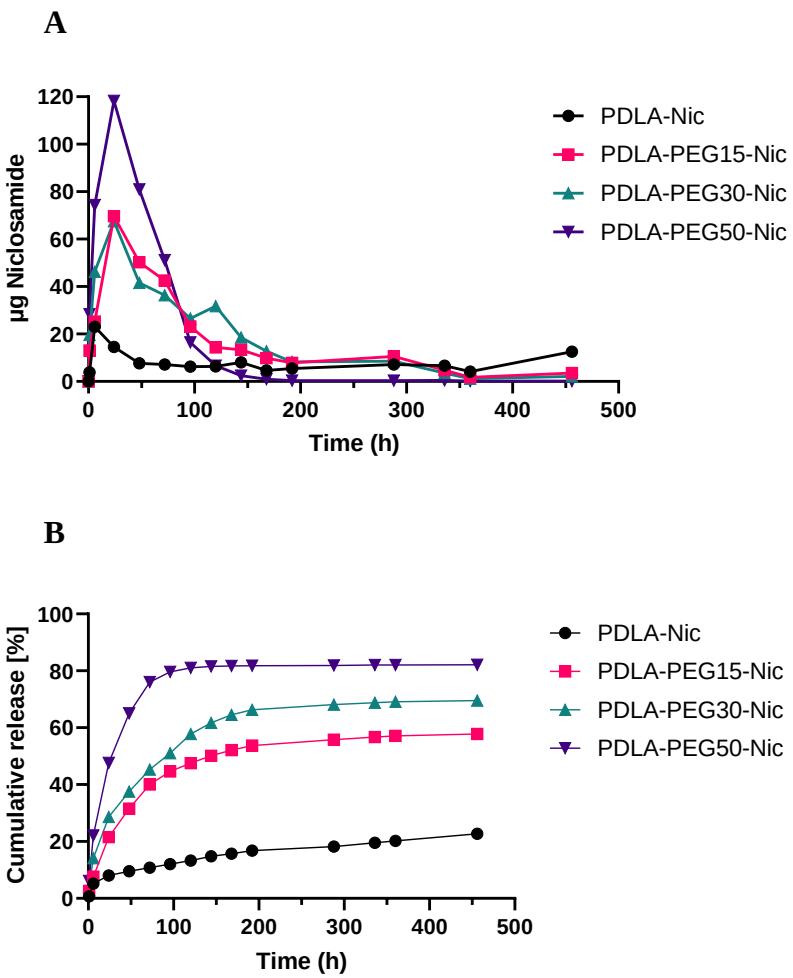

Figure 3. A) Amount of released niclosamide from different polymeric coatings. B) Cumulative niclosamide release pattern of different polymeric coatings.

CHARACTERIZATION OF NICLOSAMIDE-POLYMER COATINGS

The water contact angle was analyzed for possible modifications in the surface energy of the coated catheters. Figure 4 shows the water contact angle of catheter segments coated with different polymeric formulations. As it can be seen, there is a significant difference between LDPE catheters and LDPE catheters after plasma treatment. Additionally, a significant difference in surface energy among polymeric coatings (PDLA, PDLA-Nic, PDLA-PEG50 and PDLA-PEG50-Nic) and plasma-treated catheter was registered.

The FTIR spectra of neat niclosamide, non-loaded PDLA and PDLA-PEG50 coating, and Nic loaded PDLA and PDLA-PEG50 coatings are shown in Figure 4. The FTIR analysis for neat niclosamide showed bands at 3230 cm^{-1} , 3190 cm^{-} , 3090 cm^{-1} which correspond to -OH, =CH , -NH groups[20]. Moreover, Nic spectrum showed the characteristic bands at 1650 cm^{-1} (C=O stretching), 1610 cm^{-1}(C=C stretching), 1569 cm^{-1}(NH bending), 1518 cm^{-1}(NO_2 asymmetric stretching), 1420 cm^{-1}(CH_2 bending), 1355 cm^{-1} (CH_3 bending), 1218 cm^{-1}(C-0 stretching)[21, 22]

The PDLA coating spectra showed bands at 2995 cm^{-1} (CH_3 asymmetric stretching), 2940 cm^{-1} (CH_3 symmetric stretching), 1750 cm^{-1} (C=O stretching), 1455 cm^{-1} (CH_3 asymmetric bending), 1380 cm^{-1} (CH_3 symmetric bending), 1255 cm^{-1}(COC asymmetric stretching + C-CH_3 asymmetric rocking), 1175 cm^{-1} (CH_3 asymmetric rocking), 1115 cm^{-1}(COC symmetric stretching) , 1046 cm^{-1} (C-CH_3 stretching), 1075 cm^{-1} (COC symmetric stretching) [23-28]. The PDLA-PEG50 coating presented corresponding bands to the PDLA coating, in addition the spectra showed bands at 2887 cm^{-1}(CH_2 stretching) and 1360 cm^{-1}(CH_3 symmetric bending). Both PDLA-Nic and PDLA-PEG50-Nic presented the same peaks of PDLA-Nic and PDLA-PEG50, respectively.

The SEM micrographies of PDLA, PDLA-Nic, PDLA-PEG50 and PDLA-PEG50-Nic coatings deposited on catheter segments are shown in figure 5. SEM imaging of coated catheters with PDLA and PDLA-PEG50 coatings confirmed the functionalization and texturization of the catheter surface as their morphology presented a smooth exterior. In addition, PDLA coatings showed fissures at the surface level. On the other hand, PDLA-Nic and PDLA-PEG50-Nic coatings presented a rough morphology with visible aggregates on the surface.

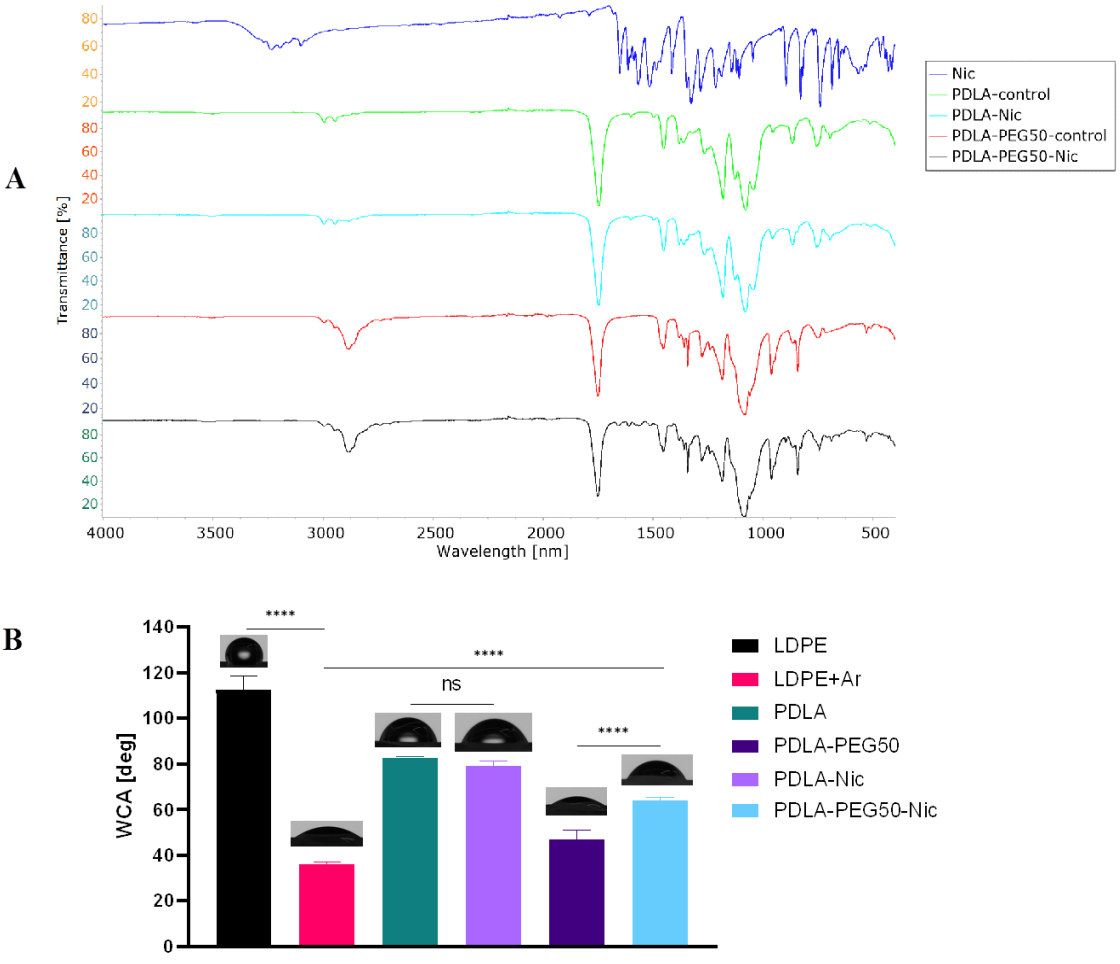

Figure 4. Panel A) FTIR spectroscopic analysis of neat Nic and polymeric coatings. Panel B) Water angle measurements of LDPE catheters and catheters coated with PDLA, PDLA-Nic, PDLA-PEG50-Nic and PDLA-PEG50.

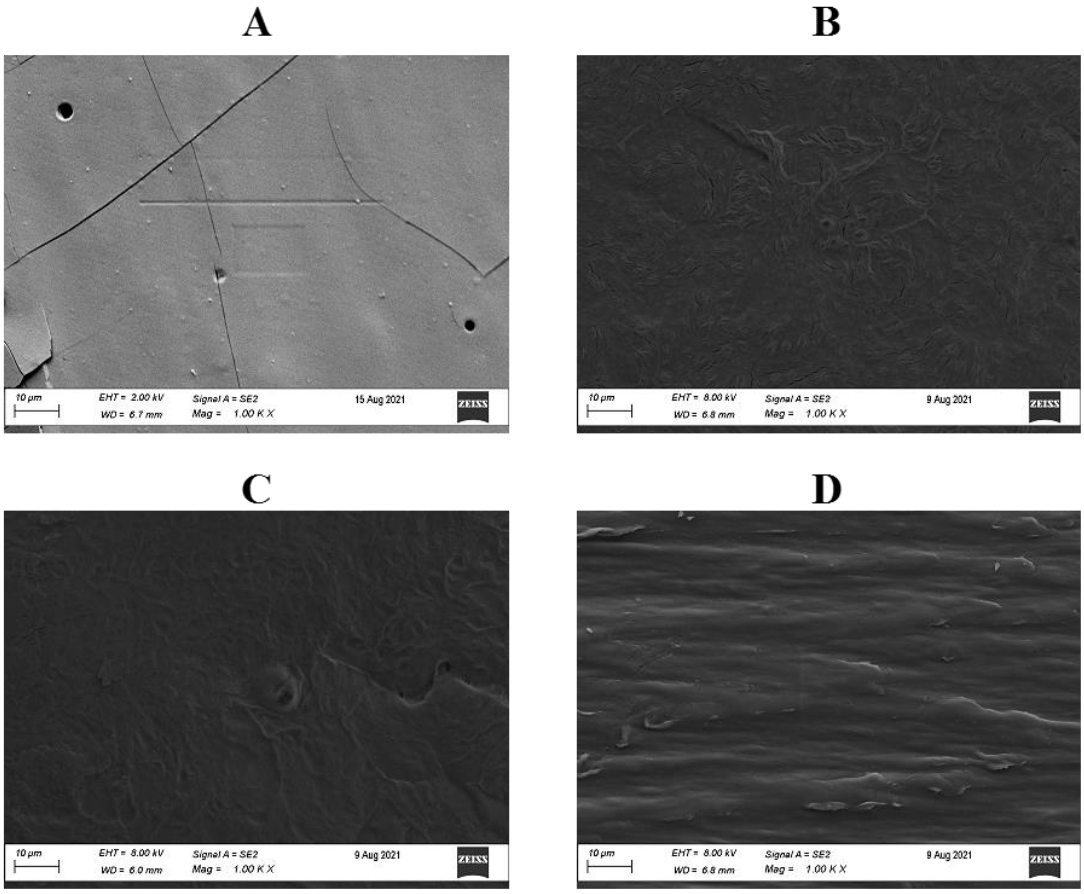

Figure 5. Representative SEM micrographies showing the surface morphology of catheter segments coated with A) PDLA coating, B) PDLA-PEG50 coating, C) PDLA-Nic coating and D) PDLA-PEG50-Nic coating. Images are visualized with a magnification of 1000x

DISK DIFFUSION ASSAY

The antibacterial capacity of PDLA-Nic and PDLA-PEG50-Nic coatings was analyzed by measuring the zone of inhibition (ZOI) produced in TSA plates inoculated with *S. aureus* ATCC 25923 and *S. aureus* ATCC 33591 over 9 days.

The catheter segments coated with PDLA and PDLA-PEG50 did not produce inhibition zone when tested against both bacterial strains, which indicates a lack of antibacterial activity from these coatings. On the contrary, catheters coated with PDLA-Nic coating displayed antibacterial activity as they produced on day 1 an inhibition zone of 5.92 and 7.8 mm against *S. aureus* ATCC 33591 and *S. aureus* ATCC 25923, respectively.

Moreover, the inhibitory activity was recorded for 9 consecutive days, achieving a ZOI diameter of approximately 1.6 mm for both strains on day 9. Catheter segments coated with PDLA-PEG50-Nic coatings, showed on day 1 a ZOI diameter of 14.45 and 13.35 mm, for S. *aureus* ATCC 33591 and *S. aureus* ATCC 25923, respectively. On day 9 the recorded diameters for this coating formulation were between 4.9 and 5.4 mm for both *S. aureus* strains

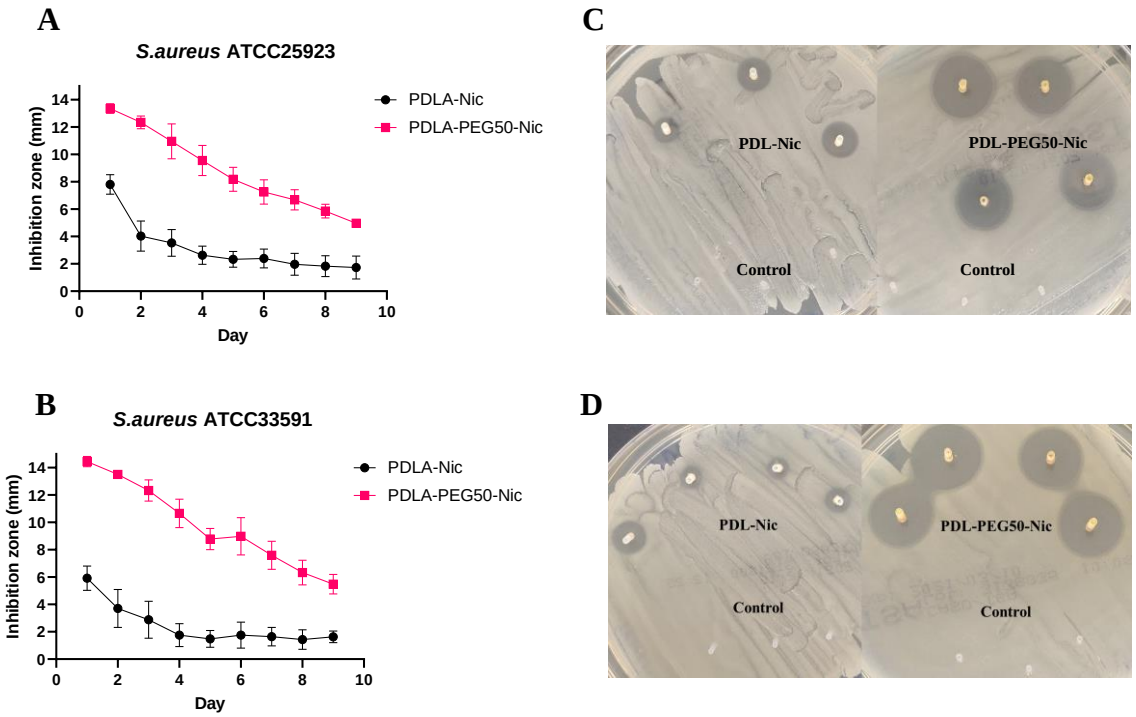

Figure 6. Zone of inhibition produced by PDLA-Nic and PDLA-PEG50-Nic coatings against A) *S. aureus* ATCC 25923 and B) *S. aureus* ATCC 33591. Representative photographs of the inhibition zone created by niclosamide-loaded coatings against C) *S. aureus* ATCC 25923 and D) *S. aureus* ATCC 33591

IN VITRO ANTIBACTERIAL ACTIVITY OF CATHETERS COATED WITH PDLA-NIC AND PDLA-PEG50-NIC

Biofilm formation on the surface of medical devices is a crucial step to develop device-associated infections[4]. The antibiofilm activity of PDLA-Nic and PDLA-PEG50-Nic coatings was examined against *S. aureus* ATCC 25923 and *S. aureus* ATCC 33591. PDLA and PDLA-PEG50 coatings were used as negative controls. Moreover, we tested how eluting niclosamide from the coatings was able to inhibit planktonic growth in the

surrounding media. As shown in Figure 7, we found that PDLA-Nic (Log reduction of 3.82) and PDLA-PEG50-Nic (Log reduction of 4.8) coatings were able to decrease bacterial colonization of *S. aureus* ATCC 25923 when compared to their respective control samples. Similarly, a reduction in biofilm formation was observed when PDLA-Nic (Log reduction of 1.5) and PDLA-PEG50-Nic (Log reduction OF 3.33) were challenged against the Methicillin resistant *S. aureus* ATCC 33591.

We also tested whether planktonic bacterial cells in the surrounding media would be affected by leaching niclosamide from the coatings. PDLA-Nic and PDLA-PEG50-Nic coatings inhibited the bacterial growth of *S. aureus* ATCC 25923 and *S. aureus* ATCC 33591 by a value of 3.96 and 2.36 LogCFU, respectively. On the other hand, PDLA-Nic coating didn't inhibit the planktonic bacterial growth whereas PDLA-PEG50-Nic coatings reduced the bacterial growth of *S. aureus* ATCC 33591.

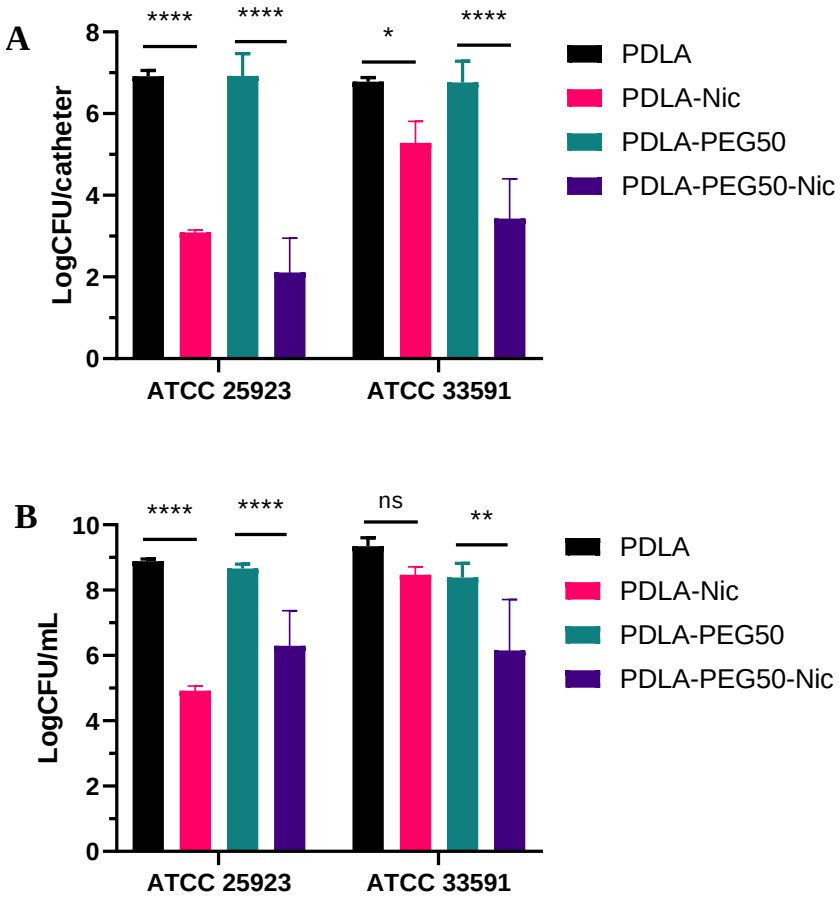

Figure 7. A) Antibiofilm activity of catheter segments coated with PDLA-Nic and PDLA-PEG50-Nic formulations against *S. aureus* ATCC 25923 and *S. aureus* ATCC 33591. B) Planktonic growth inhibition of leaching niclosamide from polymeric against S. *aureus* ATCC 25923 and *S. aureus* ATCC 33591

In accordance with the results obtained from the *in vitro* antibacterial evaluation, the reduction of the bacterial load at the surface level of catheter segments was confimed by SEM microscopy (Figure 8). As can be seen in figure 8A and 8B, *S. aureus* ATCC 25923 bacterial cells formed well defined 3D biofilm structures on the surface of PDLA and PDLA-PEG50 coated catheters. Converserly, a visible reduction on bacterial biofilm was achieved on catheters coated with PDLA-Nic (Fig. 8C) and PDLA-PEG50-Nic (Fig. 8D).

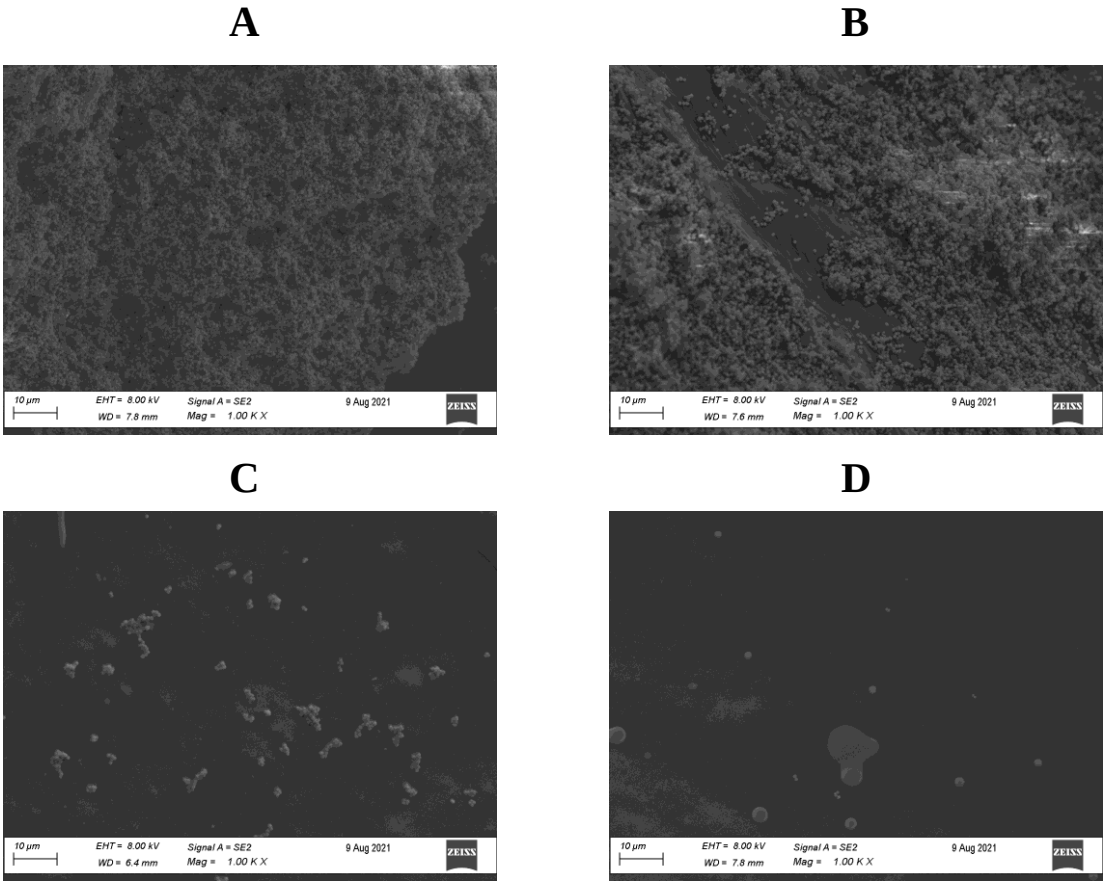

Figure 8. Representative images of biofilm formation of *S. aureus* ATCC 25923 on catheter surfaces coated with A) PDLA, B) PDLA-PEG50, C) PDLA-Nic and D) PDLA-PEG50-Nic coating formulations. Micrographies were taken at a Magnification of 1000 X

EVALUATION OF THE ANTIBACTERIAL EFFICACY OF PDL-NIC AND PDL-PEG50-NIC COATINGS USING A SUBCUTANEOUS FOREIGN BODY INFECTION MODEL

The antibacterial activity of PDLA-Nic and PDLA-PEG50-Nic coatings was further analyzed using a subcutaneous murine foreign body infection model. Coated catheter segments were subcutaneously implanted in the animals and accordingly infected with *S. aureus* ATCC 25923. After 3- and 7-days post-infection catheter segments and surrounding tissue were collected, and the bacterial load was accordingly determined (Figure 7).

Quantification of bacterial load on catheters coated with PDLA-Nic revealed that this formulation was not effective on reducing the *in vivo* biofilm formation over the experimentation time. On day 3, mice retrieved catheter segments coated with PDLA-Nic had a bacterial load value of 7.25 LogCFU which was not different from the bacterial load (6.66 LogCFU) of PDLA coated catheters. Accordingly, the bacterial load in surrounding tissue of catheters coated with PDLA-Nic (8.70 LogCFU) did not differ from the bacterial load on their PDLA control group (8.86 LogCFU). Similarly, on day 7 no significant difference was found on the bacterial load of catheters coated with PDLA-Nic (6.47 LogCFU) and PDLA (5.95 LogCFU) coatings. In agreement, on day 7 PDLA-Nic coated catheters did not reduce the bacterial colonization in surrounding tissue when compared with their control group. These results clearly indicate that PDLA-Nic coating formulations did not exert a biological effect when tested in this infection model.

As seen in Figure 7, PDLA-PEG50-Nic coatings were more effective in reducing *S. aureus* colonization on both catheter segments and surrounding tissue. On day 3 post infection, PDLA-PEG50-Nic coated catheters registered a 4.9 LogCFU reduction when compared to its respective PDLA-PEG50 control group. Accordingly, the bacterial load in surrounding tissue of PDLA-PEG50 coated catheter (6.57LogCFU) was reduced when compared to the PDLA-PEG50 tissue control group (8.16 Log CFU). Remarkably, after 7 days of infection, a LogCFU reduction of 6.52 was observed on PDLA-PEG50-Nic

coated catheters. The bacterial colonization in the respective surrounding tissue was also affected after 7 days.

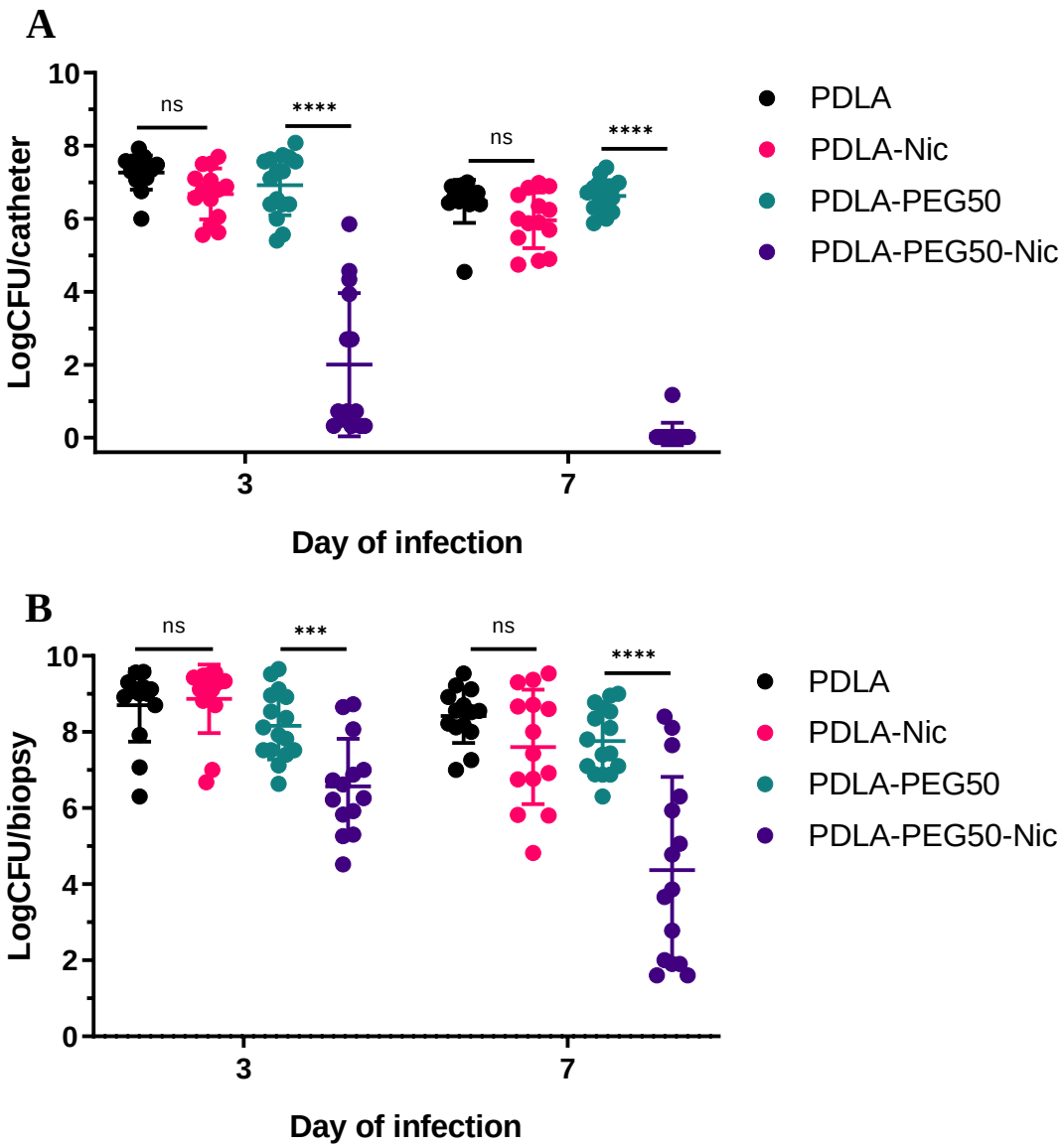

Figure 9. *In vivo* antibacterial efficacy of PDLA-Nic and PDLA-PEG50-Nic coatings using a foreign body infection model with the methicillin sensitive *S. aureus* ATCC 25923. Panel A) Bacterial load on catheter surfaces. Panel B) Bacterial colonization in catheter-surrounding tissue.

DISCUSSION AND CONCLUSION

In the present chapter the development of polymeric coatings loaded with niclosamide to combat potential biofilm development and device-associated infections that may occur with catheterization is reported. Niclosamide is a well-studied anthelmintic drug with recently described antibacterial activity[29-35]. In several studies this drug has been repurposed to combat antibacterial resistant bacteria, especially *S. aureus* which is in fact the main responsible pathogens of device-associated infections[32, 36-38]. Furthermore, this drug has been proven not toxic in several murine disease models as well as in on-going clinical trials in humans[35, 39-44].

For this reason, we decided to develop coatings by incorporating niclosamide into the polymeric matrix of PDLA and PDLA formulated with different concentrations of PEG (15, 30 and 50 % w/w). These drug-polymer formulations were used to coat catheter segments by Ink jet printing technology in order to accurately deposit predictable Nic concentrations on the catheters as well as to reduce manufacturing-related costs. Moreover, the used of 3D printing technology allowed us to deposit different coatings following complex design patterns on the catheter surface.

We then sought to modulate the release of niclosamide from the coatings at concentrations effective against *S. aureus*. Initial drug release investigations were carried out with PDLA-Nic, PDLA-PEG15-Nic, PDLA-PEG30-Nic and PDLA-PEG50-Nic coatings. The amount of Nic released from each coating differed over 456 h with an initial burst drug release during the first 24 h. The cumulative release of niclosamide from PEG containing coatings was higher than the drug release of PDLA-Nic which agrees with previous studies as PEG has been previously used to increase the aqueous solubility of Nic and thus its bioavailability[45-47]. Given the extended-release profile of PDLA-PEG50-Nic coatings, they were used for further *in vitro* and *in vivo* characterization as well as PDLA-Nic for comparison purposes.

The incorporation of niclosamide into the polymeric matrix of both PDLA-Nic and PDLA-PEG50-Nic was confirmed as there was an attenuation of the characteristic FTIR spectral bands of Nic which may indicate a covalent interaction between the drug and the polymer[48]. Several studies have reported the attenuation of the same spectral bands when Nic was formulated with different polymeric carriers[49-52]. The hydrophobicity increased in PDLA-Nic and PDLA-PEG50-Nic coatings which was expected as niclosamide is a hydrophobic drug [41]. Similarly, SEM microscopy demonstrated discernible differences in the surface morphology between non-loaded polymeric coatings (PDLA and PDLA-PEG50) and Nic loaded coatings (PDLA-Nic and PDLA-PEG50-Nic). The texturization at the surface level may result from the incorporation of Nic and the subsequent interaction with the polymeric carrier during the dying process.

Based on the material characterization studies, we next investigated whether PDLA-Nic and PDLA-PEG50-Nic coatings would be able to inhibit the *in vitro* bacterial growth and prevent biofilm formation of the methicillin sensitive *S. aureus* ATCC 25923 and the methicillin resistant *S. aureus* ATCC 33591. PDLA-Nic and PDLA-PEG50-Nic coatings presented an extended antibacterial activity as both coatings produced an inhibition zone over 9 consecutive days. This result indicated that leaching niclosamide from the coatings can diffuse through semi-solid media and exert an antibacterial activity. We further confirmed the antibacterial activity of PDLA-Nic and PDLA-PEG50-Nic coatings by quantification of biofilm formation on coated catheter surfaces. Not only did the PDLA-Nic and PDLA-PEG50-Nic coatings reduced the number of viable bacteria recovered but also reduced the number of biofilm-forming bacteria on the catheter surface as determined by SEM.

Having established by different methods the *in vitro* activity of PDLA-Nic and PDLA-PEG50-Nic coatings, we next evaluated the efficacy of such coatings using a foreign body murine infection mode. This model was selected due to its proven efficacy to evaluate the *in vivo* antibacterial activity of novel coatings, devices, and implants[53]. In this infection model, PDLA-Nic coated catheters did not

reduce the *in vivo* biofilm formation as well as the bacterial colonization in surrounding tissue. The low *in vivo* protection of PDLA-Nic coating may be due to the low release profile of the drug as most of Nic remained entrapped in the coating. In addition, niclosamide is not highly bioavailable which may diminish the local concentration of niclosamide *in vivo[41]*.

Conversely, PDLA-PEG50-Nic coatings were proved highly effective on reducing bacterial colonization in both catheter surface and the surrounding tissue. For instance, previous studies have reported that PEG-Nic formulations improve the bioavailability of this drug in animal models while increasing its biological effect[47]. In this case, the achieved local concentration of niclosamide were effective on exerting an antibacterial effect on both catheter surfaces and the surrounding tissue. Interestingly, on day 7 post infection the bacterial colonization was practically null on PDLA-PEG50-Nic coated catheters while residing bacteria in the tissue was reduced by ~4 LogCFU. Taking all together the results from *in vitro* and *in vivo* experimentation, PDLA-PEG50-Nic coatings exhibited promising efficacy which would make this coating suitable to prevent *S. aureus* device associated infections in clinical settings. Furthermore, 3D printing technology could be used to accurately coat with niclosamide formulations non only catheters but also different devices to treat other medical indications such as diabetes, cancer, viral infections, psoriasis, etc. In future studies it would be interesting to formulate coatings formulations containing Nic and different drug combinations containing to attack specific device associated infections caused.

REFERENCES

1. Rumbaugh, K.P. and K.J.N.R.M. Sauer, *Biofilm dispersion.* 2020. **18**(10): p. 571-586.
2. Donaldson, M.S., J.M. Corrigan, and L.T. Kohn, *To err is human: building a safer health system.* 2000.
3. Prevention, E.C.f.D., *Annual epidemiological report on communicable diseases in Europe*. 2008: ECDC, European Centre for Disease Prevention and Control.
4. Bryers, J.D.J.B. and bioengineering, *Medical biofilms.* 2008. **100**(1): p. 1-18.
5. VanEpps, J.S. and J.G.J.S. Younger, *Implantable device related infection.* 2016. **46**(6): p. 597.
6. Koo, H., et al., *Targeting microbial biofilms: current and prospective therapeutic strategies.* 2017. **15**(12): p. 740-755.
7. Cloutier, M., D. Mantovani, and F.J.T.i.b. Rosei, *Antibacterial coatings: challenges, perspectives, and opportunities.* 2015. **33**(11): p. 637-652.
8. Neoh, K.G., et al., *Surface modification strategies for combating catheter-related complications: recent advances and challenges.* 2017. **5**(11): p. 2045-2067.
9. León-Buitimea, A., et al., *The Demand for New Antibiotics: Antimicrobial Peptides, Nanoparticles, and Combinatorial Therapies as Future Strategies in Antibacterial Agent Design.* Frontiers in Microbiology, 2020. **11**: p. 1669.
10. Cyphert, E.L. and H.A. von Recum, *Emerging technologies for long-term antimicrobial device coatings: advantages and limitations.* Experimental biology and medicine (Maywood, N.J.), 2017. **242**(8): p. 788-798.
11. Ngo, T.D., et al., *Additive manufacturing (3D printing): A review of materials, methods, applications and challenges.* 2018. **143**: p. 172-196.
12. Barui, S.J.M.D. and Sensors, *3D inkjet printing of biomaterials: Principles and applications.* 2021. **4**(1): p. e10143.
13. Azizi Machekposhti, S., S. Mohaved, and R.J.J.E.o.o.d.d. Narayan, *Inkjet dispensing technologies: recent advances for novel drug discovery*. 2019. **14**(2): p. 101-113.
14. Scoutaris, N., S. Ross, and D.J.P.r. Douroumis, *Current trends on medical and pharmaceutical applications of inkjet printing technology.* 2016. **33**(8): p. 1799-1816.
15. Ballard, D.H., et al., *Antibiotics in 3D-printed implants, instruments and materials: Benefits, challenges and future directions.* 2019. **3**(2): p. 83-93.

16. Boehm, R.D., et al., *Inkjet printing for pharmaceutical applications.* 2014. **17**(5): p. 247-252.
17. Gu, Y., et al., *Inkjet printed antibiotic- and calcium-eluting bioresorbable nanocomposite micropatterns for orthopedic implants.* Acta Biomaterialia, 2012. **8**(1): p. 424-431.
18. Chen, X.N., et al., *Multifunctional surfaces with biomimetic nanofibres and drug-eluting micro-patterns for infection control and bone tissue formation.* Eur Cell Mater, 2012. **24**: p. 237-48.
19. Zheng, Y., et al., *Colonization of medical devices by staphylococci.* Environmental microbiology, 2018. **20**(9): p. 3141-3153.
20. Zaazaa, H.E., et al., *Kinetic study and mechanism of niclosamide degradation.* 2014. **132**: p. 655-662.
21. Van Tonder, E.C., et al., *Preparation and physicochemical characterization of 5 niclosamide solvates and 1 hemisolvate.* 2004. **5**(1): p. 86-95.
22. Ray, E., et al., *Autophagy-inducing inhalable co-crystal formulation of Niclosamide-Nicotinamide for lung cancer therapy.* 2020. **21**(7): p. 1-14.
23. Pan, P., et al., *Temperature-variable FTIR and solid-state 13C NMR investigations on crystalline structure and molecular dynamics of polymorphic poly (L-lactide) and poly (L-lactide)/poly (D-lactide) stereocomplex.* 2012. **45**(1): p. 189-197.
24. Lopes, M.S. and A.L.J.C.e.t. Jardini, *Synthesis and characterizations of poly (lactic acid) by ring-opening polymerization for biomedical applications.* 2014.
25. Wu, Y., et al., *Synthesis, characterization, and crystallization behaviors of poly (D-lactic acid)-based triblock copolymer.* 2020. **10**(1): p. 1-12.
26. Buhecha, M.D., et al., *Development and characterization of PLA nanoparticles for pulmonary drug delivery: Co-encapsulation of theophylline and budesonide, a hydrophilic and lipophilic drug.* 2019. **53**: p. 101128.
27. Zhang, J., et al., *Infrared Spectroscopic Study of CH3⊙⊙⊙ OC Interaction during Poly (l-lactide)/Poly (d-lactide) Stereocomplex Formation.* 2005. **38**(5): p. 1822-1828.
28. Tueen, B.S., *Polylactic acid: a practical guide for the processing, manufacturing, and applications of PLA.* 2019: William Andrew.
29. Xu, J., et al., *Discovery of niclosamide and its O-alkylamino-tethered derivatives as potent antibacterial agents against carbapenemase-producing and/or colistin*

resistant Enterobacteriaceae isolates. Bioorganic & medicinal chemistry letters, 2019. **29**(11): p. 1399-1402.

30. Farha, M.A. and E.D. Brown, *Drug repurposing for antimicrobial discovery.* Nature Microbiology, 2019. **4**(4): p. 565-577.
31. Das, S., A. Dasgupta, and S. Chopra, *Drug repurposing: a new front in the war against Staphylococcus aureus.* Future microbiology, 2016. **11**(8): p. 1091-1099.
32. Gwisai, T., et al., *Repurposing niclosamide as a versatile antimicrobial surface coating against device-associated, hospital-acquired bacterial infections.* Biomedical Materials, 2017. **12**(4): p. 045010.
33. Mohammad, H., et al., *Repurposing niclosamide for intestinal decolonization of vancomycin-resistant enterococci.* International journal of antimicrobial agents, 2018. **51**(6): p. 897-904.
34. Tharmalingam, N., et al., *Repurposing the anthelmintic drug niclosamide to combat Helicobacter pylori.* Scientific reports, 2018. **8**(1): p. 3701.
35. Copp, J.N., et al., *Mechanistic understanding enables the rational design of salicylanilide combination therapies for Gram-negative infections.* 2020. **11**(5): p. e02068-20.
36. Rajamuthiah, R., et al., *Repurposing salicylanilide anthelmintic drugs to combat drug resistant Staphylococcus aureus.* PloS one, 2015. **10**(4): p. e0124595.
37. Torres, N.S., et al., *Screening a commercial library of pharmacologically active small molecules against Staphylococcus aureus biofilms.* Antimicrobial agents and chemotherapy, 2016. **60**(10): p. 5663-5672.
38. Zhurina, M., et al., *Niclosamide as a promising antibiofilm agent.* Microbiology, 2017. **86**(4): p. 455-462.
39. Brunaugh, A.D., et al., *Development and evaluation of inhalable composite niclosamide-lysozyme particles: A broad-spectrum, patient-adaptable treatment for coronavirus infections and sequalae.* PloS one, 2021. **16**(2): p. e0246803.
40. Boyapally, R., et al., *Niclosamide alleviates pulmonary fibrosis in vitro and in vivo by attenuation of epithelial-to-mesenchymal transition, matrix proteins & Wnt/β-catenin signaling: A drug repurposing study.* 2019. **220**: p. 8-20.
41. Barbosa, E.J., et al., *Niclosamide repositioning for treating cancer: Challenges and nano-based drug delivery opportunities.* European Journal of Pharmaceutics and Biopharmaceutics, 2019. **141**: p. 58-69.
42. Chang, Y.-W., et al., *Pharmacokinetics of anti-SARS-CoV agent niclosamide and its analogs in rats.* Journal of Food and Drug Analysis, 2006. **14**(4).

43. Parikh, M., et al., *Phase Ib trial of reformulated niclosamide with abiraterone/prednisone in men with castration-resistant prostate cancer*. Scientific reports, 2021. **11**(1): p. 1-7.
44. Backer, V., et al., *A randomized, double-blind, placebo-controlled phase 1 trial of inhaled and intranasal niclosamide: A broad spectrum antiviral candidate for treatment of COVID-19.* The Lancet Regional Health-Europe, 2021: p. 100084.
45. Wang, G., et al., *Lipid nanoparticle formulation of niclosamide (nano NCM) effectively inhibits SARS-CoV-2 replication in vitro.* 2021. **4**(1): p. 724-737.
46. Ma, R., et al., *Injectable pegylated niclosamide (polyethylene glycol-modified niclosamide) for cancer therapy*. 2020. **108**(1): p. 30-38.
47. Zhang, X., et al., *Significantly enhanced bioavailability of niclosamide through submicron lipid emulsions with or without PEG-lipid: a comparative study*. 2015. **32**(5): p. 496-502.
48. Kowalczuk, D., *FTIR Characterization of the Development of Antimicrobial Catheter Coatings Loaded with Fluoroquinolones.* Coatings, 2020. **10**(9): p. 818.
49. Jara, M.O., Z.N. Warnken, and R.O.J.P. Williams, *Amorphous solid dispersions and the contribution of nanoparticles to in vitro dissolution and in vivo testing: Niclosamide as a case study.* 2021. **13**(1): p. 97.
50. Ray, E., et al., *Autophagy-Inducing Inhalable Co-crystal Formulation of Niclosamide-Nicotinamide for Lung Cancer Therapy*. AAPS PharmSciTech, 2020. **21**(7): p. 260.
51. Yilmaz, B., *Nifedipine, Niclosamide and Furosemid Release of A Biocompatible and Protective Hydrogel for Cancer Therapy.* 2021.
52. Jain, N.K., et al., *Niclosamide encapsulated polymeric nanocarriers for targeted cancer therapy.* 2019. **9**(46): p. 26572-26581.
53. Nowakowska, J., R. Landmann, and N.J.A. Khanna, *Foreign body infection models to study host-pathogen response and antimicrobial tolerance of bacterial biofilm.* 2014. **3**(3): p. 378-397.

CHAPTER 5

CONCLUSIONS AND NEXT STEPS

CONCLUSIONS AND NEXT STEPS

Antimicrobial resistance is considered one of the main global health issues by the World Health Organization. The possible reasons for the serious emergence of drug-resistance microbes are lack of new antimicrobials, lack of novel approaches in drug discovery. The WHO declared that there is a latent need to develop new antimicrobial agents to prevent the potential death of millions of people caused by antimicrobial resistance.

Currently, different infection-control strategies to develop novel antimicrobials have been explored, namely phage therapy, combinatorial antibiotic treatment, vaccines, antimicrobial peptides, anti-virulence agents, new molecules, and drug repurposing. Among the current approaches, drug repurposing has risen as one of the most promising strategies. Drug repurposing focus on the identification of novel medical indications for already approved drugs. Hence the development of novel antimicrobials following drug repurposing approach is faster and reduce associated costs while minimizing potential toxicity concerns.

From several high-throughput repurposing screening studies, niclosamide has been identified as of the most promising molecules exerting antibacterial activity, especially against *Staphylococcus aureus*. In this thesis project we confirmed that niclosamide inhibits not only the bacterial planktonic growth but also prevents the biofilm formation and disrupts pre-formed biofilms of *S. aureus* and *S. epidermidis*. Moreover, following a macromolecular synthesis assay we found that niclosamide impact the synthesis of DNA, RNA, proteins, lipids and peptidoglycans of which RNA and protein synthesis were greatly affected at the lowest concentrations. These results suggest that niclosamide acts at different macromolecular pathways which would reduce the risk of emergence of niclosamide resistance in *S. aureus*. For instance, it has been reported that niclosamide affects the PMF and therefore ATP production and related metabolic processes such as macromolecule synthesis. We also confirmed that niclosamide does not exert a significant antibacterial activity against Gram-negative bacteria

such as *Escherichia coli* and *Pseudomonas aeruginosa*. Hence, the combination of niclosamide with antibiotics or other novel antimicrobial agents seems attractive to develop broad-spectrum antibacterial treatments. Moreover, the chemical modification of niclosamide could provide novel molecules with enhanced antibacterial effect against both Gram-positive and Gram-negative bacteria while improving the physico-chemical properties of the molecules for novel applications.

Given the high antibacterial activity of niclosamide at low concentrations and its well-known safety profile, in this PhD thesis we selected niclosamide as an antibacterial agent to explore novel manufacturing technologies to develop antibacterial/anti-infective medical devices.

Specifically, we have used 2 different technologies to manufacture medical devices with antibacterial functionalities. In one hand, we produced niclosamide-loaded catheters via hot melt extrusion, using a modified 3D printer. In this approach, we demonstrated the *in vivo* efficacy of the niclosamide-loaded catheters, using a foreign body infection model. Moreover, we confirmed that niclosamide is suitable to be used in high temperature 3D technologies, as it can withstand about 180 °C without undergoing degradation. For future studies, we propose to 3D print novel architectures and designs to tailor made antibacterial medical devices for different health applications. In a similar manner, different polymers can be used to modulate the drug release rate as well as the mechanical properties of the devices.

On the other hand, we developed polymeric coatings loaded with niclosamide, which were then deposited on the surface of catheter segments via ink jet printing. As a proof of principle study, we developed a specific method to coat catheter segments with precise amounts of niclosamide, however we can adjust the same method to deposit the developed coatings on the surface of medical devices with different architectures and materials. Moreover, we confirmed that the developed coatings were capable of resist bacterial infections, using a foreign body infection

model. As following steps, we propose to coat diverse medical devices and evaluate the antibacterial efficacy of the developed niclosamide-loaded coatings. Novel coatings can be customized by using different polymers and niclosamide loadings which would provide specific properties to satisfy specific health applications. Finally, we also propose to further evaluate the antibacterial catheters herein described using animal models mimicking more accurately the clinical scenario of catheter associated infections.

In summary, the use of repurposed drugs for treating bacterial infections represent a promising approach to develop novel antibacterial therapeutics while minimizing the emergence of antimicrobial resistance. Moreover, 3D printing technologies arise as one of the most cost-effective strategies to fabricate tailor-made anti-infective medical devices. However, more preclinical models as well as standardized testing methods are needed to accurately evaluate de efficacy of novel anti-infective devices and thus obtain valuable extrapolatable data for future human studies.

.